Copyright Warning & Restrictions

The copyright law of the United States (Title 17, United States Code) governs the making of photocopies or other reproductions of copyrighted material.

Under certain conditions specified in the law, libraries and archives are authorized to furnish a photocopy or other reproduction. One of these specified conditions is that the photocopy or reproduction is not to be "used for any purpose other than private study, scholarship, or research." If a, user makes a request for, or later uses, a photocopy or reproduction for purposes in excess of "fair use" that user may be liable for copyright infringement,

This institution reserves the right to refuse to accept a copying order if, in its judgment, fulfillment of the order would involve violation of copyright law.

Please Note: The author retains the copyright while the New Jersey Institute of Technology reserves the right to distribute this thesis or dissertation

Printing note: If you do not wish to print this page, then select "Pages from: first page # to: last page #" on the print dialog screen

Order Number 9514441

Local thermal stress factor of pipe-nozzle

Chen, David Chihwei, Ph.D.

New Jersey Institute of Technology, 1994

U·M·I

300 N. Zeeb Rd.
Ann Arbor, MI 48106

ABSTRACT

LOCAL THERMAL STRESS FACTOR OF PIPE-NOZZLE

by
David Chihwei Chen

A comprehensive study of local thermal stresses at the juncture of pipe -nozzle is presented in this thesis. The thermal loading is assumed to be a linear thermal gradient across the thickness of the pipe and nozzle. Currently, there exists neither experimental nor analytical data that is sufficient for pressure vessel designers to analyze the local thermal stresses at the juncture of pipe-nozzle. In order to provide a comprehensive database to calculate these thermal stresses, the finite element technique is used to provide a series of local thermal stress factor plots as a function of pipe-nozzle geometrical parameters.

For the local thermal stresses on the juncture of pipe-nozzle, the longitudinal and circumferential thermal stress factors due to the thermal loading are presented in a series of plots as functions of gamma, γ (pipe mean radis/pipe thickness) and beta, β (nozzle mean radius/pipe radius). The gamma values vary from 10 to 300 and beta values vary from 0.1 to 1.0. These stress factors would complement the welding Research Council Bulletin 107 method in pipe-nozzle stress analysis which did not include the effect of local thermal stresses.

To ensure the convergence of the finite element results, two major parameters were thoroughly studied. First, to minimize the influence of boundary conditions on the

thermal stresses around the juncture of the pipe-nozzle, the geometrical parameter $alpha_p$, α_p, (pipe length/pipe mean radius) is found to be at least equal to 8.0 as well as $alpha_n$, α_n, (nozzle length/nozzle mean radius) at least to be 4.0. Next, 96 node points must be assigned at the juncture of pipe-nozzle. As a result, approximately 5000 node points and 3000 plus elements were needed for the computation. Numerical examples are also presented in this thesis to demonstrate how the thermal stress components complement the WRC 107 local stress computation due to external loadings.

LOCAL THERMAL STRESS FACTOR OF PIPE-NOZZLE

by
David Chihwei Chen

A Dissertation
Submitted to the Faculty of
New Jersey Institute of Technology
in Partial Fulfillment of the Requirements for the Degree of
Doctor of Philosophy

Department of Mechanical and Industrial Engineering

October 1994

APPROVAL PAGE

LOCAL THERMAL STRESS FACTOR OF PIPE-NOZZLE

David Chihwei Chen

Dr. Benedict C. Sun, Dissertation Advisor — Date
Associate Professor of Engineering Technology, NJIT

Dr. Rong-Yaw Chen, Committee Chair — Date
Professor of Mechanical Engineering
and Associate Chairperson and Graduate Advisor
of Mechanical Engineering, NJIT

Dr. Bernard Koplik, Committee Member — Date
Professor of Mechanical Engineering and Chairperson
of the Department of Mechanical and Industrial Engineering, NJIT

Dr. Nouri Levy, Committee Member — Date
Associate Professor of Mechanical Engineering, NJIT

Dr. C.T. Thomas Hsu, Committee Member — Date
Professor of Civil and Environmental Engineering, NJIT

BIOGRAPHICAL SKETCH

Author: David Chihwei Chen

Degree: Doctor of Philosophy in Mechanical and Industrial Engineering

Date: October 1994

Undergraduate and Graduate Education:

- Doctor of Philosophy in Mechanical and Industrial Engineering ,
  New Jersey Institute Technology,
  Newark, New Jersey, 1994

- Master of Science in Mechanical Engineering ,
  New Jersey Institute Technology,
  Newark, New Jersey, 1987

- Bachelor of Science in Mechanical Engineering ,
  Tamkang University,
  Tamsui, Taiwan, 1984

Major: Mechanical Engineering

Presentations and Publications:

David C. Chen

"On Longitudinal and Transverse Shear Spring Constants at the Juncture of Piping-nozzle." Master Thesis, NJIT
Newark, New Jersey, May 1987

Position Held:

Project Manager
Airco Gases, Engineering System Dept. D.I.E.T.
575 Mountain Ave., Murray Hill, New Jersey 07974

Professional License and Memberships:

Professional Engineer License, Pennsylvania, 1993
Member of American Society of Mechanical Engineers
Member of National Association of Corrosion Engineers

This dissertation is dedicated to
my parents and all my family members

ACKNOWLEDGMENT

The author wishes to express his sincere appreciation to his Dissertation advisor, Dr. Benedict Sun, for his guidance, friendship, and moral support throughout this research.

Special thanks to Dr. Rong-Yaw Chen, Dr. Bernard Koplik, Dr. Nouri Levy, and Dr. C. T. Thomas Hsu for serving as members of the committee and their kindly suggestions and support.

Also, the author would like to express his gratitude to his family for their love, understanding and support to the achievement of this dissertation.

TABLE OF CONTENTS

Chapter	Page
1 INTRODUCTION	1
2 LITERATURE SURVEY	4
3 BASIC THEORY	12
3.1 Derivation of Equations for Deflections Due to the Thermal Loading	12
3.2 Thermal Stress Factors	20
4 FINITE ELEMENT MODEL	24
4.1 General	24
4.2 Assumption	25
4.3 Asymptotic Studies	25
4.3.1 Asymptotic Study of Node Points at Juncture of Pipe-nozzle	25
4.3.2 Asymptotic Study of the α_p and α_n	26
4.4 Normalization Studies	26
4.4.1 Case I, II, III	26
4.4.2 Case IV	27
5 COMPARISON OF DATA	28
5.1 General	28
5.2 Comparison of Thermal Stress Factors	28
5.2.1 Case 1	28
5.2.2 Case 2	30
5.3 Comparison of Thermal Stresses	32

Chapter **Page**

6 NUMERICAL EXAMPLES 34

6.1 Example I 34

6.2 Example II 38

7 CONCLUSIONS 42

APPENDIX A THERMAL STRESS FACTOR PLOTS 43

APPENDIX B ASYMPTOTIC STUDY OF NODE POINTS AT JUNCTURE OF PIPE-NOZZLE 60

APPENDIX C ASYMPTOTIC STUDY OF α_P AND α_N 77

APPENDIX D NORMALIZATION STUDIES 110

APPENDIX E COMPARISON OF DATA - CASE 2 123

REFERENCES 132

LIST OF TABLES

Table		Page
1	Modified Stress Computation Table of WRC 107 Including Local Thermal Stresses	22
2	List of Thermal Stresses and Thermal Stress Factors Given in the Case 2	31
3	Comparison of Local Thermal Stresses at Pipe-nozzle and Theoretical Thermal Stresses at Regular Long Hollow Pipe	33
4	Material Properties of the Illustrating Pipe-nozzle Model	35
5	Geometrical Parameters and Dimensions of Example for Calculation of Local Stresses on the Pipe of Pipe-nozzle Model	35
6	Computation Table of Thermal Stress Factors on the Pipe	36
7	Modified Stress Computation Table of WRC 107 Including Local Thermal Stress on the Pipe - Numerical Example	37
8	Geometrical Parameters and Dimensions of Example for Calculation of Local Stresses on Nozzle of Pipe-nozzle Model	39
9	Computation Table of the Thermal Stress Factors on the Nozzle	39
10	Computation Table of Example for Calculation of Local Stresses on Nozzle of Pipe-nozzle Model	40
11	Local Stress Factors on the Nozzle from Lin [45]	41
D-1	Material Properties, Geometric Parameters and Dimensions of Case # 1 and Case # 2	111
D-2	Thermal Stresses & Stress Factors Comparison Table at Node Point A of Case # 1 and Case # 2	112
D-3	Thermal Stresses & Stress Factors Comparison Table at Node Point C of Case # 1 and Case # 2	113
D-4	Material Properties, Geometric Parameters and Dimensions of Case # 3 and Case # 4	114

Table **Page**

D-5 Thermal Stresses & Stress Factors Comparison Table at Node Point A of Case # 3 and Case # 4 115

D-6 Thermal Stresses & Stress Factors Comparison Table at Node Point C of Case # 3 and Case # 4 116

D-7 Material Properties, Geometric Parameters and Dimensions of Case # 5 and Case # 6 117

D-8 Thermal Stresses & Stress Factors Comparison Table at Node Point A of Case # 5 and Case # 6 118

D-9 Thermal Stresses & Stress Factors Comparison Table at Node Point C of Case # 5 and Case # 6 119

D-10 Material Properties, Geometric Parameters and Dimensions of Case # 7 and Case # 8 120

D-11 Thermal Stresses & Stress Factors Comparison Table at Node Point A of Case # 7 and Case # 8 121

D-12 Thermal Stresses & Stress Factors Comparison Table at Node Point C of Case # 7 and Case # 8 122

LIST OF FIGURES

Figure		Page
1	Typical Configuration of Pipe-nozzle Juncture under Axisymmetrical Temperature Distribution	3
2	Literature Survey Table	7
3	Cylindrical Coordinate Applied to a Cylindrical Pipe with Displacement U, V, and W in X, φ, and Z Direction Respectively	19
4	Different Loadings Applied on the Juncture of Pipe-nozzle	23
5	Data Comparison of Case 1 - Thermal Stress Factor in the Longitudinal Direction at Point A_U of the Pipe	29
1T	Thermal Stress Factor in the Longitudinal Direction at Point A_U of the Pipe	44
2T	Thermal Stress Factor in the Longitudinal Direction at Point A_L of the Pipe	45
3T	Thermal Stress Factor in the Longitudinal Direction at Point C_U of the Pipe	46
4T	Thermal Stress Factor in the Longitudinal Direction at Point C_L of the Pipe	47
5T	Thermal Stress Factor in the Circumferential Direction at Point A_U of the Pipe	48
6T	Thermal Stress Factor in the Circumferential Direction at Point A_L of the Pipe	49
7T	Thermal Stress Factor in the Circumferential Direction at Point C_U of the Pipe	50
8T	Thermal Stress Factor in the Circumferential Direction at Point C_L of the Pipe	51
9T	Thermal Stress Factor in the Longitudinal Direction at Point A_o of the Nozzle	52
10T	Thermal Stress Factor in the Longitudinal Direction at Point A_i of the Nozzle	53

Figure **Page**

11T Thermal Stress Factor in the Longitudinal Direction at Point C_o of the Nozzle 54

12T Thermal Stress Factor in the Longitudinal Direction at Point C_i of the Nozzle 55

13T Thermal Stress Factor in the Circumferential Direction at Point A_o of the Nozzle 56

14T Thermal Stress Factor in the Circumferential Direction at Point A_i of the Nozzle 57

15T Thermal Stress Factor in the Circumferential Direction at Point C_o of the Nozzle 58

16T Thermal Stress Factor in the Circumferential Direction at Point C_i of the Nozzle 59

B1 Convergence of Node Points at Juncture of Pipe-nozzle for Longitudinal Thermal Stress Factors at Point A_U of the Pipe 61

B2 Convergence of Node Points at Juncture of Pipe-nozzle for Longitudinal Thermal Stress Factors at Point A_L of the Pipe 62

B3 Convergence of Node Points at Juncture of Pipe-nozzle for Longitudinal Thermal Stress Factors at Point C_U of the Pipe 63

B4 Convergence of Node Points at Juncture of Pipe-nozzle for Longitudinal Thermal Stress Factors at Point C_L of the Pipe 64

B5 Convergence of Node Points at Juncture of Pipe-nozzle for Circumferential Thermal Stress Factors at Point A_U of the Pipe 65

B6 Convergence of Node Points at Juncture of Pipe-nozzle for Circumferential Thermal Stress Factors at Point A_L of the Pipe 66

B7 Convergence of Node Points at Juncture of Pipe-nozzle for Circumferential Thermal Stress Factors at Point C_U of the Pipe 67

B8 Convergence of Node Points at Juncture of Pipe-nozzle for Circumferential Thermal Stress Factors at Point C_L of the Pipe 68

Figure **Page**

B9 Convergence of Node Points at Juncture of Pipe-nozzle for Longitudinal Thermal Stress Factors at Point A_o of the Nozzle 69

B10 Convergence of Node Points at Juncture of Pipe-nozzle for Longitudinal Thermal Stress Factors at Point A_i of the Nozzle 70

B11 Convergence of Node Points at Juncture of Pipe-nozzle for Longitudinal Thermal Stress Factors at Point C_o of the Nozzle 71

B12 Convergence of Node Points at Juncture of Pipe-nozzle for Longitudinal Thermal Stress Factors at Point C_i of the Nozzle 72

B13 Convergence of Node Points at Juncture of Pipe-nozzle for Circumferential Thermal Stress Factors at Point A_o of the Nozzle 73

B14 Convergence of Node Points at Juncture of Pipe-nozzle for Circumferential Thermal Stress Factors at Point A_i of the Nozzle 74

B15 Convergence of Node Points at Juncture of Pipe-nozzle for Circumferential Thermal Stress Factors at Point C_o of the Nozzle 75

B16 Convergence of Node Points at Juncture of Pipe-nozzle for Circumferential Thermal Stress Factors at Point C_i of the Nozzle 76

C1 Percentage of Improvement of Larger α_p to Previous α_p for Longitudinal Thermal Stress Factors at Point A_U of the Pipe 78

C2 Percentage of Improvement of Larger α_p to Previous α_p for Longitudinal Thermal Stress Factors at Point A_L of the Pipe 79

C3 Percentage of Improvement of Larger α_p to Previous α_p for Longitudinal Thermal Stress Factors at Point C_U of the Pipe 80

C4 Percentage of Improvement of Larger α_p to Previous α_p for Longitudinal Thermal Stress Factors at Point C_L of the Pipe 81

C5 Percentage of Improvement of Larger α_p to Previous α_p for Circumferential Thermal Stress Factors at Point A_U of the Pipe 82

C6 Percentage of Improvement of Larger α_p to Previous α_p for Circumferential Thermal Stress Factors at Point A_L of the Pipe 83

Figure **Page**

C7 Percentage of Improvement of Larger α_p to Previous α_p for Circumferential Thermal Stress Factors at Point C_U of the Pipe 84

C8 Percentage of Improvement of Larger α_p to Previous α_p for Circumferential Thermal Stress Factors at Point C_L of the Pipe 85

C9 Percentage of Improvement of Larger α_p to Previous α_p for Longitudinal Thermal Stress Factors at Point A_o of the Nozzle 86

C10 Percentage of Improvement of Larger α_p to Previous α_p for Longitudinal Thermal Stress Factors at Point A_i of the Nozzle 87

C11 Percentage of Improvement of Larger α_p to Previous α_p for Longitudinal Thermal Stress Factors at Point C_o of the Nozzle 88

C12 Percentage of Improvement of Larger α_p to Previous α_p for Longitudinal Thermal Stress Factors at Point C_i of the Nozzle 89

C13 Percentage of Improvement of Larger α_p to Previous α_p for Circumferential Thermal Stress Factors at Point A_o of the Nozzle 90

C14 Percentage of Improvement of Larger α_p to Previous α_p for Circumferential Thermal Stress Factors at Point A_i of the Nozzle 91

C15 Percentage of Improvement of Larger α_p to Previous α_p for Circumferential Thermal Stress Factors at Point C_o of the Nozzle 92

C16 Percentage of Improvement of Larger α_p to Previous α_p for Circumferential Thermal Stress Factors at Point C_i of the Nozzle 93

C17 Percentage of Improvement of Larger α_n to Previous α_n for Longitudinal Thermal Stress Factors at Point A_U of the Pipe 94

C18 Percentage of Improvement of Larger α_n to Previous α_n for Longitudinal Thermal Stress Factors at Point A_L of the Pipe 95

C19 Percentage of Improvement of Larger α_n to Previous α_n for Longitudinal Thermal Stress Factors at Point C_U of the Pipe 96

C20 Percentage of Improvement of Larger α_n to Previous α_n for Longitudinal Thermal Stress Factors at Point C_L of the Pipe 97

Figure **Page**

C21 Percentage of Improvement of Larger α_n to Previous α_n for Circumferential Thermal Stress Factors at Point A_U of the Pipe 98

C22 Percentage of Improvement of Larger α_n to Previous α_n for Circumferential Thermal Stress Factors at Point A_L of the Pipe 99

C23 Percentage of Improvement of Larger α_n to Previous α_n for Circumferential Thermal Stress Factors at Point C_U of the Pipe 100

C24 Percentage of Improvement of Larger α_n to Previous α_n for Circumferential Thermal Stress Factors at Point C_L of the Pipe 101

C25 Percentage of Improvement of Larger α_n to Previous α_n for Longitudinal Thermal Stress Factors at Point A_o of the Nozzle 102

C26 Percentage of Improvement of Larger α_n to Previous α_n for Longitudinal Thermal Stress Factors at Point A_i of the Nozzle 103

C27 Percentage of Improvement of Larger α_n to Previous α_n for Longitudinal Thermal Stress Factors at Point C_o of the Nozzle 104

C28 Percentage of Improvement of Larger α_n to Previous α_n for Longitudinal Thermal Stress Factors at Point C_i of the Nozzle 105

C29 Percentage of Improvement of Larger α_n to Previous α_n for Circumferential Thermal Stress Factors at Point A_o of the Nozzle 106

C30 Percentage of Improvement of Larger α_n to Previous α_n for Circumferential Thermal Stress Factors at Point A_i of the Nozzle 107

C31 Percentage of Improvement of Larger α_n to Previous α_n for Circumferential Thermal Stress Factors at Point C_o of the Nozzle 108

C32 Percentage of Improvement of Larger α_n to Previous α_n for Circumferential Thermal Stress Factors at Point C_i of the Nozzle 109

E1 Data Comparison of Case 2 - Thermal Stress Factor in the Longitudinal Direction at Point A_o of the Nozzle 124

E2 Data Comparison of Case 2 - Thermal Stress Factor in the Longitudinal Direction at Point A_i of the Nozzle 125

Figure **Page**

E3 Data Comparison of Case 2 - Thermal Stress Factor in the Longitudinal Direction at Point C_o of the Nozzle 126

E4 Data Comparison of Case 2 - Thermal Stress Factor in the Longitudinal Direction at Point C_i of the Nozzle 127

E5 Data Comparison of Case 2 - Thermal Stress Factor in the Circumferential Direction at Point A_o of the Nozzle 128

E6 Data Comparison of Case 2 - Thermal Stress Factor in the Circumferential Direction at Point A_i of the Nozzle 129

E7 Data Comparison of Case 2 - Thermal Stress Factor in the Circumferential Direction at Point C_o of the Nozzle 130

E8 Data Comparison of Case 2 - Thermal Stress Factor in the Circumferential Direction at Point C_i of the Nozzle 131

NOMENCLATURES

α_p = pipe Length / pipe mean radius

α_n = nozzle Length / nozzle mean radius

α_T = coefficient of thermal expansion

β = nozzle mean radius / pipe mean Radius

γ = pipe mean radius / pipe thickness

μ = Poisson's ratio

κ_e = external heat transfer coefficient, ft-lb / hr-in^2-°F

κ_i = internal heat transfer coefficient, ft-lb / hr-in^2-°F

σ_T = local thermal stress, psi

E = Young's Modulus, psi

H = pipe thickness / 2 , in

h = nozzle thickness / 2 , in

K_T = local thermal stress factor

L_p = pipe length, in

L_n = nozzle length, in

M_x , M_φ = shell moment resultants, in-lb

M_{th} = thermal moment, in-lb

N_x , N_φ = shell force resultants, lb

N_{th} = thermal membrane force, lb

R_m = pipe mean radius, in

R_p = pipe outside radius, in

t_p = pipe thickness, in

r_m = nozzle mean radius, in

r_n = nozzle outside radius, in

t_n = nozzle thickness, in

T_i = internal temperature, °F

T_o = external temperature, °F

T_{nm} = mean temperature at the nozzle, °F

T_{pm} = mean temperature at the pipe, °F

T_{nd} = normal temperature different at the nozzle, °F

T_{pd} = normal temperature different at the pipe, °F

u = displacement in x direction at the nozzle, in

U = displacement in x direction at the pipe, in

v = displacement in φ direction at the nozzle, in

V = displacement in φ direction at the pipe, in

w = displacement in r direction at the nozzle, in

W = displacement in r direction at the pipe, in

subscript p = pipe

subscript n = nozzle

CHAPTER 1

INTRODUCTION

Thermal stresses analysis at the juncture of pipe-nozzle is one of the critical factor for pressure vessel design. From linear thin-shell theory, an analytical solution based on Morley's equations, which has nearly the same simple form as the well-known Donnell equations, had been presented by D. H, Van Campen [1] . To date, only a few special cases were reported based on either experimental or analytical techniques. However, these available literatures and publications are so limited that they are not sufficient to be used as a design guide for most of the pipe-nozzle stress analysis. In order to provide a comprehensive database for thermal stresses on pipe-nozzle, the finite element analysis method is used in this thesis based on the assumption that the nozzle thickness is proportional to the pipe thickness by beta ($t_n = \beta\, t_p$). It covered the following studies:

1. The data ranges of the geometrical parameters, beta, β (nozzle mean radius/pipe mean radius) are from 0.1 to 1.0, and gamma, γ (pipe mean radius/pipe thickness) are from 10 to 300.

2. For the accuracy of the results, independent of the boundary conditions, the geometrical parameters, alpha $_p$, α_p (pipe length/pipe mean radius) is at least equal to 8.0, and alpha$_n$, α_n (nozzle length/nozzle mean radius) is at least equal to 4.0.

3. For the optimization study of node point number at the pipe-nozzle juncture, 96 node points are required at the juncture of the pipe-nozzle full model.

4. The resulting thermal stresses on both the pipe and the nozzle around the pipe-nozzle juncture are normalized as thermal stress factors and presented in a series of sixteen plots as function of β and γ. These plots cover the membrane and bending stresses in longitudinal and circumferential directions on both the inside and the outside surfaces of the pipe, as well as the nozzle, at point A and C on X-Z and Y-Z planes, respectively. A typical configuration of the pipe-nozzle is shown in Figure 1.

These local thermal stress may be used in conjunction with local stresses from other external loadings, such as radial load, circumferential moment and longitudinal moment as well as shear stresses induced by shear forces and torsional moment, which had been published by Welding Research Council Bulletin 107 [2].

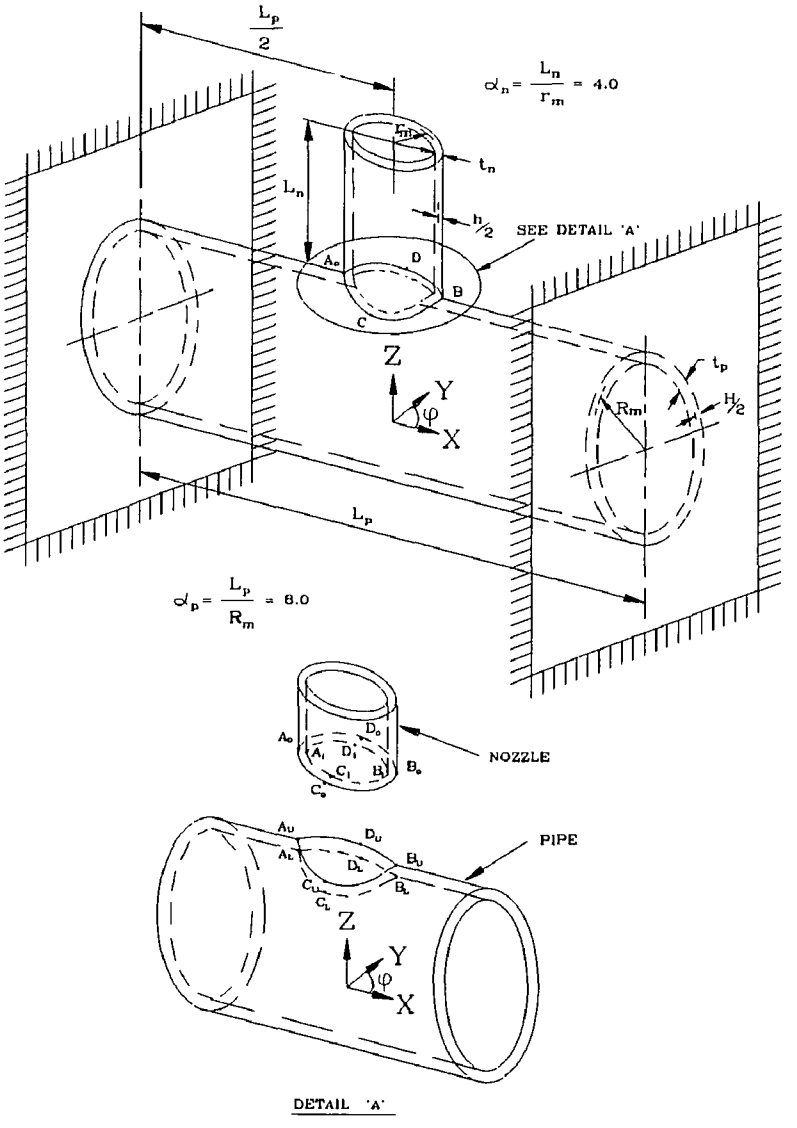

Figure 1 Typical configuration of pipe-nozzle juncture under axisymmetrical temperature distribution

CHAPTER 2

LITERATURE SURVEY

Since the middle of 1960's, some studies on local stresses around pipe-nozzle juncture using theoretical [3][4][5] and experimental [6][7][8][9] analyses due to mechanical and thermal loadings had been published. In 1968, Manschot [10] presented a numerical computing method for thermal stresses in thin-walled, tee-type cylinder. In 1969, Van Campen [1] introduced a solution of the Morley partial differential shell equation and numerical method to calculate the local thermal stress of an equal size tee ($\beta \cong 1$), and Cranch, et. al., [11] had an investigation on thermal stresses of circular pipe attached to a spherical shell and provided some normalized thermal stress factor plots with geometrical parameter beta, β, (attached cylinder pipe mean radius/ spherical shell mean radius) is equal to 0.03 , and gamma , γ, (shell mean radius/shell thickness) is equal to 169.

After the 1970s, the finite element method had been applied by some researchers [12]. Also, the large computer and the Finite Element Analysis, FEA, code had been employed to analyze the thermal stresses around the cylinder-to-cylinder juncture [13]. In the meantime, quite a few of the revised theoretical and experimental [16][17] studies on the same topic had been published. Van Campen, et. al. [14] in 1972 and Fullard [15] in 1973, both presented the local thermal stresses on the intersection of small diameter ratio of nozzle-to-shell with β less than 0.4. In 1977, Cesari [18] developed a 2-D equivalent nozzle-cylinder model to study the local thermal stresses on the juncture of nozzle-to-cylinder. In his case study, a special case with $\beta = 0.12$, and $\gamma = 28.57$

(vessel radius = 191.4 mm, vessel thickness = 6.7 mm and nozzle radius = 24.675 mm, nozzle thickness = 1.35 mm) had been analyzed. Independently also, Gantayst, et.al. [19] in 1977, presented a finite element procedure and the associated programs for the analysis of thin and thick walled tubular tee joint under thermal loading with beta of 0.5, and gamma of 100.

In the similar study field, a conical nozzle on spherical shell had been published by Jayaraman, et. al. [20]. Meanwhile, transient thermal stresses on pipe-nozzle had been presented by either theoretical method [21] or numerical approach [22][23] in 1970s.

In the beginning of the 1980s, Bryson, et. al. [24], Truc, et. al. [25], and Ranjan, et. al [26] respectively, had presented a variety of improved thermal stress analysis methods on the pipe-nozzle. In 1986, Lapoint, et. al. [27], and in 1988, Baldur, et. al. [28], had relative studies on thermal stresses of the intersection area with β = 0.2, 0.4, 0.6, and γ = 5, 15, 25. Respectively, a reinforced nozzle on a cylinder due to thermal loads had been studied with theoretical methods [30][31][32] and a numerical method [33]. Also, some applications of thermal stresses analysis methods on cylinder-nozzle had been presented [29][34][35]. Strel'chenko, et. al. [36][37] had studied the temperature stress in T-shaped intersection cylindrical shell with beta of 0.2 and gamma of 62.5 and 100, by means of finite differential method (FDM).

In 1991, Moini, et. al. [38] discussed the specified boundary displacement method to measure stress concentration due to geometrical discontinuity. Furuhashi, et. al. [39][40] developed a simplified method of stress analysis of nozzle subjected to a thermal loading, which can save costs and time in the calculation of thermal stresses on nozzle-shell connection. Their results was for a special geometry with β of 0.254 and γ of 57.14.

From the above literature survey, it is obvious that normalized thermal stress factor plots with extended range of β and γ values are necessary to facilitate the local thermal stress computations of pipe-nozzle.

The above publications and developments are chronologically tabulated as shown in Figure 2.

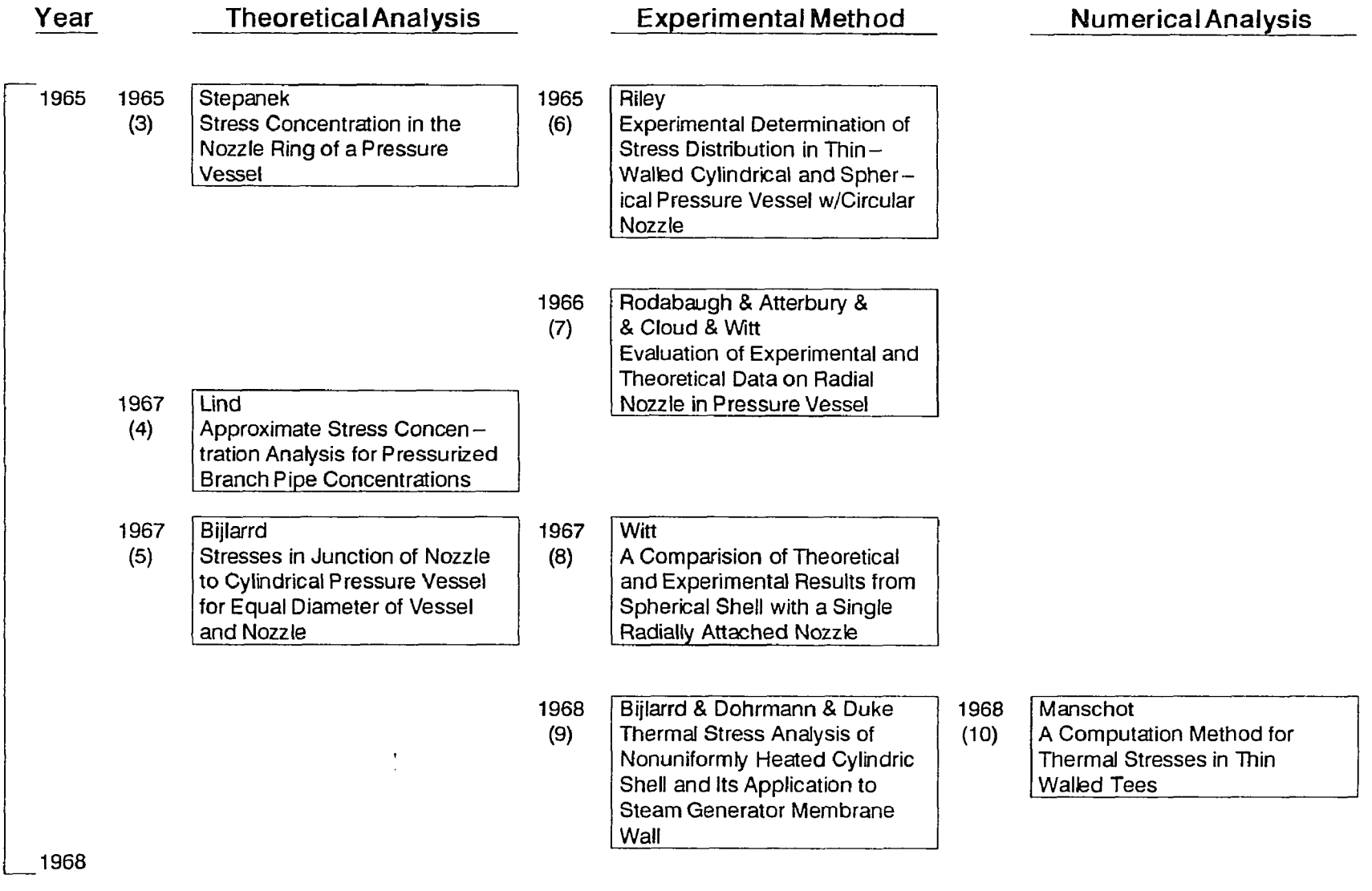

Figure 2 Literature survey table

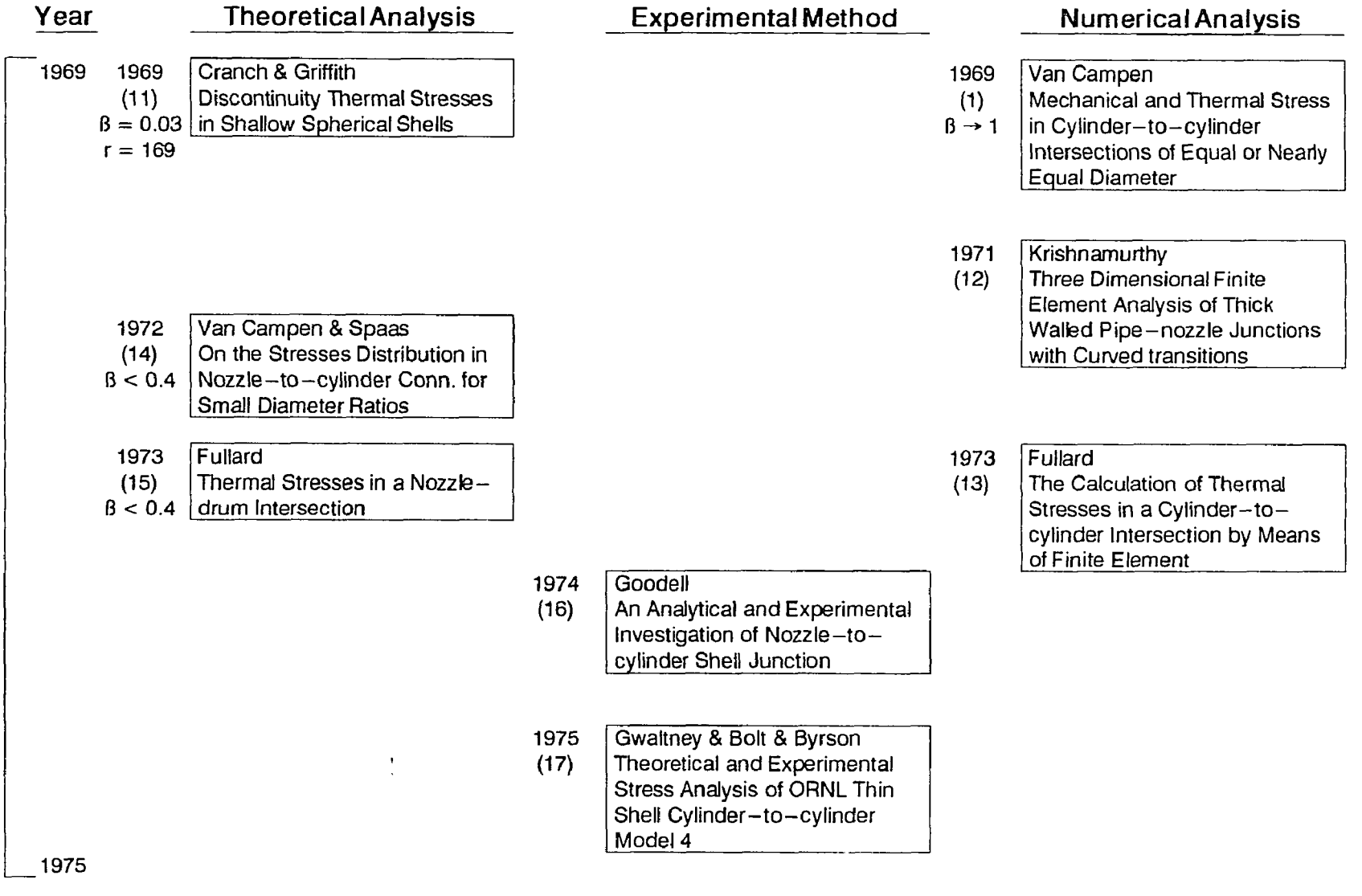

Figure 2 Literature survey table (cont'd)

Year	Theoretical Analysis	Experimental Method	Numerical Analysis
1976			
			1977 (18) ß = 0.13 r = 28.6 — Cesari: Equivalent Nozzle in Thermo-mechanical Problems
			1977 (19) ß = 0.5 r = 100 — Gantayat & Powell: Finite Element Analysis of Thin and Thick Walled Tubular Tee Joints
	1978 (20) — Jayaraman & Rao: Thermal Stresses in a Spherical Shell with a Conical Nozzle		1978 (22) — Brown: Thermal Transient Stress Analysis of Cylinder-to-cylinder Structures by the Finite Element Method
	1978 (21) — Gupta & Rao & Narayanan & Gangadharan: Theroelastic Analysis of Non-axisymmetrical Heated Thick Cylindrical Shell		
			1979 (23) — Brown: On the Mechanical and Thermal Transient Analysis of Cylinder-to-cylinder Vessels by a Finite Element Method
	1981 (24) — Bryson & Johnson & Bass: Stresses in Reinforced Nozzle-cylinder Attachments – a Parametrical Study	1981 (25) — Truc & Bazerbui: Experimental Thermal Stresses at Attachment/Cylinder Intersections	
			1982 (26) — Ranjan & Brooks & Huet: An Improved Method of Stress Analysis for Cylinder-to-cylinder Intersection
1982			

Figure 2 Literature survey table (cont'd)

Year	Theoretical Analysis	Experimental Method	Numerical Analysis
1983			
1986 (29)	Stikvoort Piping Reactions on Pressure Vessel Nozzles		
1987 (27) ß = 0.2, 0.4, 0.6 r = 5, 15, 25			Lapointe & Laberge & Baldur Plate–cylinder Intersections Subjected to Thermal Loads
1988 (30)	Sundaravadiveler & Hariharan & Ganapath Formula for Variation of Stress Concentration around Inter–section in Tubular Jount		
1988 (33)			Kuo & Hsu Stress Analysis of Rienforced Nozzle–Cylindrical Shell Intersection under Internal Pressure or Nozzle Radial Thermal Expansion
1988 (31)	Brooks Shell Solution for Reinforced Cylinder to Sphere Intersection		
1988 (28) ß = 0.2, 0.4, 0.6 r = 5, 15, 25			Baldur & Laberge Numerical Design Method for Thermally Loaded Plate–cylinder Intersections
1988 (34)	Savchenko & Nakonechvyi Stress Concentration around Opening in Conical Shells		
1989 (35)			Lam & Trauner Finite Element Analysis of a Desuperheater Vessel Steam Inlet Nozzle Subjected to Thermal Loads
1989 (32)	Kumar & Singh Analysis of Pad–reinforced Nozzle in Pressure Vessel Head		
1989			

Figure 2 Literature survey table (cont'd)

Year	Theoretical Analysis	Experimental Method	Numerical Analysis
1989			
1989 (36) ß = 0.2 r = 62.5, 100	Strel'chenko & Strel'chenko & Sheptun Stress State of a Variable Thickness Cylindrical Shell with a Constant Thickness Branch Pipe		
			1989 (39) ß = 0.254 r = 57.14 Watashi & Furuhashi & Imasu A Simplified Method for Stress Estimation of Nozzles
1991 (38)	Moini & Mitchell Stress Analysis of Thick–Walled Pressure Vessel Nozzle Junction		
			1991 (40) ß = 0.254 r = 57.14 Furuhashi & Watashi A Simplified Method of Stress Calculation of Nozzle Subjected to Thermal Transient
1991 (37) ß = 0.2 r = 62.5, 100	Strel'chenko & Strel'chenko & Sheptun Temperature Stress in T–shaped Intersecting Cylindrical Shells of Constant and Variable Thickness		
1994			

Figure 2 Literature survey table (cont'd)

CHAPTER 3

BASIC THEORY

The purpose of this study is to investigate the axisymmetrical thermal stresses around the juncture of a pipe-nozzle. Figure 1 shows a configuration of this model.

3.1 Derivation of Equations for Deflections due to the Thermal Loading

Consider the thermoelastic state of circular pipe, intersecting with a nozzle at right angle, under the influence of a steady state temperature gradient. The thickness of the pipe may vary according to any law but shall be symmetrical relative to the median surfaces, and the ratio of nozzle thickness / pipe thickness shall be unity. In deriving the basic relations of thin-shell theory, the Kirchhoff-Love hypotheses are used. The material from which the shells are made is assumed to be homogeneous and isotropic. The thermal loading is assumed to be such that geometrically linear thin-shell theory may be used. In addition, it is assumed that the stress in the shells do not exceed the elastic limit of the material. In view of the linearity of this study, the overall stress at the pipe-nozzle juncture is expressed as the sum of the stress states arising under the action of a steady temperature field. When a steady axisymmetric temperature field acts on the piping -nozzle, the forces and the displacement of the basic state are determined by solving the thermoelastic problem [36][43] for each of the shells.

The resolving equations of the thermoelastic problem for the pipe shell and nozzle shell with a linear temperature distribution over the thickness shall be

$$T_n(x) = T_{nm}(x) + \frac{2h}{t_n(x)} T_{nd}(x) \qquad (1)$$

$$T_p(z) = T_{pm}(z) + \frac{2H}{t_p(z)} T_{pd}(z) \qquad (2)$$

where $T_m = (T_o + T_i) / 2$ is the mean temperature of a normal element of the shell; $T_d = (T_o - T_i) / 2$ is the normal temperature difference; T_o and T_i are the temperatures at the external ($h = t_n /2$, $H = t_p /2$) and internal ($h = -t_n /2$, $H = - t_p /2$) shell surface. Refer to Figure 1. Take the displacement forms

$$\frac{\partial^4 w_t}{\partial z^4} + \frac{2}{D_{n11}} \frac{\partial D_{n11}}{\partial z} \frac{\partial^3 w_t}{\partial z^3} + \frac{1}{D_{n11}} \frac{\partial^2 D_{n11}}{\partial z^2} \frac{\partial^2 w_t}{\partial z^2} + \frac{R_n^2 (C_{n11} C_{n22} - C_{n12})}{D_{n11} C_{n11}} w_t =$$

$$\alpha_t \frac{R_n^3 (C_{n11} C_{n22} - C_{n12})}{D_{n11} C_{n11}} T_{nm} + \frac{2\alpha_t R_n^3}{D_{n11} t_n^3} \{ (\frac{\partial^2 D_{n11}}{\partial z^2} + \frac{\partial^2 D_{n12}}{\partial z^2}) t_n^2 -$$

$$2(\frac{\partial D_{n11}}{\partial z} + \frac{\partial D_{n12}}{\partial z}) \frac{\partial t_n}{\partial z} t_n + (D_{n11} + D_{n12}) [2(\frac{\partial t_n}{\partial z})^2 - \frac{\partial^2 t_n}{\partial z^2} t_n] \} T_{nd} \qquad (3)$$

$$\frac{\partial^4 W_t}{\partial y^4} + \frac{R_p^2 (C_{p11} C_{p22} - C_{p12})}{D_{p11} C_{p11}} W_t = \alpha_t \frac{R_p^3 (C_{p11} C_{p22} - C_{p12})}{D_{p11} C_{p11}} T_{pm} \qquad (4)$$

where α_T is the coefficient of linear temperature expansion; also

$$D_{n11} = \frac{E t_n^3(x)}{12(1-\mu^2)} ; \qquad D_{p11} = \frac{E t_p^3(z)}{12(1-\mu^2)} \qquad (5a)$$

$$C_{n11} = C_{n22} = \frac{E t_n(x)}{1-\mu^2} ; \qquad C_{p11} = C_{p22} = \frac{E t_p(z)}{1-\mu^2} \qquad (5b)$$

$$C_{n12} = \frac{\mu E t_n(x)}{1-\mu^2}\ ; \qquad C_{p12} = \frac{\mu E t_p(z)}{1-\mu^2} \tag{5c}$$

$$D_{n12} = \frac{\mu E t_n(x)}{12(1-\mu^2)}\ ; \qquad D_{p12} = \frac{\mu E t_p(z)}{12(1-\mu^2)} \tag{5d}$$

At the ends of the shells, the transverse forces and moments are zero.

The solution of Eqs. (3) and (4) relative to w_t and W_t allows the components of the basic state of the shells under the action of the axisymmetric temperature to be determined from the formula

$$u_t = \alpha_t R_n (T_{nm})(z - z_0)\ ; \qquad U_t = \alpha_t R_p T_{pm} \tag{6}$$

$$m_{xt} = \frac{D_{n11}}{R_n^2}\frac{\partial^2 w_t}{\partial z^2} - \frac{2\alpha_t (D_{n11}+D_{n12})}{t_n(z)} T_{nd}\ ;$$

$$m_{yt} = \frac{D_{n12}}{R_n^2}\frac{\partial^2 w_t}{\partial z^2} - \frac{2\alpha_t (D_{n12}+D_{n22})}{t_n(z)} T_{nd} \tag{7a}$$

$$M_{Xt} = \frac{D_{p11}}{R_p^2}\frac{\partial^2 W_t}{\partial x^2} - \frac{2\alpha_t (D_{p11}+D_{p12})}{t_p} T_{pd}\ ;$$

$$M_{Yt} = \frac{D_{p12}}{R_p^2}\frac{\partial^2 W_t}{\partial x^2} - \frac{2\alpha_t (D_{p12}+D_{p22})}{t_p} T_{pd} \tag{7b}$$

Finding the forces and moments entails determining the functions of T_p and T_d which are found from the resolving heat-conduction equations for the pipe,

$$\frac{\partial^2 T_{pm}}{\partial y^2} + \frac{1}{y}\frac{\partial T_{pm}}{\partial y} - \frac{R_p}{t_p}(\kappa e + \kappa_i) T_{pm} - \frac{R_p^2}{t_p}(\kappa e - \kappa_i - \frac{2}{R_p}) T_{pd}$$

$$= -\frac{R_p^2}{t_p}(\kappa e T_{pe}^{\infty} + \kappa_i T_{pi}^{\infty}) \tag{8a}$$

$$\frac{\partial^2 T_{pd}}{\partial y^2} + \frac{1}{y}\frac{\partial T_{pd}}{\partial y} - [\frac{12R_p^2}{t_p^2} + \frac{3R_p^2}{t_p}(\kappa e + \kappa_i)]T_{pd} - \frac{3R_p^2}{t_p}(\kappa e - \kappa_i)Tpm$$

$$= -\frac{3R_p^2}{t_p}(\kappa e T_{pe}^{\infty} - \kappa_i T_{pi}^{\infty}) \qquad (8b)$$

and for the nozzle,

$$\frac{\partial^2 T_{nd}}{\partial z^2} + \frac{\partial t_n}{\partial z}\frac{1}{t_n}\frac{\partial T_{nd}}{\partial z} - [(\frac{\partial t_n}{\partial z})^2\frac{1}{t_n^2} + \frac{\partial t_n}{\partial z}\frac{1}{t_n} + \frac{12R_n^2}{t_n^2} + \frac{3R_n^2}{t_n}(\kappa e + \kappa_i)]T_{nd}$$

$$-\frac{3R_n^2}{t_n}(\kappa e - \kappa_i)Tnm = -\frac{3R_n^2}{t_n}(\kappa e T_{ne}^{\infty} - \kappa_i T_{ni}^{\infty}) \qquad (9a)$$

$$\frac{\partial^2 T_{nm}}{\partial z^2} + \frac{\partial t_n}{\partial z}\frac{1}{t_n}\frac{\partial T_{nm}}{\partial z} - \frac{R_n^2}{t_n}(\kappa e + \kappa_i)Tnm - \frac{R_n^2}{t_n}(\kappa e - \kappa_i - \frac{2}{R_n})T_{nd}$$

$$= -\frac{R_n^2}{t_n}(\kappa e T_{ne}^{\infty} + \kappa_i T_{ni}^{\infty}) \qquad (9b)$$

where T_e^{∞} and T_i^{∞} are the temperatures of the media in which the pipe/nozzle surfaces h = + t_n / 2 , h = - t_n / 2 , and H = + t_p / 2 , H = - t_p / 2 are immersed ; κ_e and κ_i are the relative heat transfer coefficients at the shell surfaces.

At the ends of the pipe and nozzle, it is assumed that the heat-conduction equations for the pipe,

$$y\frac{\partial^2 T_{pm}}{\partial y^2} + \frac{\partial T_{pm}}{\partial y} + \frac{2R_p^2 y}{R_p t_p}T_{pd} = 0 \ ;$$

$$\frac{2y}{t_p}\frac{\partial^2 T_{pd}}{\partial y^2} + \frac{2}{t_p}\frac{\partial T_{pd}}{\partial y} = 0 \qquad (10)$$

and for the nozzle,

$$\frac{\partial^2 T_{nm}}{\partial z^2} + \frac{2R_n}{t_n} T_{nd} = 0 \ ;$$

$$\frac{2}{t_n}\frac{\partial^2 T_{nd}}{\partial z^2} - \frac{4}{t_n}\frac{\partial t_n}{\partial z}\frac{\partial T_{nd}}{\partial z} - \frac{2}{t_n^4}[\frac{\partial^2 t_n}{\partial z^2} t_n^2 - 2t_n(\frac{\partial t_n}{\partial z})^2] = 0 \qquad (11)$$

are satisfied.

The components characterizing the thermal stresses of nozzle are found using the homogeneous system of equilibrium equations

$$\frac{\partial n_x}{\partial z} + \frac{\partial n_{xy}}{\partial \varphi} = 0 \ ; \qquad \frac{\partial n_y}{\partial \varphi} + \frac{\partial n_{xy}}{\partial z} = 0 \ ;$$

$$ny + \frac{\partial q_x}{\partial z} + \frac{\partial q_y}{\partial \varphi} = 0 \qquad (12a)$$

$$\frac{\partial m_x}{\partial z} + \frac{\partial m_{xy}}{\partial \varphi} - q_x R_n = 0 \ ; \qquad \frac{\partial m_y}{\partial \varphi} + \frac{\partial m_{xy}}{\partial z} - q_y R_n = 0 \qquad (12b)$$

for the pipe

$$y\frac{\partial N_y}{\partial y} + \frac{\partial N_{y\varphi}}{\partial \varphi} + Ny - N_\varphi = 0 \ ; \qquad y\frac{\partial N_{y\varphi}}{\partial y} + \frac{\partial N_\varphi}{\partial \varphi} + 2Ny_\varphi = 0 \qquad (13a)$$

$$y\frac{\partial M_y}{\partial y} + \frac{\partial M_{y\varphi}}{\partial \varphi} + My - M_\varphi - yRpQy = 0 \ ;$$

$$y\frac{\partial M_{y\varphi}}{\partial y} + \frac{\partial M_\varphi}{\partial \varphi} + 2My_\varphi - yRpQ_\varphi = 0 \qquad (13b)$$

The elasticity law for the pipe and nozzle could be written in the form

$$nx = C_{n11}\zeta_{n1} + C_{n12}\zeta_{n2} \ ; \qquad ny = C_{n22}\zeta_{n2} + C_{n12}\zeta_{n1}$$

$$nxy = C_{n33}\xi_{n1}\ ; \qquad mx = -(D_{n11}\varpi_{n1} + D_{n12}\varpi_{n2})$$

$$my = -(D_{n22}\varpi_{n2} + D_{n12}\varpi_{n1})\ ; \quad mxy = -2D_{n33}\tau_{n1} \tag{14a}$$

$$Ny = C_{p11}\zeta_{p1} + C_{p12}\zeta_{p2}\ ; \qquad N\varphi = C_{p22}\zeta_{p2} + C_{p12}\zeta_{p1}$$

$$Ny\varphi = C_{p33}\zeta_{p1}\ ; \qquad My = -(D_{p11}\varpi_{p1} + D_{p12}\varpi_{p2})$$

$$M\varphi = -(D_{p22}\varpi_{p2} + C_{p12}\varpi_{p1})\ ; \quad My\varphi = -2D_{p33}\tau_{p1} \tag{14b}$$

where

$$C_{n11} = C_{n22} = \frac{Et_n(z)}{1-\mu^2}\ ; \qquad C_{n12} = \frac{\mu Et_n(z)}{1-\mu^2}\ ; \qquad C_{n33} = \frac{Et_n(z)}{2(1+\mu)} \tag{15a}$$

$$D_{n11} = D_{n22} = \frac{Et_n^3(z)}{12(1-\mu^2)}\ ; \quad D_{n12} = \frac{\mu Et_n^3(z)}{12(1-\mu^2)}\ ; \quad D_{n33} = \frac{Et_n^3(z)}{24(1+\mu)} \tag{15b}$$

$$C_{p11} = C_{p22} = \frac{Et_p}{1-\mu^2}\ ; \qquad C_{p12} = \frac{\mu Et_p}{1-\mu^2}\ ; \qquad C_{p33} = \frac{Et_p}{2(1+\mu)} \tag{15c}$$

$$D_{p11} = D_{p22} = \frac{Et_p^3}{12(1-\mu^2)}\ ; \quad D_{p12} = \frac{\mu Et_p^3}{12(1-\mu^2)}\ ; \quad D_{p33} = \frac{Et_p^3}{24(1+\mu)} \tag{15d}$$

The geometric equations of deformation and change in curvature for the pipe and nozzle are as followings

$$\zeta_{n1} = \frac{1}{R_n}\frac{\partial u}{\partial z}\ ; \qquad \zeta_{n2} = \frac{1}{R_n}\left(\frac{\partial v}{\partial \varphi} + w\right)\ ; \quad \xi_{n1} = \frac{1}{R_n}\left(\frac{\partial v}{\partial z} + \frac{\partial u}{\partial \varphi}\right)$$

$$\varpi_{n1} = -\frac{1}{R_n^2}\frac{\partial^2 w}{\partial z^2}\ ; \qquad \varpi_{n2} = -\frac{1}{R_n^2}\frac{\partial^2 w}{\partial \varphi^2}\ ; \qquad \tau_{n1} = -\frac{1}{R_n^2}\frac{\partial^2 w}{\partial z \partial \varphi} \tag{16a}$$

$$\zeta_{p1} = \frac{1}{R_n}\frac{\partial U}{\partial y} + \frac{\sin^2\varphi}{R_p}W \; ; \qquad \zeta_{p2} = \frac{1}{yR_n}\frac{\partial V}{\partial \varphi} + \frac{1}{yR_n}U + \frac{\cos^2\varphi}{R_p}W \; ;$$

$$\xi_{p1} = \frac{1}{R_n}\frac{\partial V}{\partial y} + \frac{1}{yR_n}\frac{\partial U}{\partial \varphi} - \frac{1}{yRn}V + \frac{\sin^2\varphi}{Rp}W \; ;$$

$$\varpi_{p1} = -\frac{1}{R_p^2}\frac{\partial^2 W}{\partial y^2} \; ; \qquad \varpi_{p2} = -\frac{1}{y^2R_p^2}\frac{\partial^2 W}{\partial \varphi^2} - \frac{1}{yR_p^2}\frac{\partial W}{\partial \varphi} \; ;$$

$$\tau_{p1} = \frac{1}{y^2R_R^2}\frac{\partial W}{\partial y} - \frac{1}{yR_p^2}\frac{\partial W}{\partial y \partial \varphi} \; ; \qquad (16b)$$

Eliminating the transverse forces q_x ,q_y, Q_Y , and Q_φ in Eqs. (12a), (12b), (13a), and (13b) and substituting the forces and moments from Eqs. (14a), (14b) and (15a) to (15b), resolving systems of partial differential equations with variable coefficients for pipe and nozzle in terms of the displacements u, v, w, and U, V, W and their derivatives are obtained.

The geometry of the piping-nozzle structure and the form of loading considered permit variable separation in the resolving equations and the matching boundary conditions. Satisfying the symmetry conditions of the stress-strain state relative to the longitudinal symmetric plane, including the shell axes, and the transverse plane, perpendicular to the longitudinal plane which contains the axis of the nozzle, the solution of the problem is sought in series from

$$u = \sum u_n(z)\sin n\varphi \; ; \qquad v = \sum v_n(z)\sin n\varphi \; ;$$

$$w = \sum w_n(z)\cos n\varphi \; ; \qquad U = \sum U_n(y)\cos n\varphi \; ;$$

$$V = \sum V_n(y)\sin n\varphi \;; \qquad W = \sum W_n(y)\cos n\varphi \tag{17}$$

where u, v, and w are the displacements on the nozzle and U, V, and W, are the displacement on the pipe. The displacements in X, Y(φ), and Z direction are shown in Figure 3.

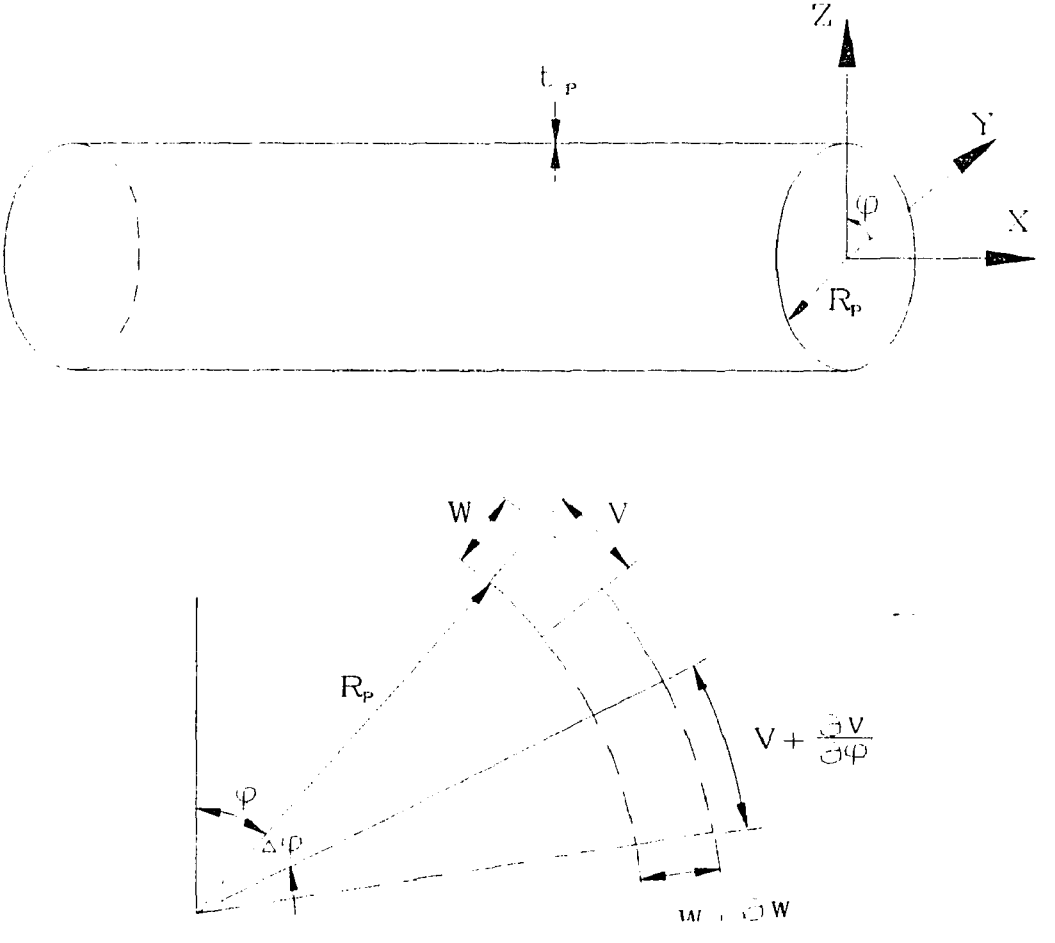

Figure 3 Cylindrical coordinate applied to a cylindrical pipe with displacements U, V, and W in X, φ, and Z direction respectively

After substituting Eqs. (17) into the resolving equations for the pipe and nozzle, the method of variable separation is undertaken. As a result, two new systems of differential equations with variable coefficients are obtained. Variable separation is also undertaken in the matching boundary condition of the pipe and nozzle.

3.2 Thermal Stress Factors

In order to present different configurations of the pipe-nozzle model, all the thermal stresses are represented in dimensionless form as thermal stress factors. For thin shells, the assumption of a linear temperature gradient through the thickness is a good approximation so that the temperature distribution will become

$$T = T_{avg} + \frac{\Delta T}{t} dt \tag{18}$$

where T_{avg} is the average wall temperature and ΔT is the difference between the outside and the inside wall temperature; t is the thickness of pipe or nozzle and there is a point at distance dt from the median surface in th meridional direction. From Timoshenko's Theory of Elasticity [43] , the thermal membrane force, N_{th} and thermal moment, M_{th} are

$$N_{th} = \frac{Et\alpha_T T_{avg}}{(1-\mu)} \quad (19)\,; \qquad M_{th} = -\frac{Et^2\alpha_T \Delta T}{12(1-\mu)} \tag{20}$$

therefore it can be derivative from the thermal stress as

$$\sigma_T = K_T \frac{E\alpha_T \Delta T}{2(1-\mu)} \tag{21}$$

where K_T is defined as the thermal stress factor which can be expressed as

$$K_T = \frac{2(1-\mu)}{E\alpha_T \Delta T} \bullet \sigma_T \qquad (22)$$

By the finite element method, all the thermal stress factors on the longitudinal and circumferential directions and sign notations for thermal stresses on the pipe of pipe-nozzle are added into a summarized Table 1 (Ref. Fig. 4) which had been presented by WRC 107 [2]. Data presented in various plots are shown in the Appendix A from Figure 1T to 8T for the longitudinal and circumferential thermal stress factors on the pipe, and Figure from 9T to 16T for the longitudinal and circumferential thermal stress factors on the nozzle. Numerical examples of thermal stresses on the pipe and the nozzle are given in Chapter 6.

Table 1 Modified stress computation table of WRC 107 including local thermal stresses

Form Fig.	Read Curves for Stress Factor	Compute Absolute Values of Stress & Enter Result (psi)	A_U	A_L	B_U	B_L	C_U	C_L	D_U	D_L
3C[1]	$\frac{N_\varphi}{P/R_m}$	$K_n[\frac{N_\varphi}{P/R_m}]\frac{P}{R_mT}$ =	-	-	-	-	-	-	-	-
1C[1]	$\frac{M_\varphi}{P}$	$K_b[\frac{M_\varphi}{P}]\frac{6P}{T^2}$ =	-	+	-	+	-	+	-	+
3A[1]	$\frac{N_\varphi}{M_C/(R_m^2\beta)}$	$K_n[\frac{N_\varphi}{M_C/(R_m^2\beta)}]\frac{M_C}{R_m^2\beta T}$ =					-	-	+	+
1A[1]	$\frac{M_\varphi}{M_C/(R_m\beta)}$	$K_b[\frac{M_\varphi}{M_C/(R_m\beta)}]\frac{6M_C}{R_m\beta T^2}$ =					-	+	+	-
3B[1]	$\frac{N_\varphi}{M_L/(R_m^2\beta)}$	$K_n[\frac{N_\varphi}{M_L/(R_m^2\beta)}]\frac{M_L}{R_m^2\beta T}$ =	-	-	+	+				
1B or 1B-1[1]	$\frac{M_\varphi}{M_L/(R_m\beta)}$	$K_b[\frac{M_\varphi}{M_L/(R_m\beta)}]\frac{6M_L}{R_m\beta T^2}$ =	-	+	+	-				
5T-8T Circumferential	$\frac{2(1-\mu)}{E\alpha_T\Delta T}$	$[\frac{E\alpha_T\Delta T}{2(1-\mu)}]\frac{2(1-\mu)}{E\alpha_T\Delta T}$ =	+	-	+	-	+	-	+	-
Add algebraically summation of circumferential stresses, σ_φ =										
4C[1]	$\frac{N_X}{P/R_m}$	$K_a[\frac{N_X}{P/R_m}]\frac{P}{R_mT}$ =	-	-	-	-	-	-	-	-
2C[1]	$\frac{M_X}{P}$	$K_b[\frac{M_X}{P}]\frac{6P}{T^2}$ =	-	+	-	+	-	+	-	+
4A[1]	$\frac{N_X}{M_C/(R_m^2\beta)}$	$K_a[\frac{N_X}{M_C/(R_m^2\beta)}]\frac{M_C}{R_m^2\beta T}$ =					-	-	+	+
2A[1]	$\frac{M_X}{M_C/(R_m\beta)}$	$K_b[\frac{M_X}{M_C/(R_m\beta)}]\frac{6M_C}{R_m\beta T^2}$ =					-	+	+	-
4B[1]	$\frac{N_X}{M_L/(R_m^2\beta)}$	$K_a[\frac{N_X}{M_L/(R_m^2\beta)}]\frac{M_L}{R_m^2\beta T}$ =	-	-	+	+				
2B or 2B-1[1]	$\frac{M_X}{M_L/(R_m\beta)}$	$K_b[\frac{M_X}{M_L/(R_m\beta)}]\frac{6M_L}{R_m\beta T^2}$ =	-	+	+	-				
1T-4T Longitudinal	$\frac{2(1-\mu)}{E\alpha_T\Delta T}$	$[\frac{E\alpha_T\Delta T}{2(1-\mu)}]\frac{2(1-\mu)}{E\alpha_T\Delta T}$ =	+	-	+	-	+	-	+	-
Add algebraically summation of longitudinal stresses, σ_X =										
Shear stress due to the Torsion, M_T	$\tau_{\varphi x} = \tau_{x\varphi} = \frac{M_T}{2\pi r_m^2 T}$		+	+	+	+	-	-	-	-
Shear stress due to the Load, V_C	$\tau_{x\varphi} = \frac{V_C}{\pi r_m T}$		+	+	-	-				
Shear stress due to the load, V_L	$\tau_{x\varphi} = \frac{V_L}{\pi r_m T}$						+	+	-	-
Add Algebraically for Summation of Shear Stresses, $\tau_{\varphi x}$ =										
COMBINED STRESS INTENSITY, S										
1) When σ_φ and σ_x have like signs	$\sigma_1 = \frac{1}{2}[\sigma\varphi + \sigma_x] + \frac{1}{2}\sqrt{(\sigma\varphi - \sigma_x)^2 + 4\tau^2}$ =									
2) When σ_φ and σ_x have unlike signs	$\sigma_2 = \frac{1}{2}[\sigma\varphi + \sigma_x] - \frac{1}{2}\sqrt{(\sigma\varphi - \sigma_x)^2 + 4\tau^2}$ =									
3) Stress intensity at each point	$S = Max(\sigma_1, \sigma_2, \lvert\sigma_1 - \sigma_2\rvert)$ =									
4) Maximum stress intensity of the pipe-nozzle										

Note 1 : refer to figures in WRC 107 [2]

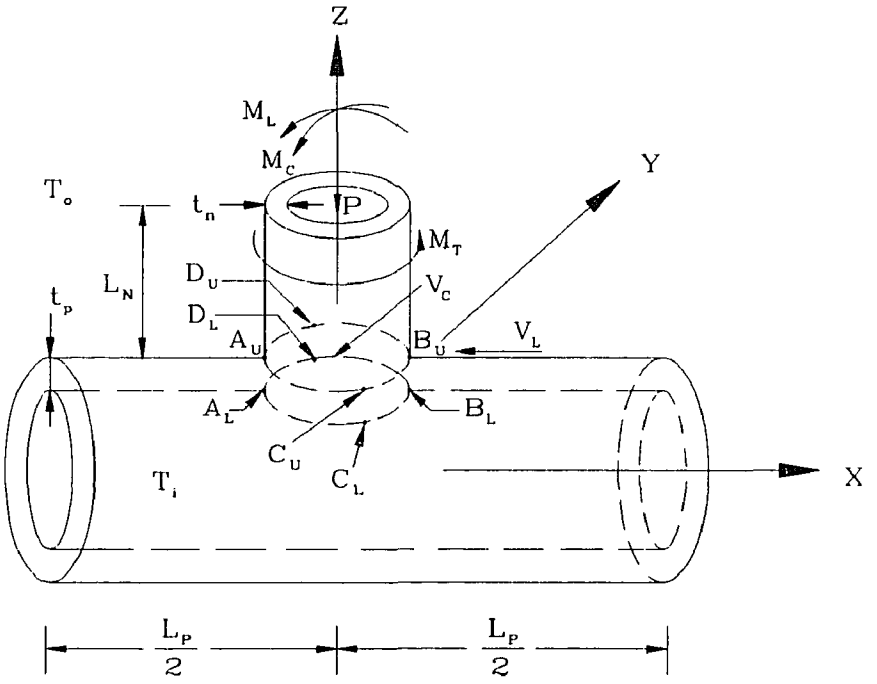

P = Radial Load, lb.
V_C = Circumferential Shear, lb.
V_L = Longitudinal Shear, lb.
T_o = Outside Temperature, °F
T_i = Inside Temperature, °F
M_C = Circumferential Moment, lb.-in.
M_L = Longitudinal Moment, lb.-in.
M_T = Torsional Moment, lb.-in.
M_{th} = Thermal Moment, lb.-in.

Figure 4 Different loadings applied on the juncture of piping-nozzle (ref. to Table-1, computation and sign notation sheet for local stresses of piping-nozzle)

CHAPTER 5

FINITE ELEMENT MODEL

4.1 General

Because there is no suitable mathematical model and exact solution available in simulating the real pipe-nozzle geometry, a finite element analysis (FEA) has been utilized in this thesis. It is understood that the finite element analysis method with computer simulation has provided an increasingly important role in engineering design and analysis. It also performs speedy and reliable calculations and develops a comprehensive, accurate, and efficient procedure for local thermal stress analysis at the juncture of pipe-nozzle.

However, the varying sizes of the pipe-nozzle at the juncture, cause difficulties in obtaining accurate and economical solutions by the finite element method. Therefore, it is extremely important to develop the proper number of nodes and generate sufficient meshes to provide a efficient finite element model.

In this thesis, ten full size finite element models, each with a specific beta value, were developed. Each model with approximately 5000 node points and 3000 elements, were generated by the ALGOR finite element program with "Superdraw" computer code. [41][42]. All the computations were performed on a 486/DX-66 personal computer with 8 Mega RAM and 300 Mega Bytes Harddrive memory. It took about 10,000 seconds of CUP running time for each computation.

4.2 Assumption

For the analysis, the following assumptions were applied:

1. The material is assumed to be homogeneous and isotropic, and obeys Hook's law. The resulting stresses are within the proportional limit of the material.

2. The influences of self-weight are neglected.

3. The internal pressure is the same as ambient pressure.

4. There are no transitions, fillets, or reinforcing pad at the junction.

5. The steady state temperature distribution is linear and the inside temperature is higher than the outside temperature.

4.3 Asymptotic Studies

For optimum accuracy and convergence within the framework of the program, the finite element model of quadrilateral thin shell is adopted. Two important asymptotic studies were introduced:

4.3.1 Asymptotic Study of Node Points at Juncture of Pipe-nozzle

Figures B1 to B16 in Appendix B showed the convergence of various thermal stresses at point A and C (Figure 1). As the number of node points on the pipe-nozzle juncture model increased to 96, all the thermal stresses converged asymptotically. In this case, the density of mesh on the juncture of pipe-nozzle satisfied the asymptotic requirement to avoid any influence of the mesh element to the thermal stress values.

4.3.2 Asymptotic Study of the α_p and α_n

As for the influence of boundary parameters, α_p (pipe length / pipe mean radius) and α_n (nozzle length / nozzle mean radius), to the solution of various thermal stresses, Figures C1 - C16 in Appendix C showed the percentage of improvement with larger α_p to the previous α_p and Figures C17-C32 showed the percentage of improvement with larger α_n to the previous α_n. It is evident that $\alpha_p = 8$ and $\alpha_n = 4$ are the optimum quantities that boundary conditions would not have any significal effect on the outcome of the thermal stresses at the pipe-nozzle juncture.

4.4 Normalization studies

Normalization studies are made to verify the validity of using geometrical parameters, beta, β (nozzle mean radius / pipe mean Radius) and gamma, γ (pipe mean radius / pipe thickness) to express the local thermal stresses . There are four different cases discussed as followings and numerical data are listed in Appendix D.

4.4.1 Case I, II, III

Case I assumed that $\alpha_p = 8$, $\alpha_n = 4$, $\beta = 0.6$, and $\gamma = 50$. By using two distinct geometries, both having the same geometric parameters , i.e. α, β, and γ , and δT, Table D-1 to D-3 in Appendix D showed that both models have identical local thermal stress results when model #2 is twice the size of the model #1. This verified the validity of using α_p , α_n , β, and γ as geometrical parameters to express the local thermal stresses.

Case II had model #3 and #4 with $\alpha_p = 8$, $\alpha_n = 4$, $\beta = 0.3$, and $\gamma = 100$, the local

thermal stresses are listed in Table D-4 to D-6, respectively.

Case III had model #5 and #6 with $\alpha_p = 8$, $\alpha_n = 4$, $\beta = 0.9$, and $\gamma = 20$, the local thermal stresses were listed in Table D-7 to D-9 respectively.

Again, from Table D-4, D-5, D-6 and D-7, D-8, D-9, the geometric parameters of α_p, α_n, β, and γ were valid.

4.4.2 Case IV

Case IV had two models (#7 & #8) which showed that the normalization of thermal stresses with stress factors $\frac{2\times\sigma\times(1-\mu)}{E\times\alpha_t\times\Delta T}$ are valid when the temperature for each model was assigned 400 °F and 900 °F, respectively. Table D-10 to D-12 tabulates the local thermal stresses and stress factors.

CHAPTER 5

COMPARISON OF DATA

5.1 General

For the thermal loading, the thermal stress factors induced by the steady state thermal gradient are compared with the related literatures cited in Chapter 2. Basically, there is no sufficient numerical data that can be used for comparison purposes.

5.2 Comparison of Thermal Stress Factors

There are two cases being discussed as followings:

5.2.1 Case 1

F. Cesari [18], presented a model with a pipe radius = 191.4 mm, pipe thickness = 6.7 mm and nozzle radius = 24.675 mm, nozzle thickness =1.350 mm, where the value of beta, β is equal to 0.129 as well as gamma, γ is equal to 28.57. The structure was subdivided into 96 elements with 66 node points and there were only 16 node points at the juncture of the pipe-nozzle. The temperature difference between internal and external pipe-nozzle was 25 ° C. The Young's Modulus, the coefficient of thermal expansion and the Poisson's ration were given as 1.7×10^5 N/mm^2 , 1.85×10^{-5} mm/mm °C , and 0.3, respectively. The maximum thermal stress found at node point C (Figure 1) was 406 N/mm^2 . In this manner, the thermal stress factor, K_T , at node point C can be calculated as the following :

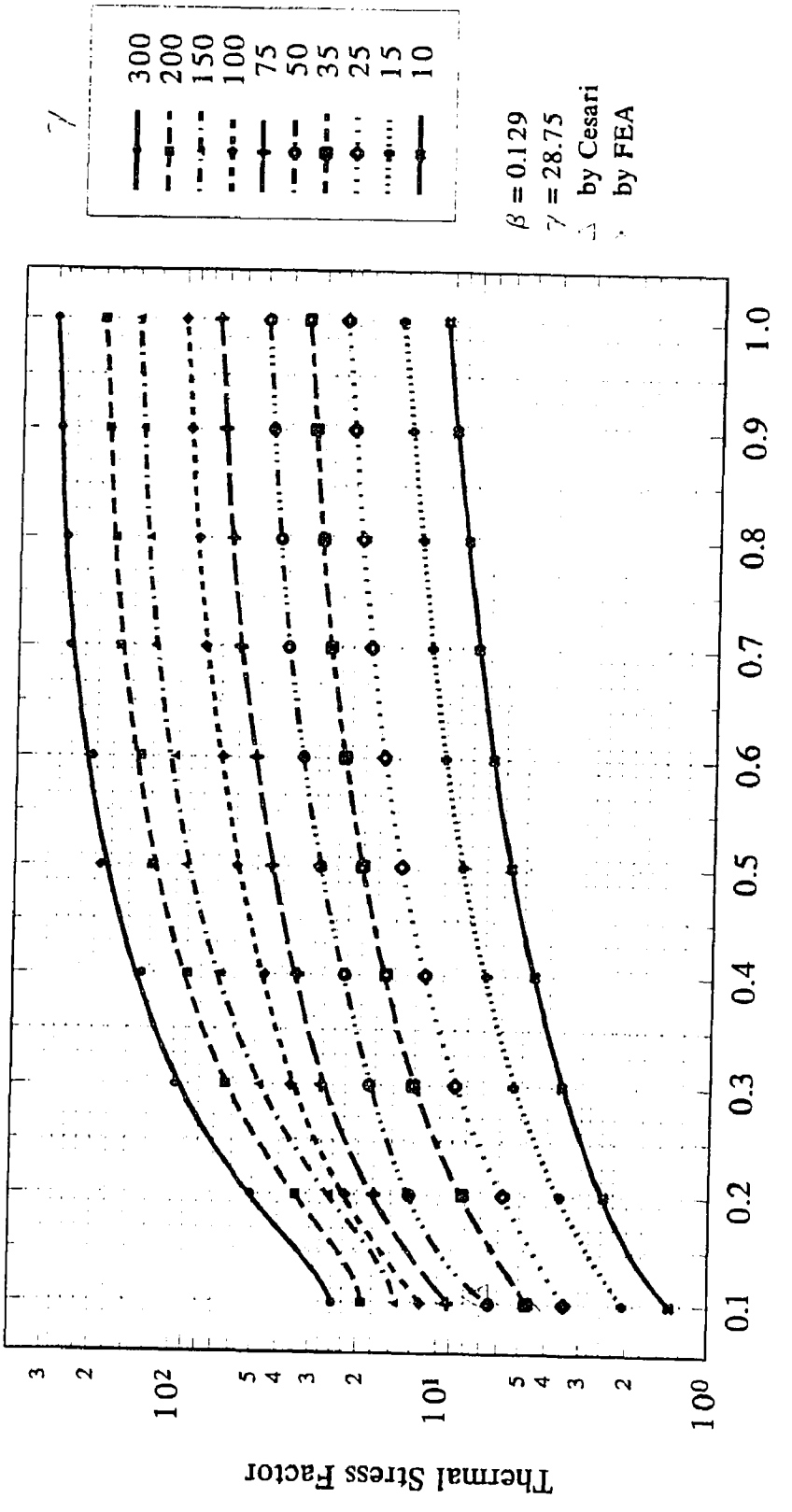

Figure 5 Data comparison of case 1 - thermal stress factor in longitudinal direction at point A_U of the pipe

$$K_T = \frac{\sigma_T \times 2 \times (1-\mu)}{E \times \alpha_T \times \Delta T} = \frac{406 \times 2 \times (1-0.3)}{1.7 \times 10^5 \times 1.85 \times 10^{-5} \times 25} = 7.23$$

from Figure T3 in Appendix A, with $\beta = 0.129$, and $\gamma = 28.75$, the local thermal stress factor should be approximately equal to 5.5.

Compared these two thermal stress factors, there is a percentage of derivation of 23%. One may detect that Cesari's results did not have sufficient node points or meshes to ensure the accuracy of the results. Additionally, his paper did not take into consideration of the boundary condition of the pipe as well as nozzle. Figure 5 shown the comparison of thermal stress factor between FEM data and Cesari's data.

5.2.2 Case 2

A paper presented by A. S. Strel'chenko, et. al [36], had a model with the pipe radius = 0.25 m, pipe thickness = 0.0125 m and nozzle radius = 0.05 m, nozzle thickness = 0.0025 m, where the value of beta, β is equal to 0.2 and gamma, γ is equal to 20. In this study, a numerical finite-difference method (FDM) was employed to solve the differential equations and FORTRAN IV program was developed to calculate the stress values. The temperature difference between internal and external of the pipe-nozzle was 30 °K. The Young's Modulus, the coefficient of linear thermal expansion, and Poisson's ration were given as 205.8 GPa, 1 x 10^{-5} m/m-°K , and 0.28, respectively. The thermal stresses and thermal stress factors were given in Table 2 based on the equation $K_T = \frac{\sigma_T \times 2 \times (1-\mu)}{E \times \alpha_T \times \Delta T}$.

Table 2 List of thermal stresses and thermal stress factors given in the case 2 by A.S Strel'chenko [36] and by FEA data of this thesis

	Thermal Stresses, MPa			
in the longitudinal direction at node point of the nozzle	A_o	A_i	C_o	C_i
by A.S. Strel'chenko [36]	129.3	108.1	35.4	17.6
by FEA Data	145	109	120	111

in the circumferential direction at node point of the nozzle	A_o	A_i	C_o	C_i
by A.S. Strel'chenko [36]	91.8	25.1	25.1	39.8
by FEA Data	190	192	214	175

	Thermal Stress Factors			
in the longitudinal direction at node point of the nozzle	A_o	A_i	C_o	C_i
by A.S. Strel'chenko [36]	3.02	2.52	0.86	0.41
by FEA Data	3.4	2.6	2.8	2.6

in the circumferential direction at node point of the nozzle	A_o	A_i	C_o	C_i
by A.S. Strel'chenko [36]	3.02	0.59	0.59	0.93
by FEA Data	4.4	4.5	5	4.1

As a result of comparison for these thermal stress factors showed in figures E1 to E8 in Appendix E, there exists a minimum percentage of derivation of approximately 3.2%. Also FEA data are all greater than that of Strel'chenko's data, which imply that the FEA results are much more conservative. However, in Strel'chenko's paper, the length of pipe and nozzle were not reported, it may explain the discrepancy of the results.

5.3 Comparison of Thermal Stresses with a long hollow cylinder

A comparison of local thermal stresses at the juncture of pipe-nozzle and theoretical thermal stresses at the regular long hollow pipe is made as in the following:

The maximum theoretical thermal stress at the regular long hollow pipe without nozzle can be calculated by using equations (23) and (24) [44]

$$\sigma_{t_a} = \sigma_{z_a} = -\frac{E \times \alpha_T \times \Delta T}{2 \times (1-\mu)} \qquad (23) \quad \text{for the inside surface ;}$$

$$\sigma_{t_b} = \sigma_{z_b} = \frac{E \times \alpha_T \times \Delta T}{2 \times (1-\mu)} \qquad (24) \quad \text{for the outside surface}$$

where subscript t refers to the circumferential direction and the z refers to the axial direction of the pipe.

Comparison of the local thermal stresses at pipe-nozzle and the theoretical thermal stresses at a regular long hollow pipe are tabulated in Table 3, which one may observe that,

1. The longitudinal local thermal stresses at node points A_U , A_L , B_U , and B_L on the pipe region of pipe-nozzle are smaller than the theoretical thermal stresses on a regular long hollow cylinder. On the contrary, the longitudinal local thermal stresses at C_U , C_L , D_U , and D_L on the pipe region of pipe-nozzle are greater than the theoretical thermal stresses on a regular long hollow cylinder.

2. Both longitudinal and circumferential local thermal stresses on the outside surface of the pipe of pipe-nozzle are greater than the theoretical thermal stresses on a regular long hollow cylinder and on the inside surface, neither local thermal stress is greater than the theoretical thermal stress on the regular cylinder.

3. All the local thermal stresses on the nozzle are greater than the theoretical thermal stresses on the regular long hollow cylinder.

Table 3 Comparison of local thermal stresses at pipe-nozzle and theoretical thermal stresses at regular long hollow pipe

Longitudinal Direction	A_U	A_L	B_U	B_L	C_U	C_L	D_U	D_L
Local thermal stresses on pipe region of pipe-nozzle	25630	-21730	25630	-21730	65185	-61285	65185	-61285
Theoretical thermal stresses on regular long hollow pipe	55714	-55,714	55714	-55,714	55714	-55,714	55714	-55,714
Circumferential Direction	A_U	A_L	B_U	B_L	C_U	C_L	D_U	D_L
Local thermal stresses on pipe region of pipe-nozzle	71315	-48470	71315	-48470	27300	-22840	27300	-22840
Theoretical thermal stresses on regular long hollow pipe	55714	-55,714	55714	-55,714	55714	-55,714	55714	-55,714

Longitudinal Direction	A_o	A_i	B_o	B_i	C_o	C_i	D_o	D_i
Local thermal stresses on nozzle region of pipe-nozzle	111420	-42342	111420	-42340	83565	-68245	83565	-68245
Theoretical thermal stresses on regular long hollow pipe	55714	-55,714	55714	-55,714	55714	-55,714	55714	-55,714
Circumferential Direction	A_o	A_i	B_o	B_i	C_o	C_i	D_o	D_i
Local thermal stresses on nozzle region of pipe-nozzle	125348	-118384	125348	-118384	115600	-114206	115600	-114206
Theoretical thermal stresses on regular long hollow pipe	55714	-55,714	55714	-55,714	55714	-55,714	55714	-55,714

CHAPTER 6

NUMERICAL EXAMPLES

To calculate the local stresses on the pipe of pipe-nozzle due to external loadings with steady state thermal gradient, an example is given as in the following :

6.1 Example I

A 12.75 inch O.D. pipe is intersected by a 5.325 inch diameter nozzle. Both pipe and nozzle thickness are 0.375 inch. The pipe mean radius, R_m , can be caucluated as (pipe O.D. - pipe thickness) / 2 = (12.75 - 0.375) / 2 = 6.188 inch, as well as nozzle mean radius, r_m , is equal to (5.325 - 0.375) / 2 = 2.475 inch.. As a result, beta, $\beta = r_m / R_m = 0.4$ and gamma, $\gamma = R_m / t_p = 16.5$. However, alpha$_p$, α_p (Pipe length / pipe mean radius) is equal to 8 and alpha$_n$, α_n (Nozzle length / nozzle mean radius) is equal to 4 , in accordance with the previous discussion. A 500 °F internal temperature and 100 °F environmental temperature are assumed in this example and the material of both pipe and nozzle are 347 stainless steel. The material properties of this pipe-nozzle model are listed in Table 4. Table 5 shown its geometrical parameters and its dimensions.

The thermal stresses were calculated by taking the dimensionless thermal stress factors (K_T) from Appendix A, which are also listed in Table 6, and then multipling it with $\frac{E \times \alpha_T \times \Delta T}{2 \times (1-\mu)}$. Table 7 is the modified stress computation table from WRC 107 which taken into account the local stresses on the pipe of the pipe-nozzle due to external loading, as well as local thermal stresses.

For the external loadings (refer to Figure 4), it assumed that

Radial Load, p = 400 lb. (downward)

Circumferential Moment, M_C = 500 lb.-in.

Longitudinal Moment, M_L = 500 lb.-in.

Torsional Moment, M_T = 500 lb.-in.

Circumferential Shear Force, V_c = 300 lb.

Longitudinal Shear Force, V_L = -400 lb. (to the right)

Table 4 Material properties of the illustrating pipe-nozzle model

α_T = Thermal Expansion Coefficience	6.50e-06	in/in-°F
E = Young's Modulus	3.00e+07	psi
μ = Poisson's ratio	0.3	
T_i = Internal Temperature	500	°F
T_o = Environmental Temperature	100	°F
$\delta T = T_i - T_o$	400	°F
Pipe Material	347 SS	
Nozzle Material	347 SS	

Table 5 Geometrical parameters and dimensions of example for calculation of local stresses on pipe of pipe-nozzle model

α_p = Pipe length / pipe mean radius	8	
α_n = Noz. length / noz. mean radius	4	
β = Noz. mean rad. / pipe mean rad.	0.4	
γ = Pipe mean rad. / pipe thk.	16.5	
L_p = Pipe length	49.5	ins
L_n = Nozzle length	9.9	ins
R_m = Pipe mean radius	6.188	ins
r_m = Nozzle mean radius	2.475	ins
t_p = Pipe thickness	0.375	ins
t_n = Nozzle thickness	0.375	ins

In Table 6, the longitudinal thermal stress factors at node point A_U and A_L are read from Figure 1T and 2T of the Appendix A, as wll as C_U and C_L from Figure 3T and 4T. Because of the axisymmetry on the pipe-nozzle geometry, numerical value at node point B_U should be identical as the value at A_U . Similarly, for B_L is equal to A_L , D_U is equal to C_U , and D_L is equal to C_L. With regard to circumferential thermal stress factors, they are from Figures 5T to 8T of the Appendix A.

Table 6 Computation table of thermal stress factors on pipe

Read values from thermal stress factor plots	A_U	A_L	B_U	B_L	C_U	C_L	D_U	D_L
in the circumferential direction from figure 5T-8T	1.28	-0.87	1.28	-0.87	0.49	-0.41	0.49	-0.41
in the longitudinal direction from figure 1T-4T	0.46	-0.39	0.46	-0.39	1.17	-1.1	1.17	-1.1

Two calculations are given as followings to illustrate how the thermal stresses can be obtained :

The thermal stress factor in the circumferential direction at node point A_U (Figure 1), which can be found from Figure 5T in the Appendix A, is equal to 1.28. Therefore, the thermal stress is able to be computed by the formula

$$\frac{K_T \times E \times \alpha_T \times \Delta T}{2\times(1-\mu)} = \frac{1.28\times 3.0\times 10^7 \times 6.5\times 10^{-6}\times 400}{2\times(1-0.3)} = 71{,}315 \text{ psi}$$

By the same way, the thermal stress factor in the longitudinal direction at A_U is given from Figure 1T as 0.46 and the thermal stress should be reckoned as

$$\frac{K_T \times E \times \alpha_T \times \Delta T}{2\times(1-\mu)} = \frac{0.46\times 3.0\times 10^7 \times 6.5\times 10^{-6}\times 400}{2\times(1-0.3)} = 25630 \text{ psi}$$

Table 7 Modified stress computation table of WRC 107 including local thermal stresses on the pipe- numerical example

Form Fig.	Read Curves for Stress Factor	Compute Absolute Values of Stress & Enter Result (psi)	A_U	A_L	B_U	B_L	C_U	C_L	D_U	D_L
3C(1)	$\frac{N_\varphi}{P/R_m} = 1.22$	$K_n[\frac{N_\varphi}{P/R_m}]\frac{P}{R_mT} =$	-210	-210	-210	-210	-210	-210	-210	-210
1C(1)	$\frac{M_\varphi}{P} = 0.0423$	$K_b[\frac{M_\varphi}{P}]\frac{6P}{T^2} =$	-723	723	-723	723	-723	723	-723	723
3A(1)	$\frac{N_\varphi}{M_C/(R_m^2\beta)} = 1.237$	$K_n[\frac{N_\varphi}{M_C/(R_m^2\beta)}]\frac{M_C}{R_m^2\beta T} =$					-62	-62	62	62
1A(1)	$\frac{M_\varphi}{M_C/(R_m\beta)} = 0.130$	$K_b[\frac{M_\varphi}{M_C/(R_m\beta)}]\frac{6M_C}{R_m\beta T^2} =$					-647	647	647	-647
3B(1)	$\frac{N_\varphi}{M_L/(R_m^2\beta)} = 2.64$	$K_n[\frac{N_\varphi}{M_L/(R_m^2\beta)}]\frac{M_L}{R_m^2\beta T} =$	-132	-132	132	132				
1B or 1B-1(1)	$\frac{M_\varphi}{M_L/(R_m\beta)} = 0.032$	$K_b[\frac{M_\varphi}{M_L/(R_m\beta)}]\frac{6M_L}{R_m\beta T^2} =$	-158	158	158	-158				
5T-8T Circumferential	$\frac{2(1-\mu)}{E\alpha_T\Delta T} = table-6$	$[\frac{E\alpha_T\Delta T}{2(1-\mu)}]\frac{2(1-\mu)}{E\alpha_T\Delta T} =$	71,315	-48,470	71,315	-48,470	27,300	-22,840	27,300	-22,840
Add algebraically summation of circumferential stresses, $\sigma_\varphi =$			70,092	-47,932	70,671	-47,984	25,656	-21,742	27,076	-22,912
4C(1)	$\frac{N_X}{P/R_m} = 2.030$	$K_a[\frac{N_X}{P/R_m}]\frac{P}{R_mT} =$	-350	-350	-350	-350	-350	-350	-350	-350
2C(1)	$\frac{M_X}{P} = 0.023$	$K_b[\frac{M_X}{P}]\frac{6P}{T^2} =$	-387	387	-387	387	-387	387	-387	387
4A(1)	$\frac{N_X}{M_C/(R_m^2\beta)} = 2.955$	$K_a[\frac{N_X}{M_C/(R_m^2\beta)}]\frac{M_C}{R_m^2\beta T} =$					-148	-148	148	148
2A(1)	$\frac{M_X}{M_C/(R_m\beta)} = 0.062$	$K_b[\frac{M_X}{M_C/(R_m\beta)}]\frac{6M_C}{R_m\beta T^2} =$					-306	306	306	-306
4B(1)	$\frac{N_X}{M_L/(R_m^2\beta)} = 1.196$	$K_a[\frac{N_X}{M_L/(R_m^2\beta)}]\frac{M_L}{R_m^2\beta T} =$	-60	-60	60	60				
2B or 2B-1(1)	$\frac{M_X}{M_L/(R_m\beta)} = 0.056$	$K_b[\frac{M_X}{M_L/(R_m\beta)}]\frac{6M_L}{R_m\beta T^2} =$	-278	278	278	-278				
1T-4T Longitudinal	$\frac{2(1-\mu)}{E\alpha_T\Delta T} = table-6$	$[\frac{E\alpha_T\Delta T}{2(1-\mu)}]\frac{2(1-\mu)}{E\alpha_T\Delta T} =$	25,630	-21,730	25,630	-21,730	65,185	-61,285	65,185	-61,285
Add algebraically summation of longitudinal stresses, $\sigma_X =$			24,555	-21,475	25,231	-21,910	63,995	-61,090	64,902	-61,406
Shear stress due to the Torsion, M_T		$\tau_{\varphi x} = \tau_{x\varphi} = \frac{M_T}{2\pi r_m^2 T} =$	27	27	27	27	-27	-27	-27	-27
Shear stress due to the Load, V_C		$\tau_{x\varphi} = \frac{V_C}{\pi r_m T} =$	92	92	-92	-92				
Shear stress due to the load, V_L		$\tau_{x\varphi} = \frac{V_L}{\pi r_m T} =$					122	122	-122	-122
Add Algebraically for Summation of Shear Stresses, $\tau_{\varphi X} =$			119	119	-64	-64	95	95	-149	-149
COMBINED STRESS INTENSITY, S										
1) When σ_φ and σ_x have like signs		$\sigma_1 = \frac{1}{2}[\sigma\varphi + \sigma x] + \frac{1}{2}\sqrt{(\sigma\varphi - \sigma_x)^2 + 4\tau^2} =$	70,093	-21,476	70,671	-21,910	63,995	-21,742	64,902	-22,912
2) When σ_φ and σ_x have unlike signs		$\sigma_2 = \frac{1}{2}[\sigma\varphi + \sigma x] - \frac{1}{2}\sqrt{(\sigma\varphi - \sigma_x)^2 + 4\tau^2} =$	24,556	-47,933	25,231	-47,986	25,656	-61,090	27,076	-61,406
3) Stress intensity at each point		$S = Max(\sigma_1, \sigma_2, \lvert\sigma_1 - \sigma_2\rvert) =$	70,093	-47,933	70,671	-47,986	63,995	-61,090	64,902	-61,406
4) Maximum stress intensity of the pipe-nozzle					70,671					

Note (1) : refer to figures in the WRC 107 [2]

After all the calculations of thermal stresses been done, the data can be input into Table 7 to complement the WRC 107 computation table and obtain the maximum stress intensity. However, these local stresses are only applied on the pipe portion. For the local thermal stresses on the nozzle, should be combined with local stresses due to external loadings, which presented by Lin [45].

6.2 Example II

A second example is given here to compute the local stresses on the nozzle region of pipe-nozzle due to external loadings with steady state thermal gradient:

A pipe with O.D. of 100.25 inch, thickness, t_p of 0.25 inch, and a nozzle with O.D. of 12.75 inch, also has a thickness, t_n of 0.25 inch. The pipe mean radius, R_m is equal to 50 inch and the nozzle mean radius, r_m is equal to 6.25 inch.

Therefore, beta can be obtained as $\beta = \frac{r_m}{R_m} = 0.125$, and gamma as $\gamma = \frac{R_m}{t_p} = 200$.

The same external loadings and material properties as the example one were using in this calculation. The geometrical parameters and dimensions of this example is shown in Table 8.

Again, the thermal stress factors of the nozzle are calculated by taking the dimensionless thermal stress factor from Figures 9T to 16T of the Appendix A and they are shown in Table 9. Table 10 is the modified stress computation table with thermal stresses on the nozzle region of the pipe-nozzle.

Table 8 Geometrical parameters and dimensions of example for calculation of local stresses on nozzle of pipe-nozzle model

α_p = Pipe length / pipe mean radius	8	
α_n = Noz. length / noz. mean radius	4	
β = Noz. mean rad. / pipe mean rad.	0.125	
γ = Pipe mean rad. / pipe thk.	200	
L_p = Pipe length	400	ins
L_n = Nozzle length	24.9	ins
R_m = Pipe mean radius	50	ins
r_m = Nozzle mean radius	6.25	ins
t_p = Pipe thickness	0.25	ins
t_n = Nozzle thickness	0.25	ins

Table 9 Computation table of the thermal stress factor on nozzle

Read values from thermal stress factor plots	A_o	A_i	B_o	B_i	C_o	C_i	D_o	D_i
in the circumferential direction from figure 13T to 16T	2.25	-1.125	2.25	-1.125	2.075	-2.05	2.075	-2.05
in the longitudinal direction from figure 9T to 12T	2.0	-0.76	2.0	-0.76	1.5	-0.76	1.5	-0.76

Table 11 lists the local thermal stress factors due to different external loadings from Lin [45].

Table 10 Computation table of example for calculation of local stresses on nozzle of pipe-nozzle model

Form Fig.	Read Curves for Stress Factor	Compute Absolute Values of Stress & Enter Result (psi)	A_o	A_i	B_o	B_i	C_o	C_i	D_o	D_i
11P & 15P[1]	$\frac{N_\varphi}{P/R_m}$ = *Table* - 11	$Kn[\frac{N_\varphi}{P/R_m}]\frac{P}{R_mT}$ =	-154	-154	-154	-154	-49	-49	-49	-49
9P & 13P[1]	$\frac{M_\varphi}{P}$ = *Table* - 11	$K_b[\frac{M_\varphi}{P}]\frac{6P}{T^2}$ =	-461	461	-461	461	-1,920	1,920	-1,920	1,920
7MC[1]	$\frac{N_\varphi}{M_C/(R_m^2\beta)}$ = *Table* - 11	$Kn[\frac{N_\varphi}{M_C/(R_m^2\beta)}]\frac{M_C}{R_m^2\beta T}$ =					-20	-20	20	20
5MC[1]	$\frac{M_\varphi}{M_C/(R_m\beta)}$ = *Table* - 11	$K_b[\frac{M_\varphi}{M_C/(R_m\beta)}]\frac{6M_C}{R_m\beta T^2}$ =					-553	553	553	-553
7ML[1]	$\frac{N_\varphi}{M_L/(R_m^2\beta)}$ = *Table* - 11	$Kn[\frac{N_\varphi}{M_L/(R_m^2\beta)}]\frac{M_L}{R_m^2\beta T}$ =	-112	-112	112	112				
5ML[1]	$\frac{M_\varphi}{M_L/(R_m\beta)}$ = *Table* - 11	$K_b[\frac{M_\varphi}{M_L/(R_m\beta)}]\frac{6M_L}{R_m\beta T^2}$ =	-86	86	86	-86				
13T-16T Circumferential	$\frac{2(1-\mu)}{E\alpha_T\Delta T}$ = *table* - 9	$[\frac{E\alpha_T\Delta T}{2(1-\mu)}]\frac{2(1-\mu)}{E\alpha_T\Delta T}$ =	125,348	-118,384	125,348	-118,384	115,600	-114,206	115,600	-114,206
Add algebraically summation of circumferential stresses, σ_φ =			124,536	-118,103	124,931	-118,051	113,058	-111,802	114,205	-112,867
12P & 16P[1]	$\frac{N_X}{P/R_m}$ = *Table* - 11	$Ka[\frac{N_X}{P/R_m}]\frac{P}{R_mT}$ =	-18	-18	-18	-18	-870	-870	-870	-870
10P & 14P[1]	$\frac{M_X}{P}$ = *Table* - 11	$K_b[\frac{M_X}{P}]\frac{6P}{T^2}$ =	-1,306	1,306	-1,306	1,306	-499	499	-499	499
8MC[1]	$\frac{N_X}{M_C/(R_m^2\beta)}$ = *Table* - 11	$Ka[\frac{N_X}{M_C/(R_m^2\beta)}]\frac{M_C}{R_m^2\beta T}$ =					-123	-123	123	123
6MC[1]	$\frac{M_X}{M_C/(R_m\beta)}$ = *Table* - 11	$K_b[\frac{M_X}{M_C/(R_m\beta)}]\frac{6M_C}{R_m\beta T^2}$ =					-184	184	184	-184
8ML[1]	$\frac{N_X}{M_L/(R_m^2\beta)}$ = *Table* - 11	$Ka[\frac{N_X}{M_L/(R_m^2\beta)}]\frac{M_L}{R_m^2\beta T}$ =	-16	-16	16	16				
6ML[1]	$\frac{M_X}{M_L/(R_m\beta)}$ = *Table* - 11	$K_b[\frac{M_X}{M_L/(R_m\beta)}]\frac{6M_L}{R_m\beta T^2}$ =	-258	258	258	-258				
9T-12T Longitudinal	$\frac{2(1-\mu)}{E\alpha_T\Delta T}$ = *table* - 9	$[\frac{E\alpha_T\Delta T}{2(1-\mu)}]\frac{2(1-\mu)}{E\alpha_T\Delta T}$ =	111,420	-42,340	111,420	-42,340	83,565	-68,245	83,565	-68,245
Add algebraically summation of longitudinal stresses, σ_X =			109,822	-40,811	113,151	-41,294	81,888	-68,555	82,503	-68,678
Shear stress due to the Torsion, M_T	$\tau_{\varphi x} = \tau_{x\varphi} = \frac{M_T}{2\pi r_m^2 T}$ =		5	5	5	5	-5	-5	-5	-5
Shear stress due to the Load, V_C	$\tau_{x\varphi} = \frac{V_C}{\pi r_m T}$ =		40	40	-40	-40				
Shear stress due to the load, V_L	$\tau_{x\varphi} = \frac{V_L}{\pi r_m T}$ =						20	20	-20	-20
Add Algebraically for Summation of Shear Stresses, $\tau_{\varphi x}$ =			45	45	-35	-35	15	15	-25	-25
COMBINED STRESS INTENSITY, S										
1) When σ_φ and σ_x have like signs	$\sigma_1 = \frac{1}{2}[\sigma\varphi + \sigma x] + \frac{1}{2}\sqrt{(\sigma\varphi - \sigma x)^2 + 4\tau^2}$ =		124,536	-40,811	124,931	-41,294	113,058	-68,555	114,205	-68,678
2) When σ_φ and σ_x have unlike signs	$\sigma_2 = \frac{1}{2}[\sigma\varphi + \sigma x] - \frac{1}{2}\sqrt{(\sigma\varphi - \sigma x)^2 + 4\tau^2}$ =		109,822	-118,103	113,151	-118,051	81,888	-111,802	82,503	-112,867
3) Stress intensity at each point	$S = Max(\sigma_1, \sigma_2, \lvert\sigma_1 - \sigma_2\rvert)$ =		124,536	-118,103	124,931	-118,051	113,058	-111,802	114,205	-112,867
4) Maximum stress intensity of the pipe-nozzle					124,931					

Note (1) : refer to figures from Lin, Sun, and Koplik. [45]

Table 11 Local stress factors on the nozzle from Lin, Sun, and Koplik [45]

Read values from Stress Factor Plots	A_o	A_i	B_o	B_i	C_o	C_i	D_o	D_i
From Figure 11P	0.895	0.895	0.895	0.895				
From Figure 15P					0.285	0.285	0.285	0.285
From Figure 9P	0.027	0.027	0.027	0.027				
From Figure 13P					0.112	0.112	0.112	0.112
From Figure 7MC					0.4	0.4	0.4	0.4
From Figure 5MC					0.111	0.111	0.111	0.111
From Figure 7ML	2.24	2.24	2.24	2.24				
From Figure 5ML	0.017	0.017	0.017	0.017				
From Figure 12P	0.104	0.104	0.104	0.104				
From Figure 16P					5.046	5.046	5.046	5.046
From Figure 10P	0.078	0.078	0.078	0.078				
From Figure 14P					0.03	0.03	0.03	0.03
From Figure 8MC					2.456	2.456	2.456	2.456
From Figure 6MC					0.037	0.037	0.037	0.037
From Figure 8ML	0.319	0.319	0.319	0.319				
From Figure 6ML	0.052	0.052	0.052	0.052				

CHAPTER 7

CONCLUSIONS

Since the finite element techniques is capable of simulating the true geometry of the pipe-nozzle configuration, node points and boundary condition studies prior to production runs ensure that the local thermal stress factors presented in this thesis are accurate and reliable. These local thermal stress factor plots are shown in Figures 1T to 16T of Appendix A. Again, these local thermal stress factors may be used in conjunction with WRC 107 with other external loadings.

By studying the Figures 1T to 16T of Appendix A, the following conclusions may be made:

1. When the gamma value increases, all the thermal stress factor values are increasing, i.e., the thinner the shell, the higher the local thermal stress.

2. At the node points A and B of the pipe, the local longitudinal thermal stresses are always less than the local circumferential thermal stresses, on the contrary, at the node points C and D of the pipe, the local longitudinal thermal stresses are always greater than the local circumferential thermal stresses.

3. On the nozzle, the local circumferential thermal stresses are always greater than the local longitudinal thermal stresses.

APPENDIX A

THERMAL STRESS FACTOR PLOTS

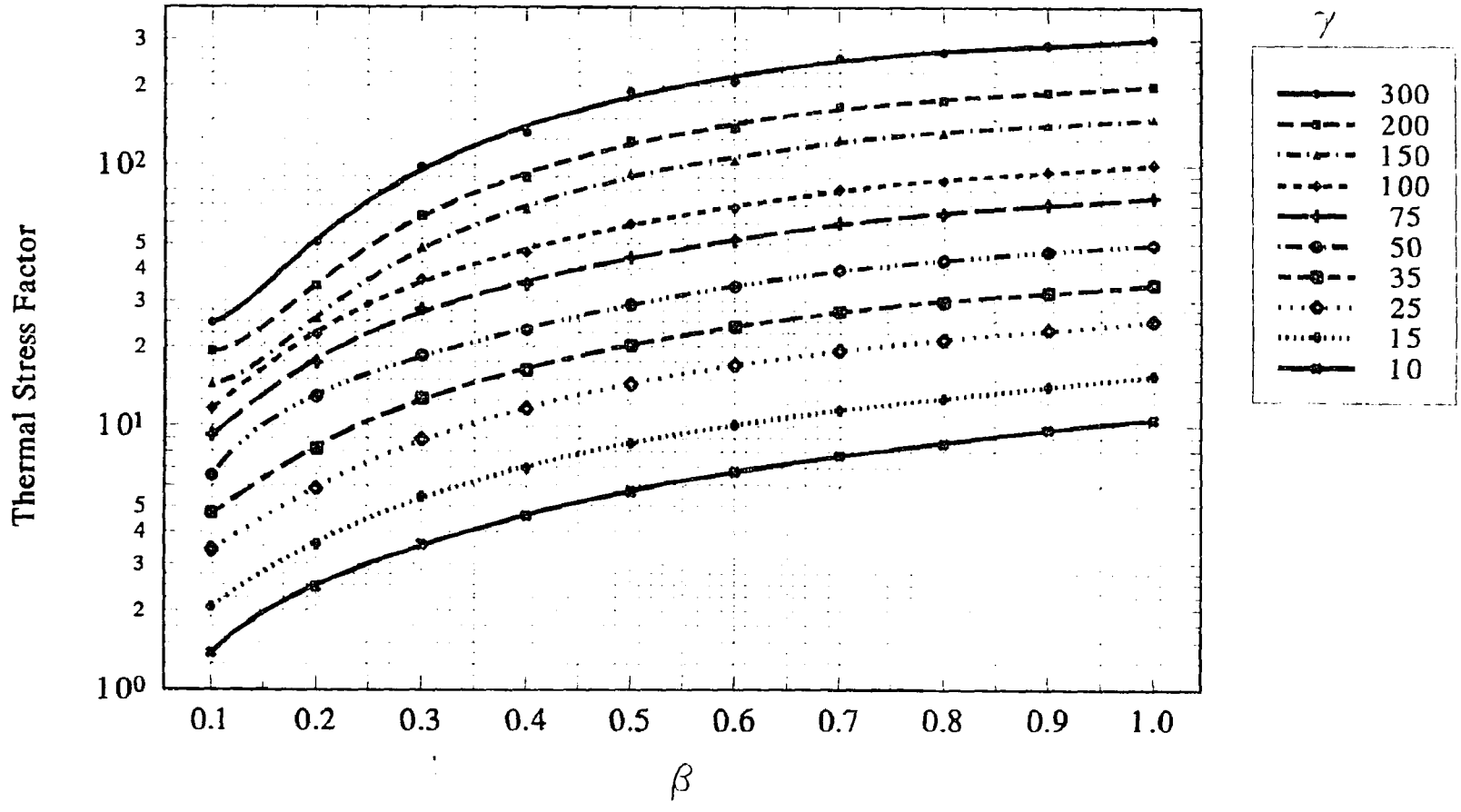

Figure 1T Thermal stress factor in the longitudinal direction at point A_{t_j} of the pipe

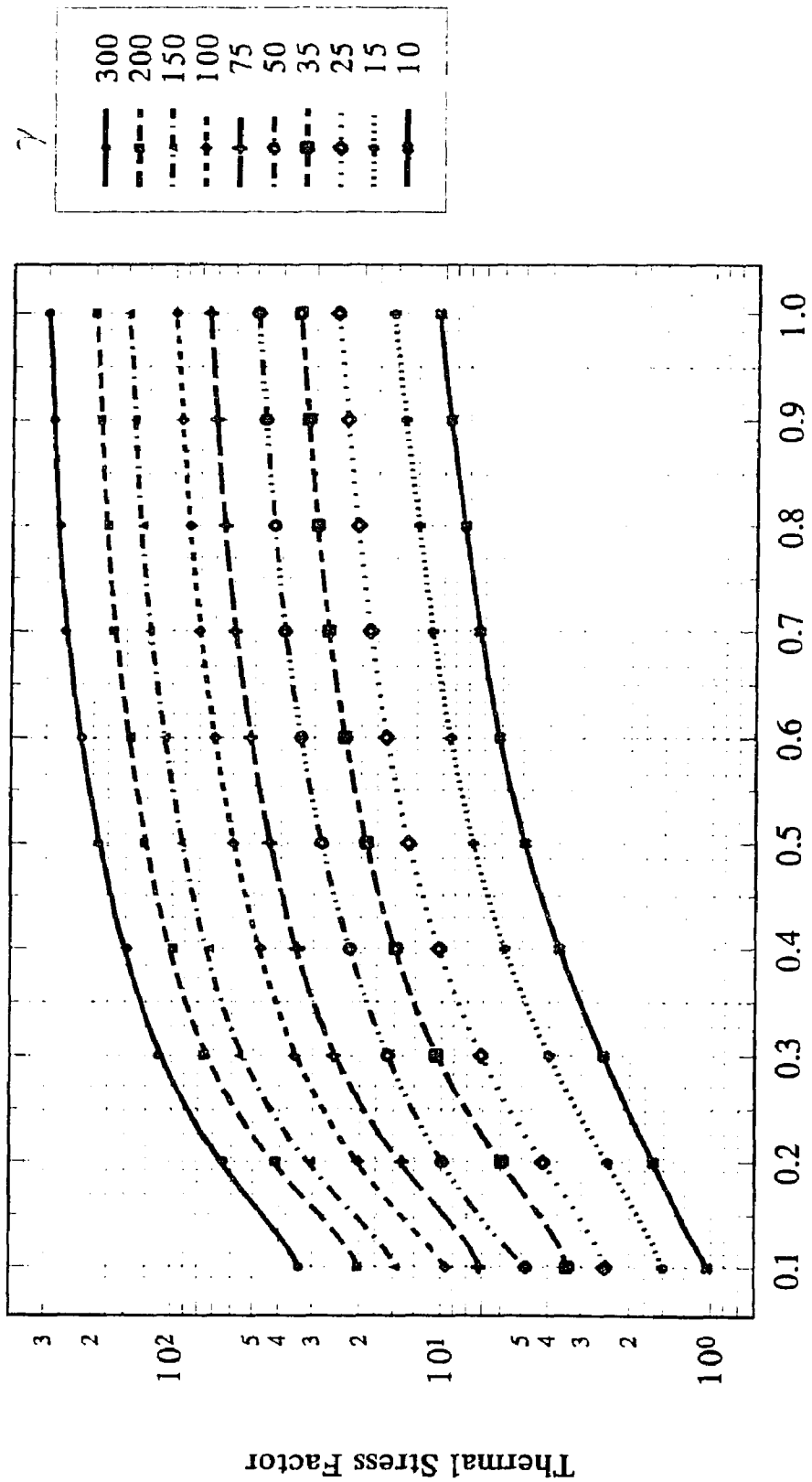

Figure 2T Thermal stress factor in the longitudinal direction at point A_1 of the pipe

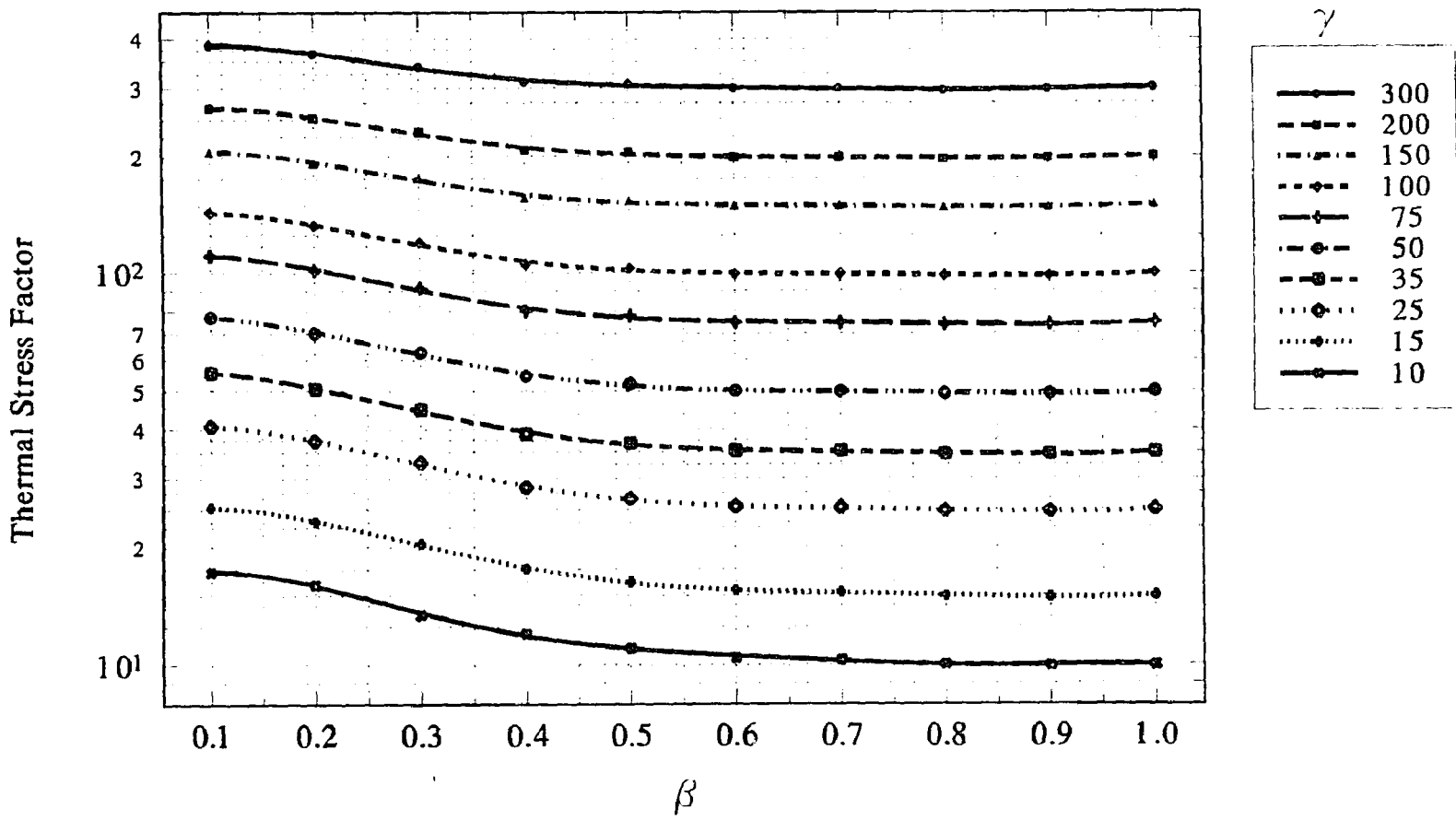

Figure 3T Thermal stress factor in the longitudinal direction at point C_U of the pipe

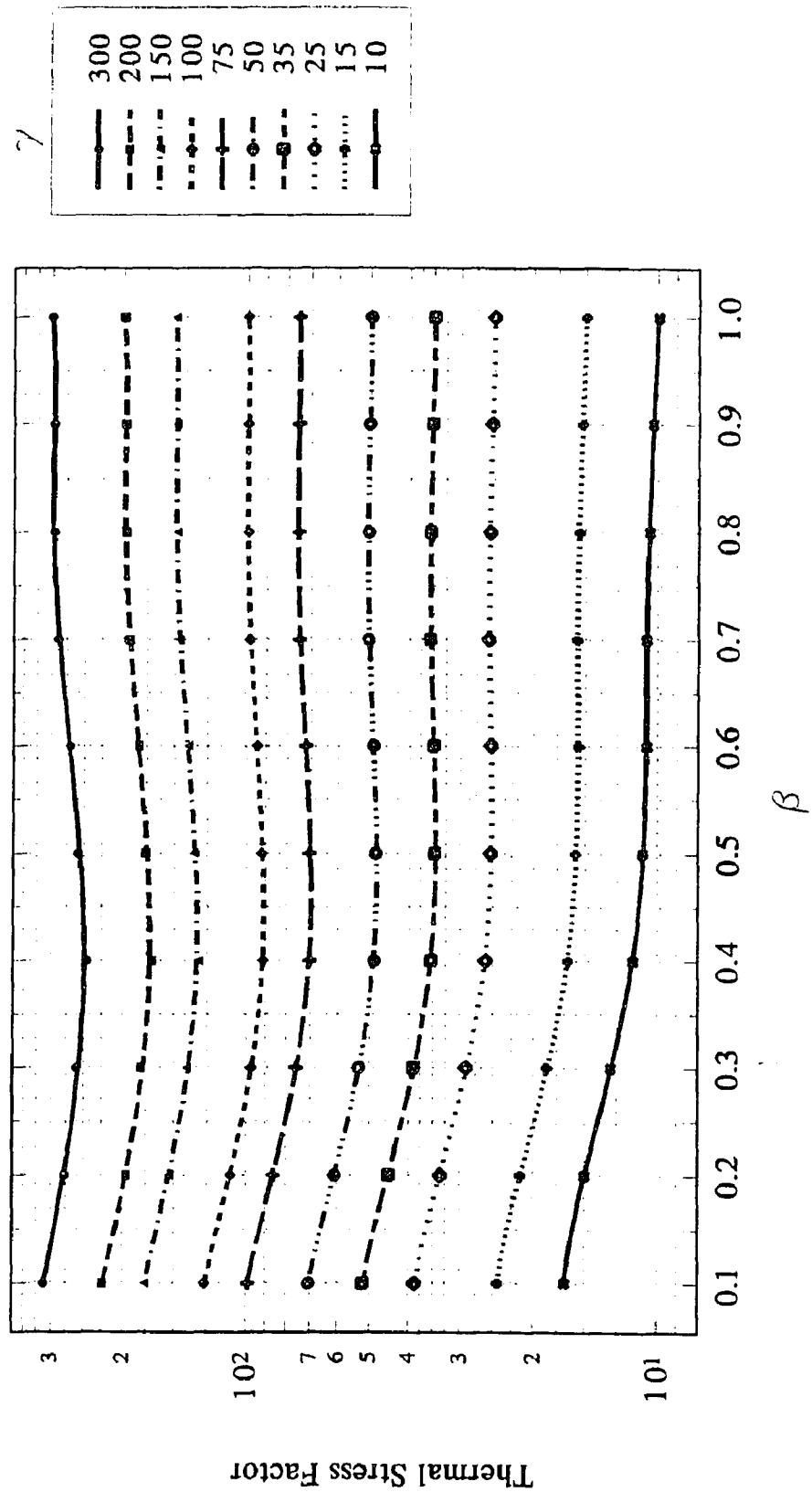

Figure 4T Thermal stress factor in the longitudinal direction at point C_1 of the pipe

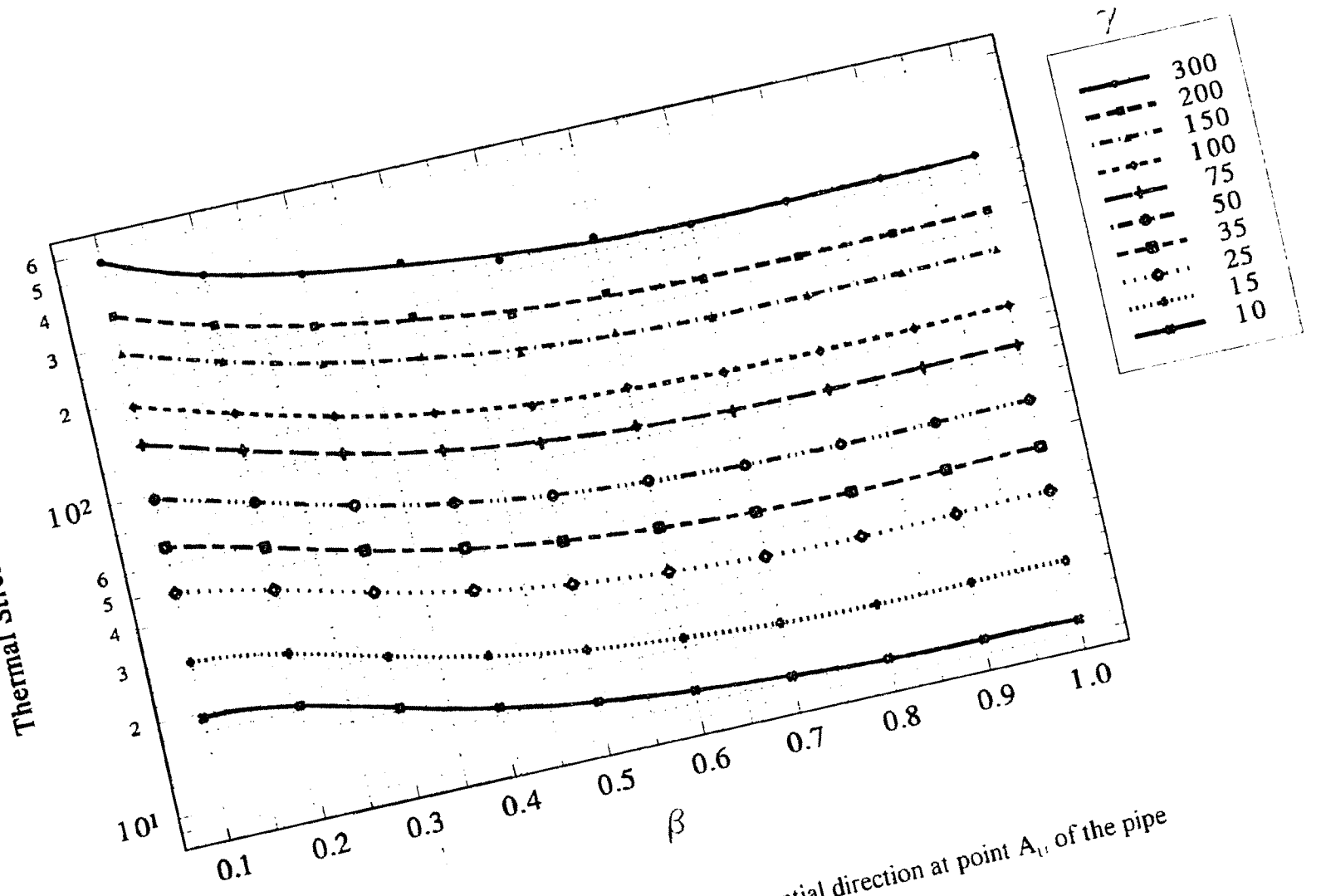

Figure 5T Thermal stress factor in the circumferential direction at point A_0 of the pipe

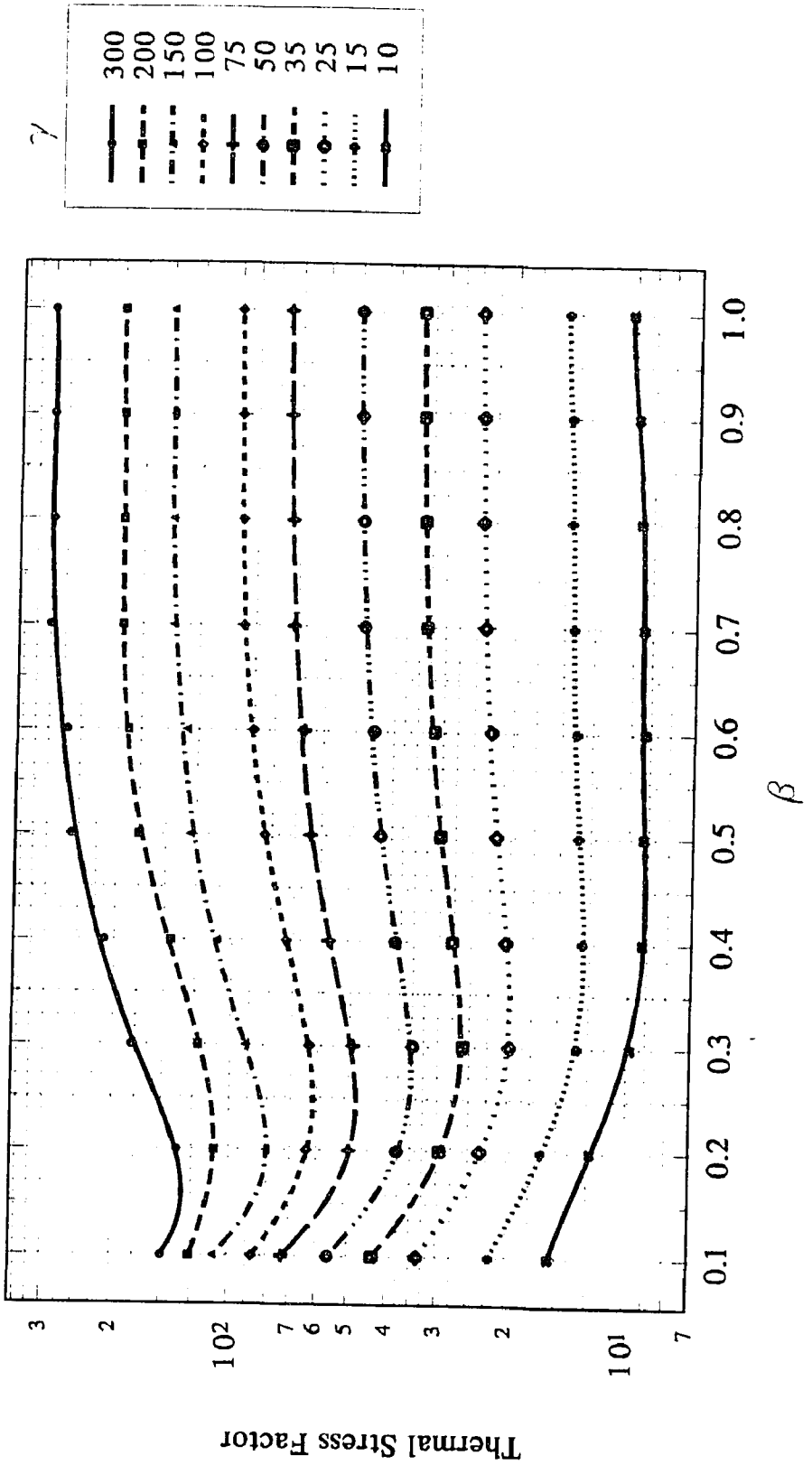

Figure 6T Thermal stress factor in the circumferential direction at point A_1 of the pipe

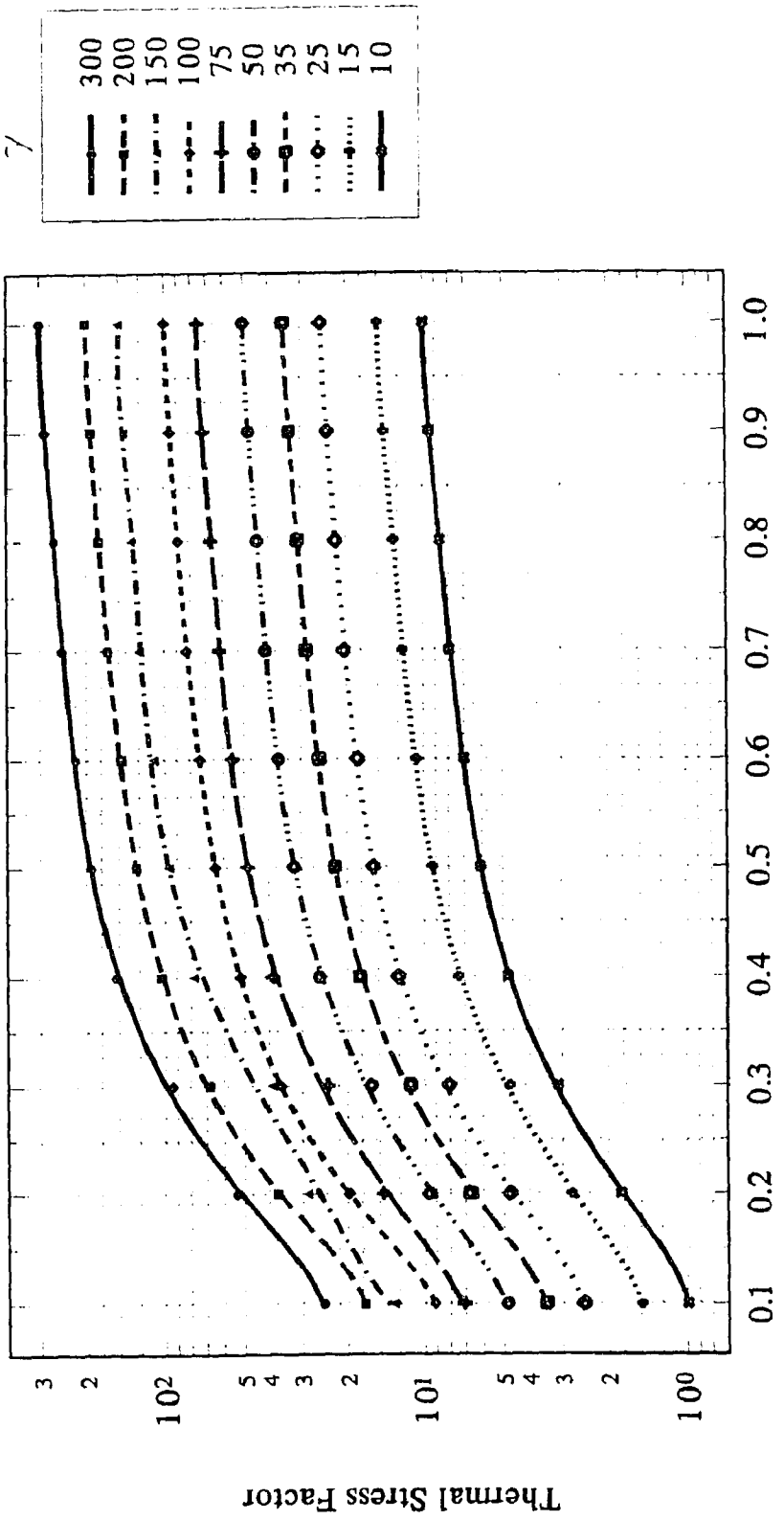

Figure 7T Thermal stress factor in the circumferential direction at point C_1 of the pipe

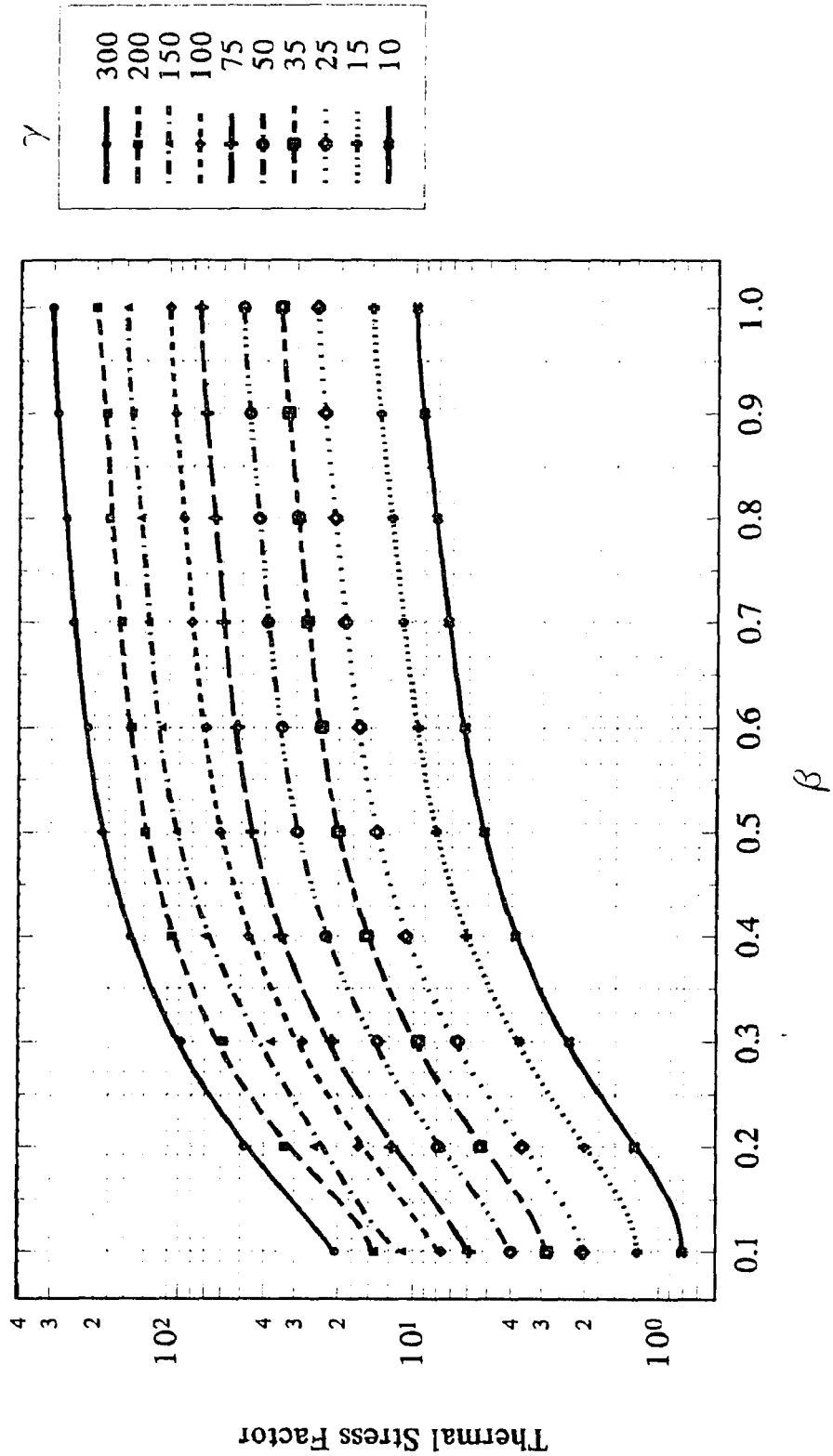

Figure 8T Thermal stress factor in the circumferential direction at point C_1 of the pipe

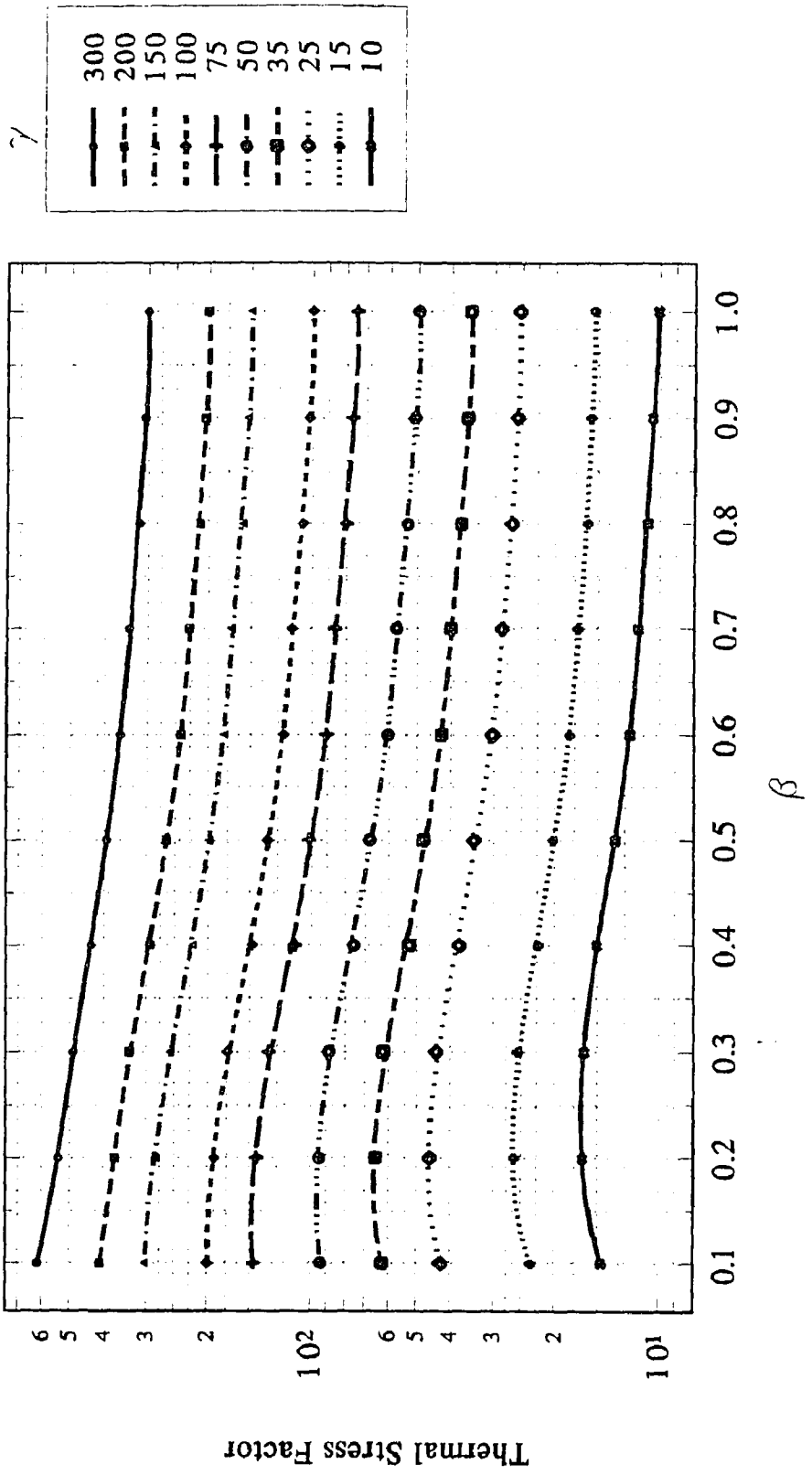

Figure 9T Thermal stress factor in the longitudinal direction at point A_1 of the nozzle

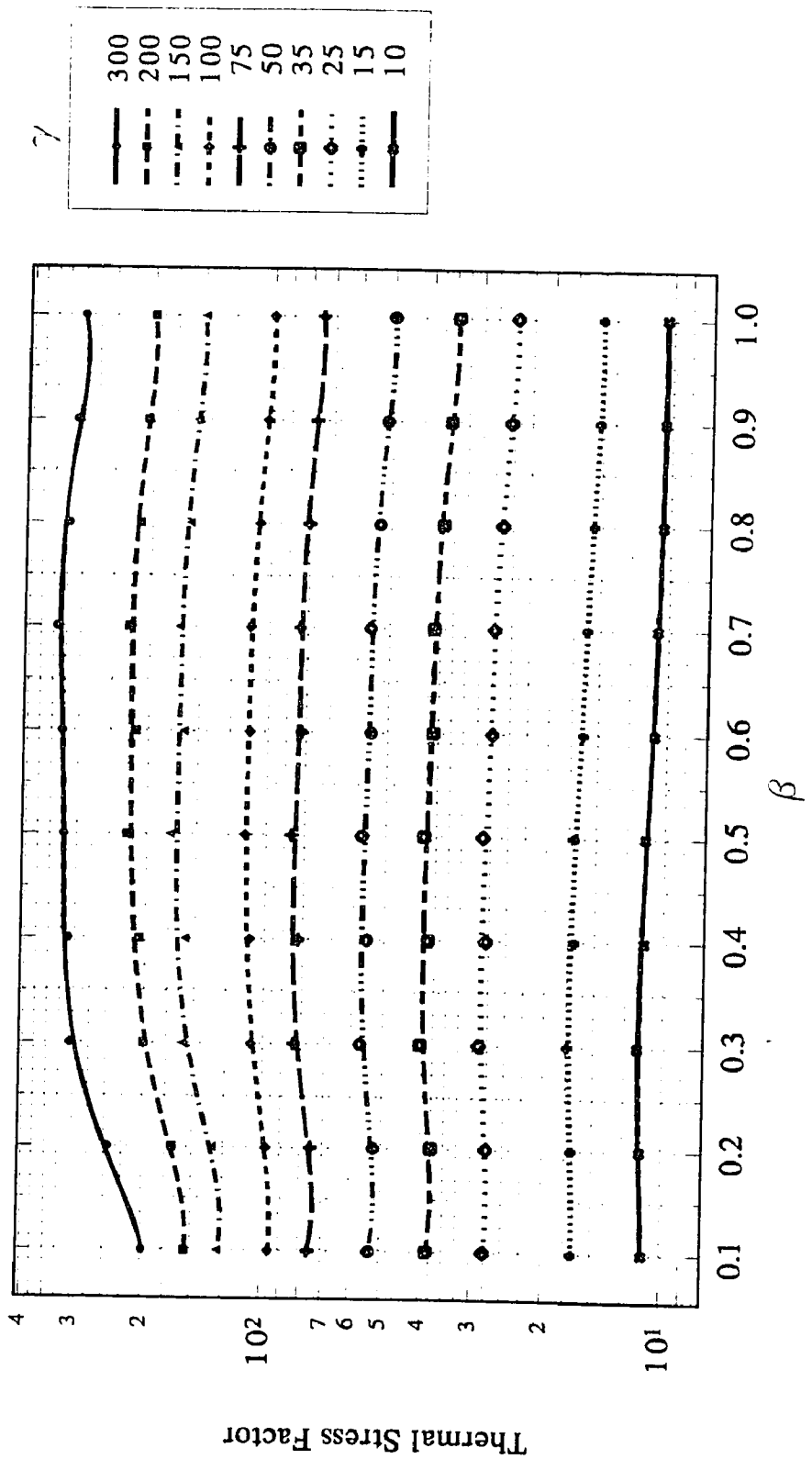

Figure 10T Thermal stress factor in the longitudinal direction at point A_1 of the nozzle

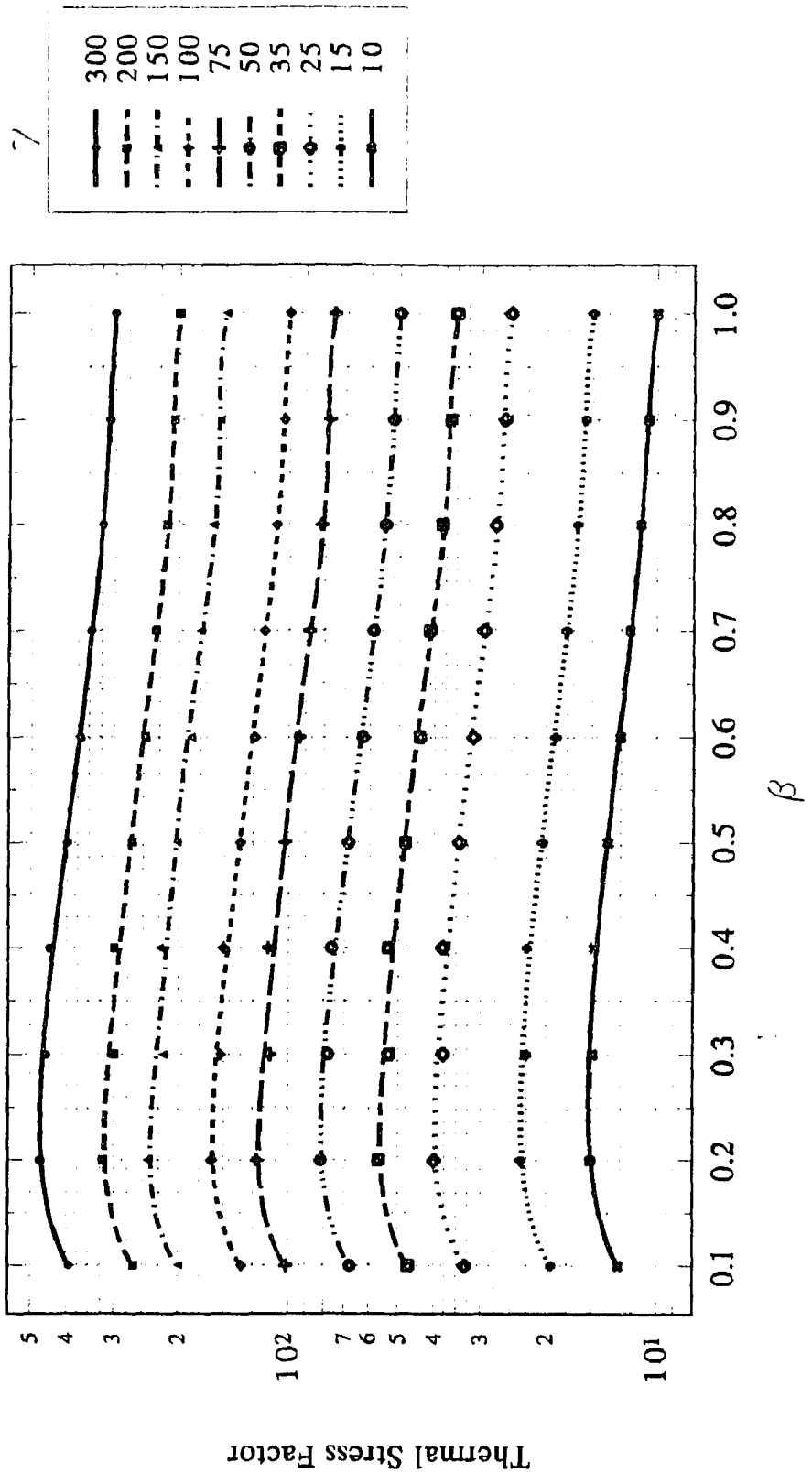

Figure 11T Thermal stress factor in the longitudinal direction at point C_o of the nozzle

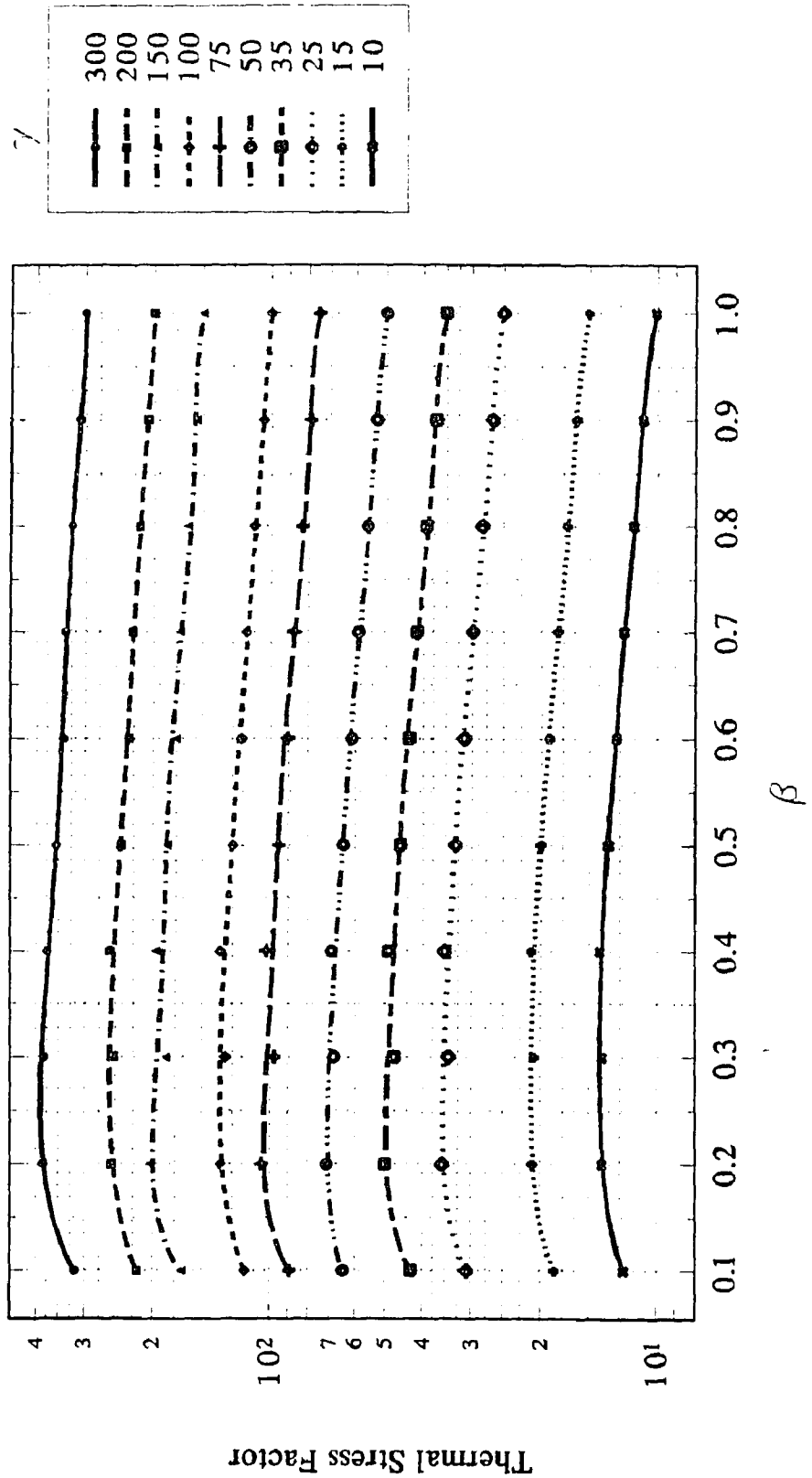

Figure 12T Thermal stress factor in the longitudinal direction at point C_1 of the nozzle

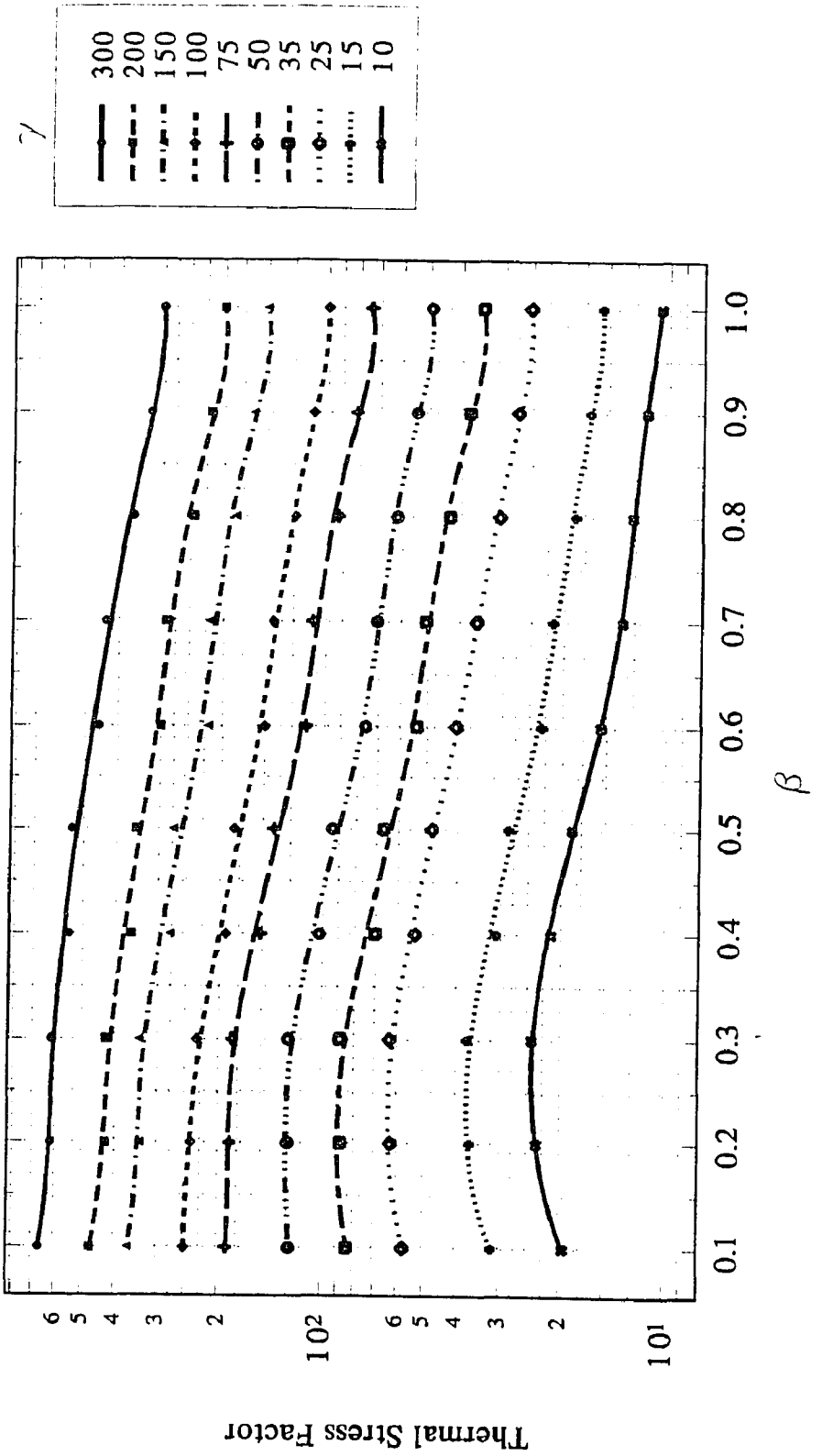

Figure 13T Thermal stress factor in the circumferential direction at point A_0 of the nozzle

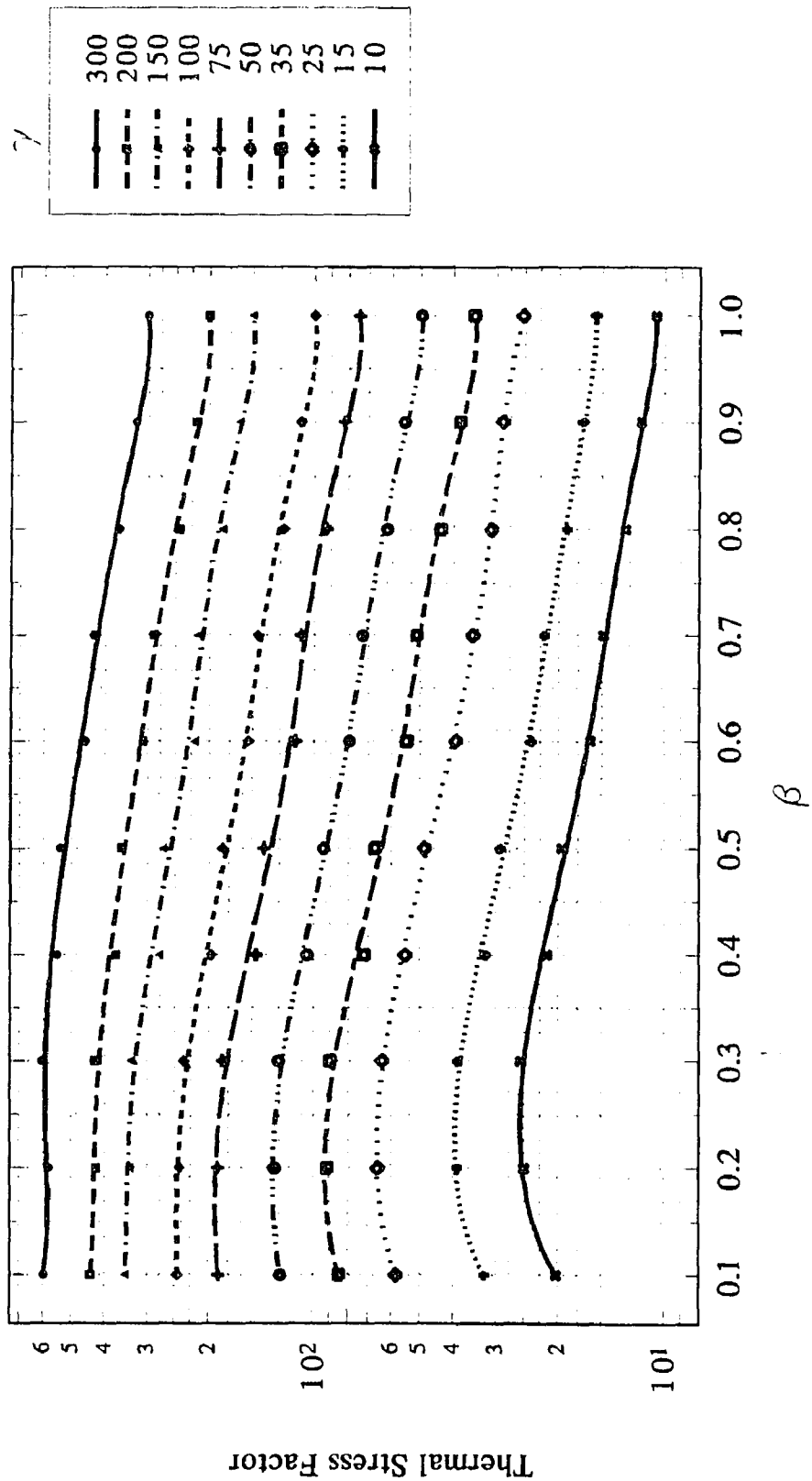

Figure 14T Thermal stress factor in the circumferential direction at point A_1 of the nozzle

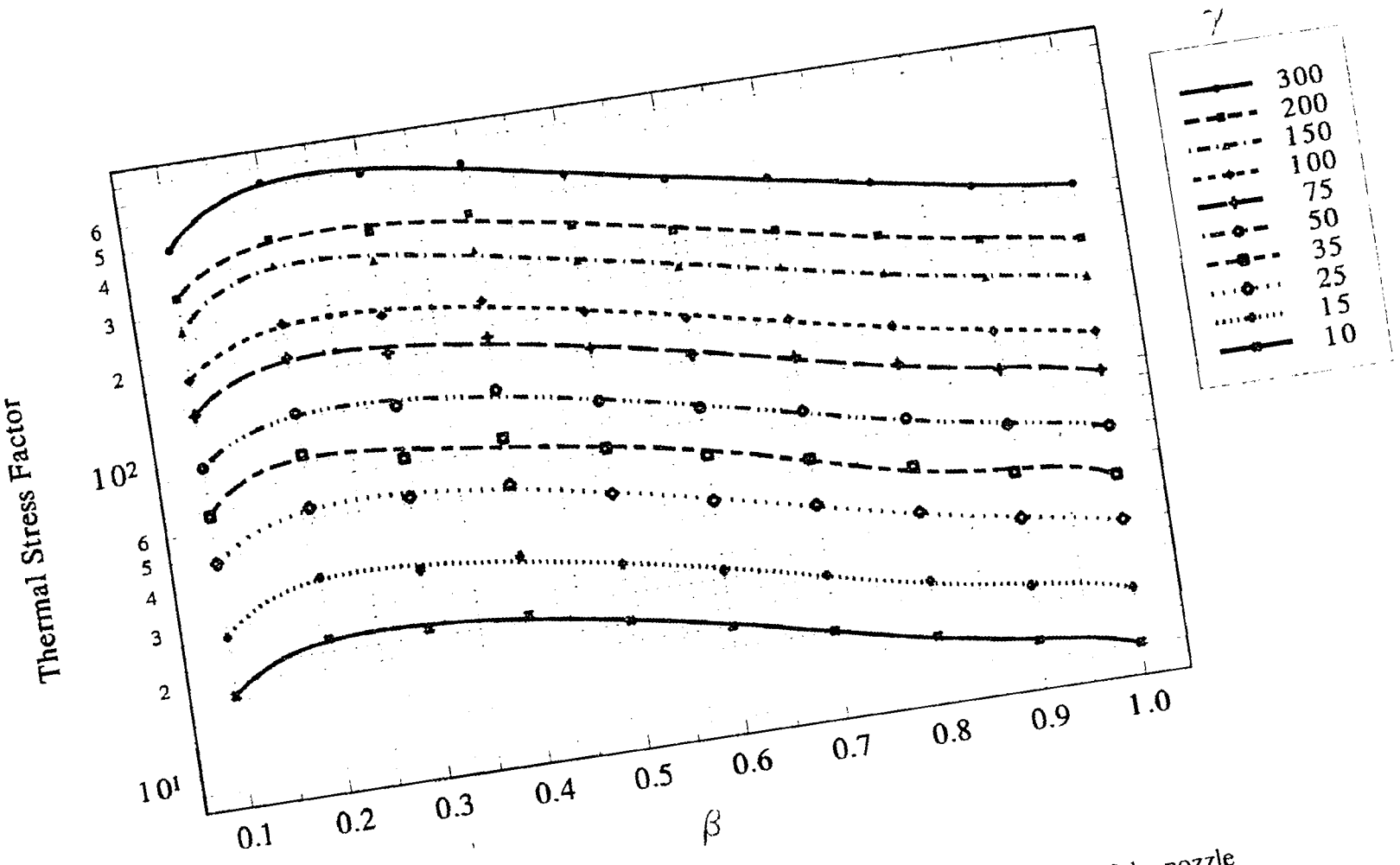

Figure 15T Thermal stress factor in the circumferential direction at point C_o of the nozzle

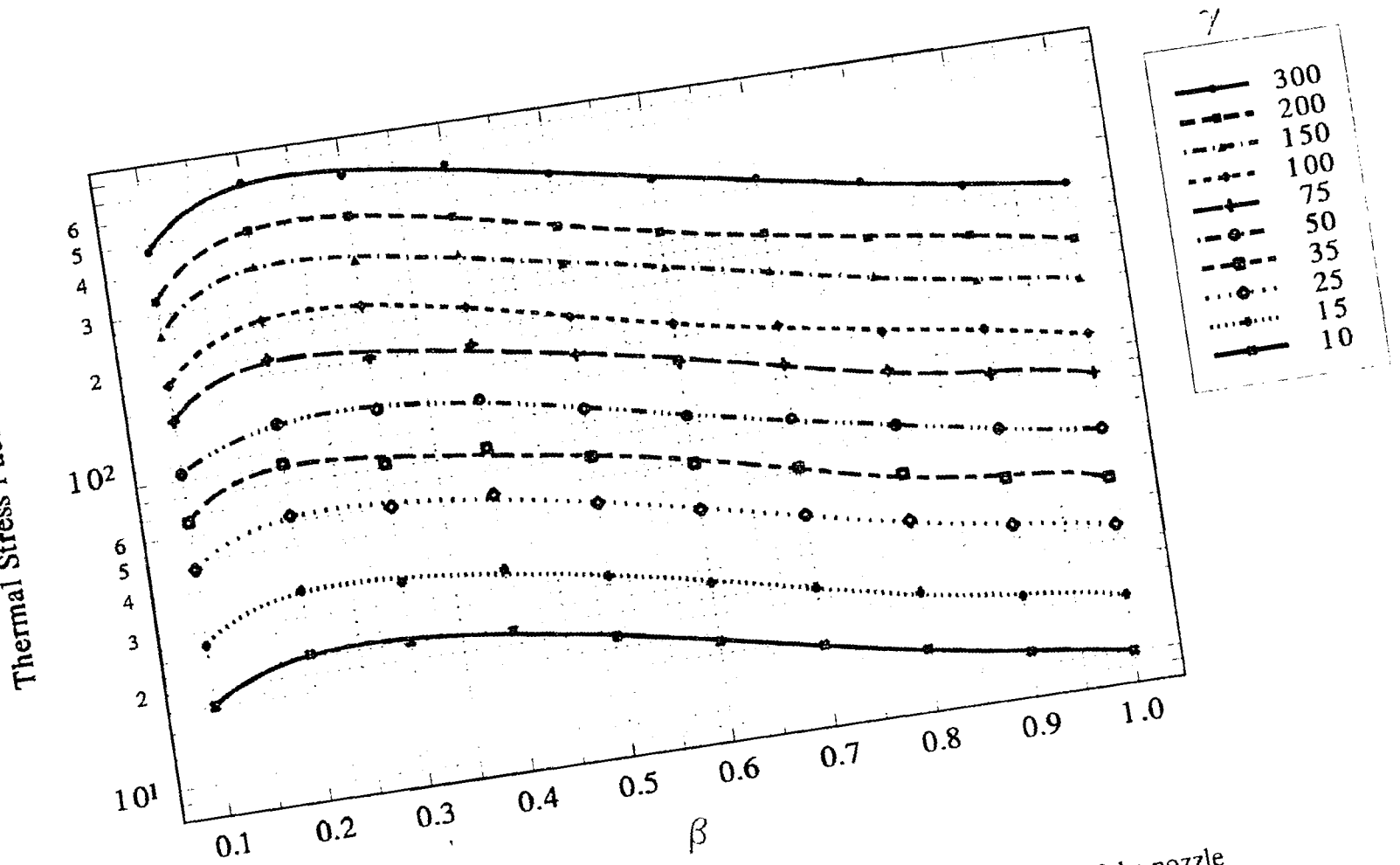

Figure 16T Thermal stress factor in the circumferential direction at point C_i of the nozzle

APPENDIX B

ASYMPOTIC STUDY OF NODE POINTS AT THE JUNCTURE OF PIPE-NOZZLE

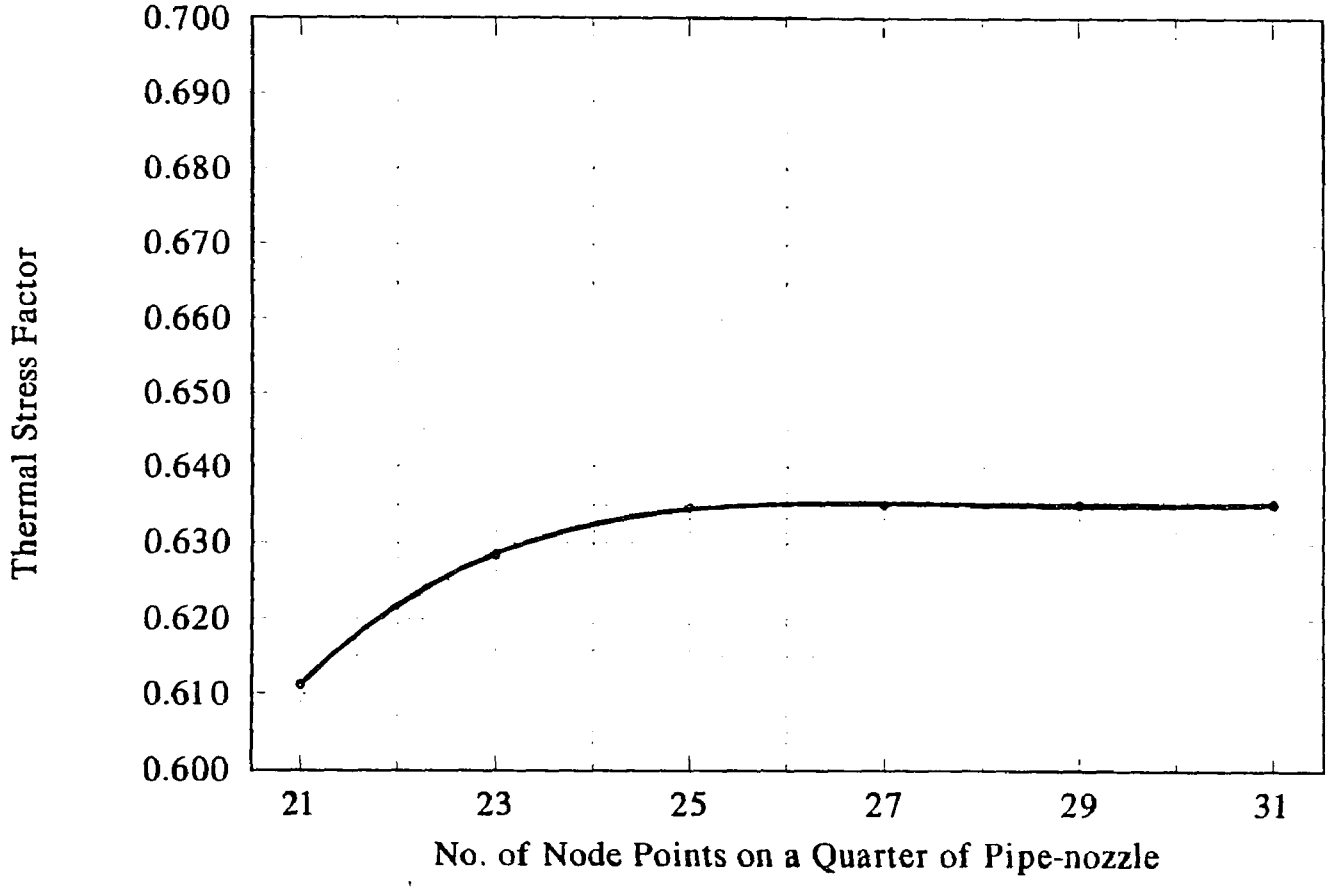

Figure B1 Convergence of node points at the juncture of pipe-nozzle for longitudinal thermal stress factor at point A_t of the pipe

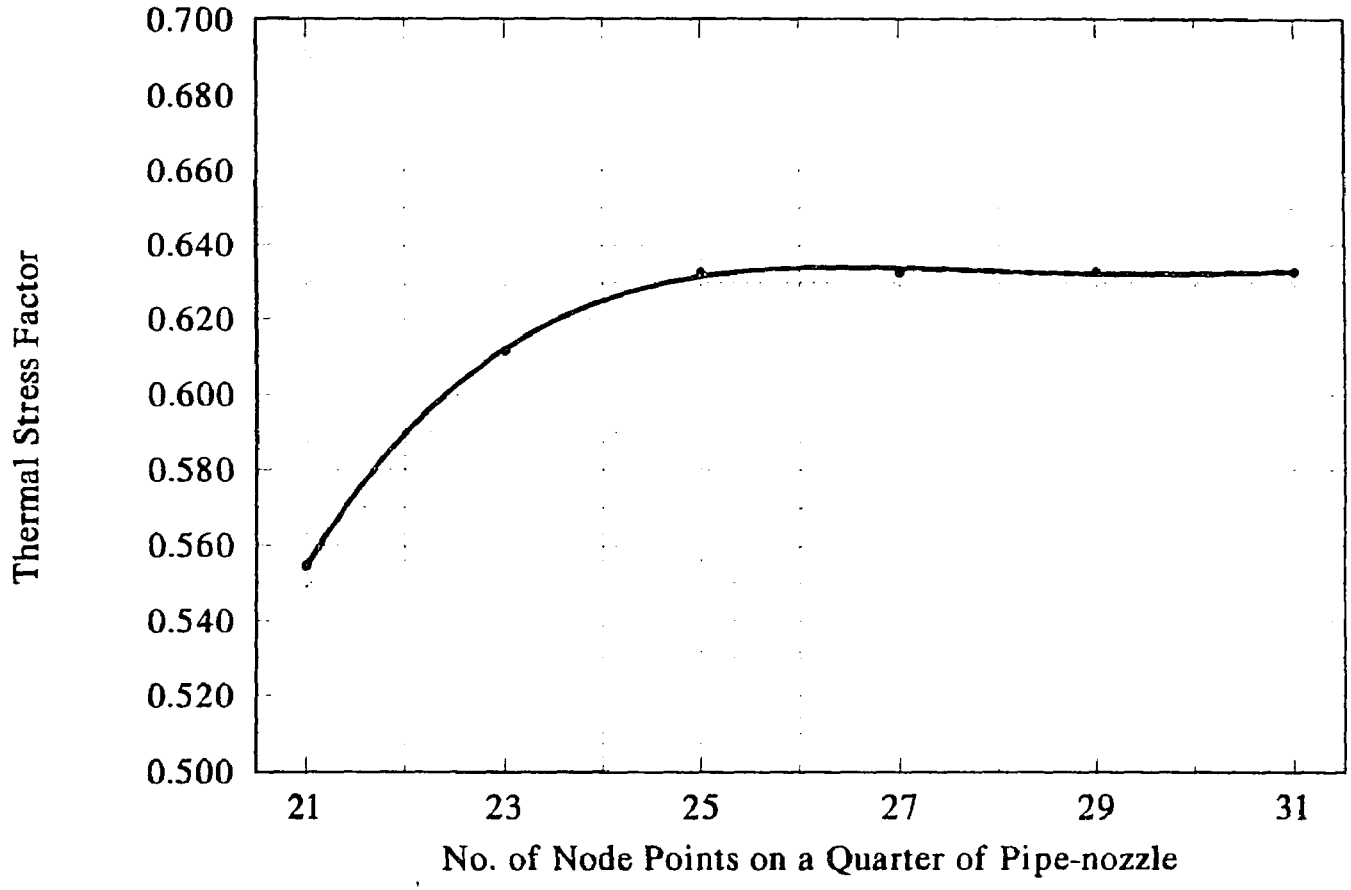

Figure B2 Convergence of node points at the juncture of pipe-nozzle for longitudinal thermal stress factor at point A_1 of the pipe

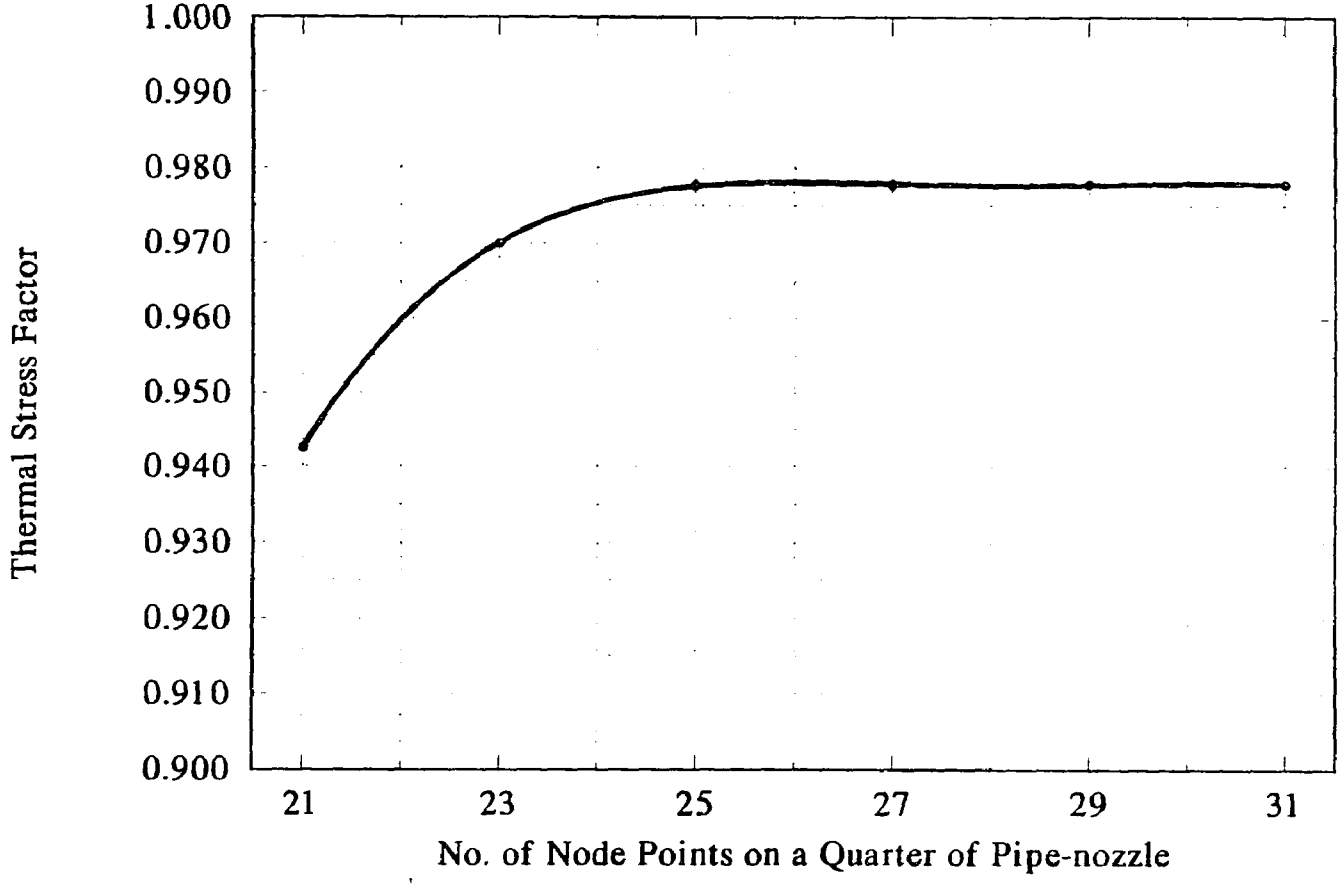

Figure B3 Convergence of node points at the juncture of pipe-nozzle for longitudinal thermal stress factor at point C_1 of the pipe

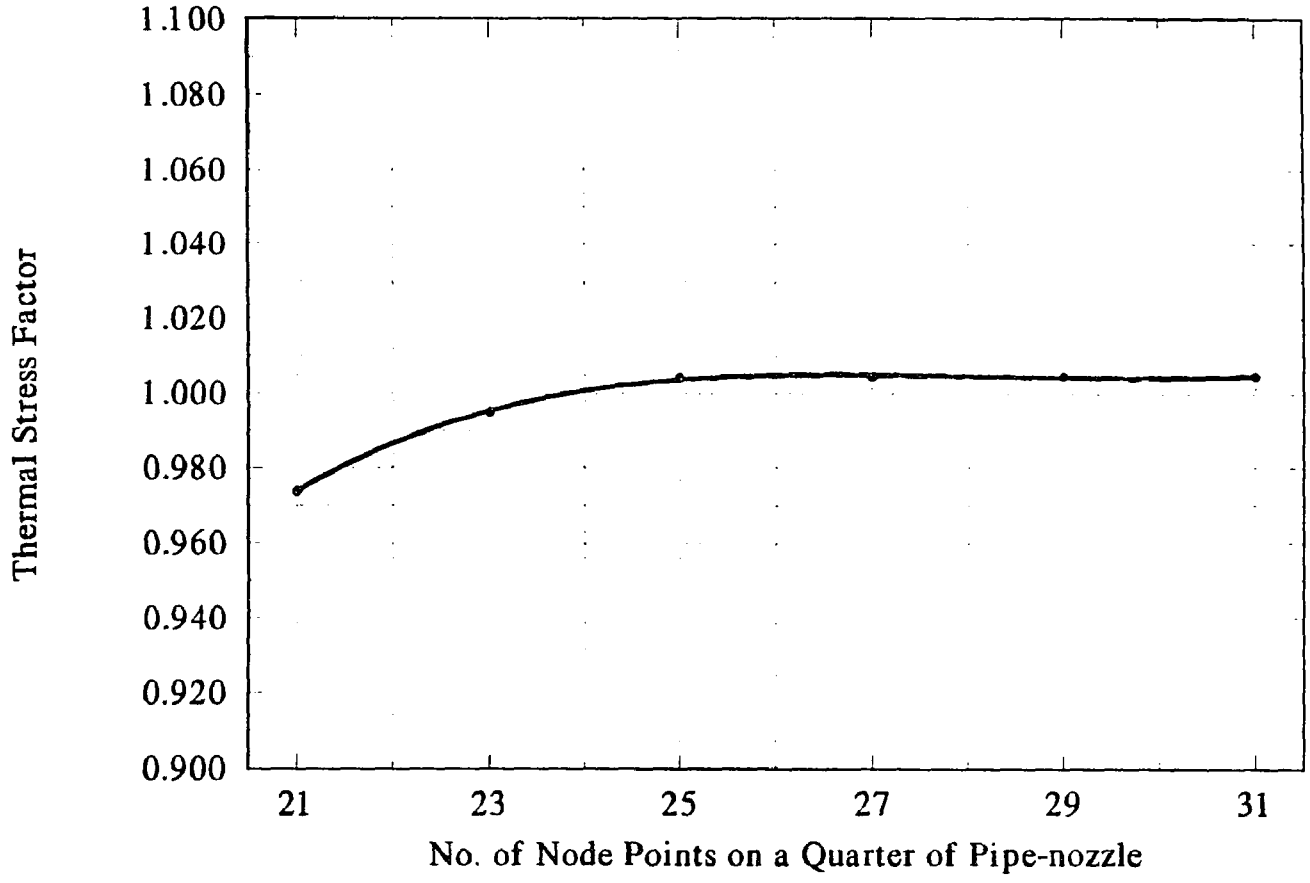

Figure B4 Convergence of node points at the juncture of pipe-nozzle for longitudinal thermal stress factor at point C_1 of the pipe

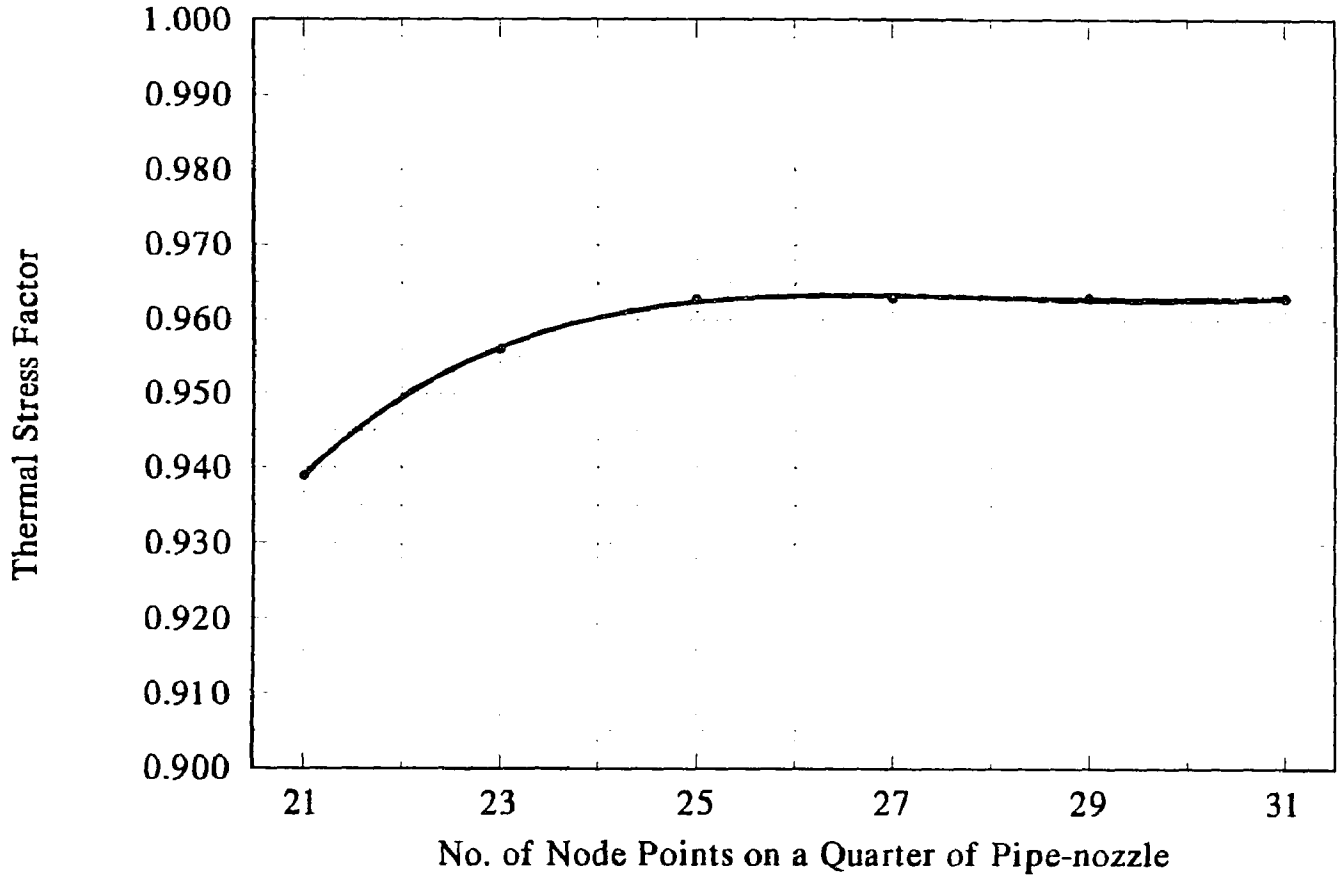

Figure B5 Convergence of node points at the juncture of pipe-nozzle for circumferential thermal stress factor at point A_1 of the pipe

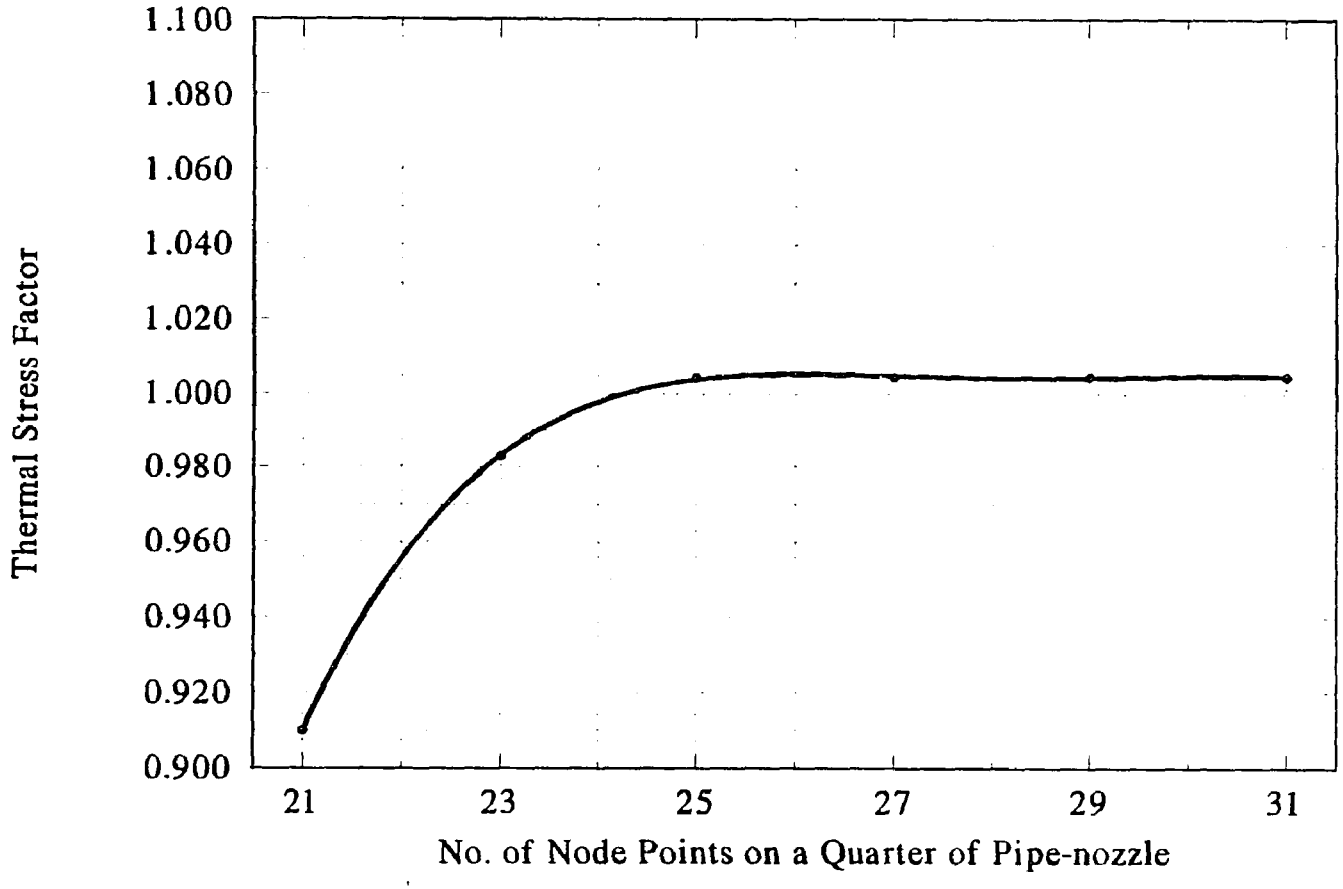

Figure B6 Convergence of node points at the juncture of pipe-nozzle for circumferential thermal stress factor at point A_i of the pipe

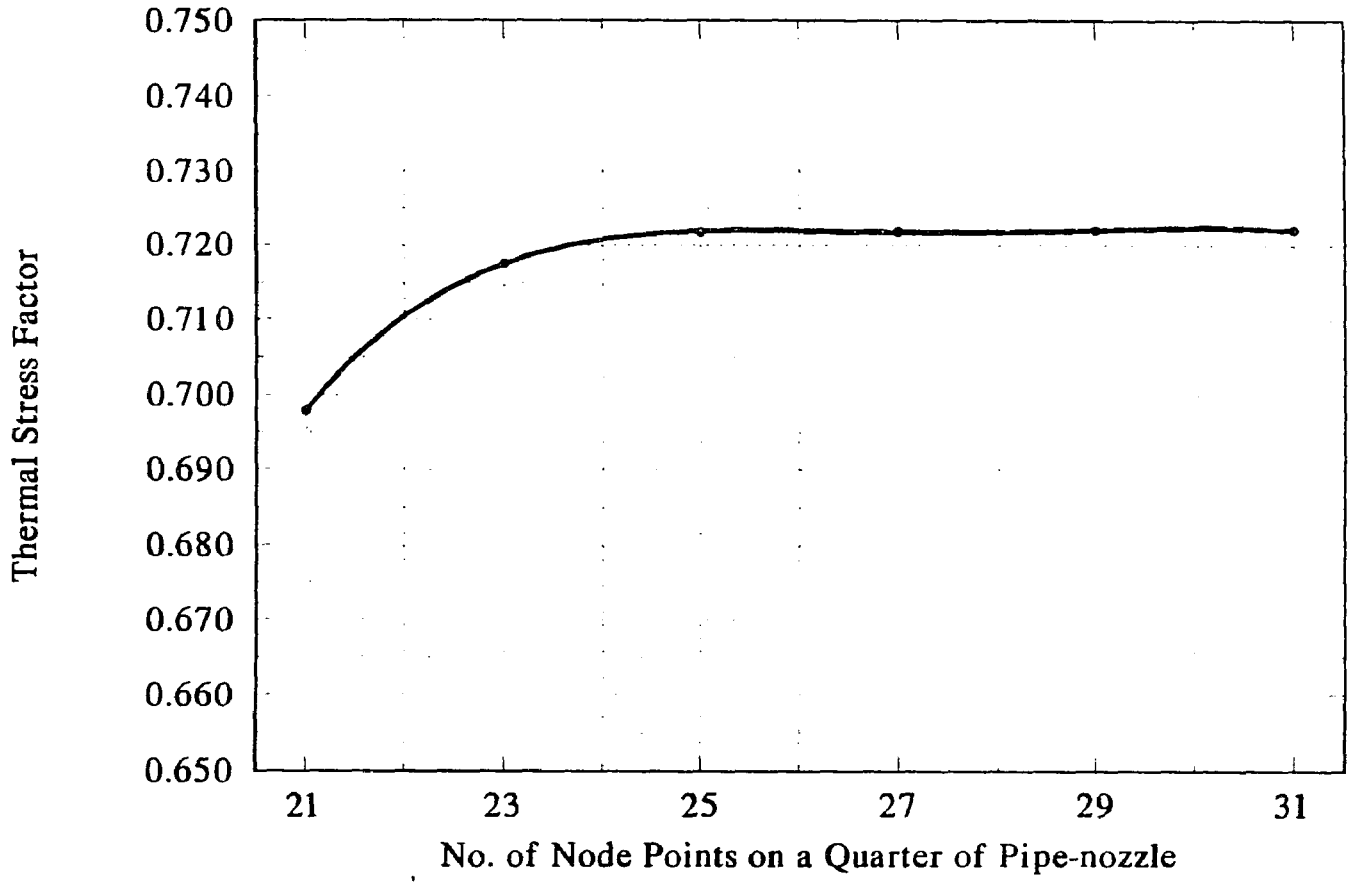

Figure B7 Convergence of node points at the juncture of pipe-nozzle for circumferential thermal stress factor at point C_1 of the pipe

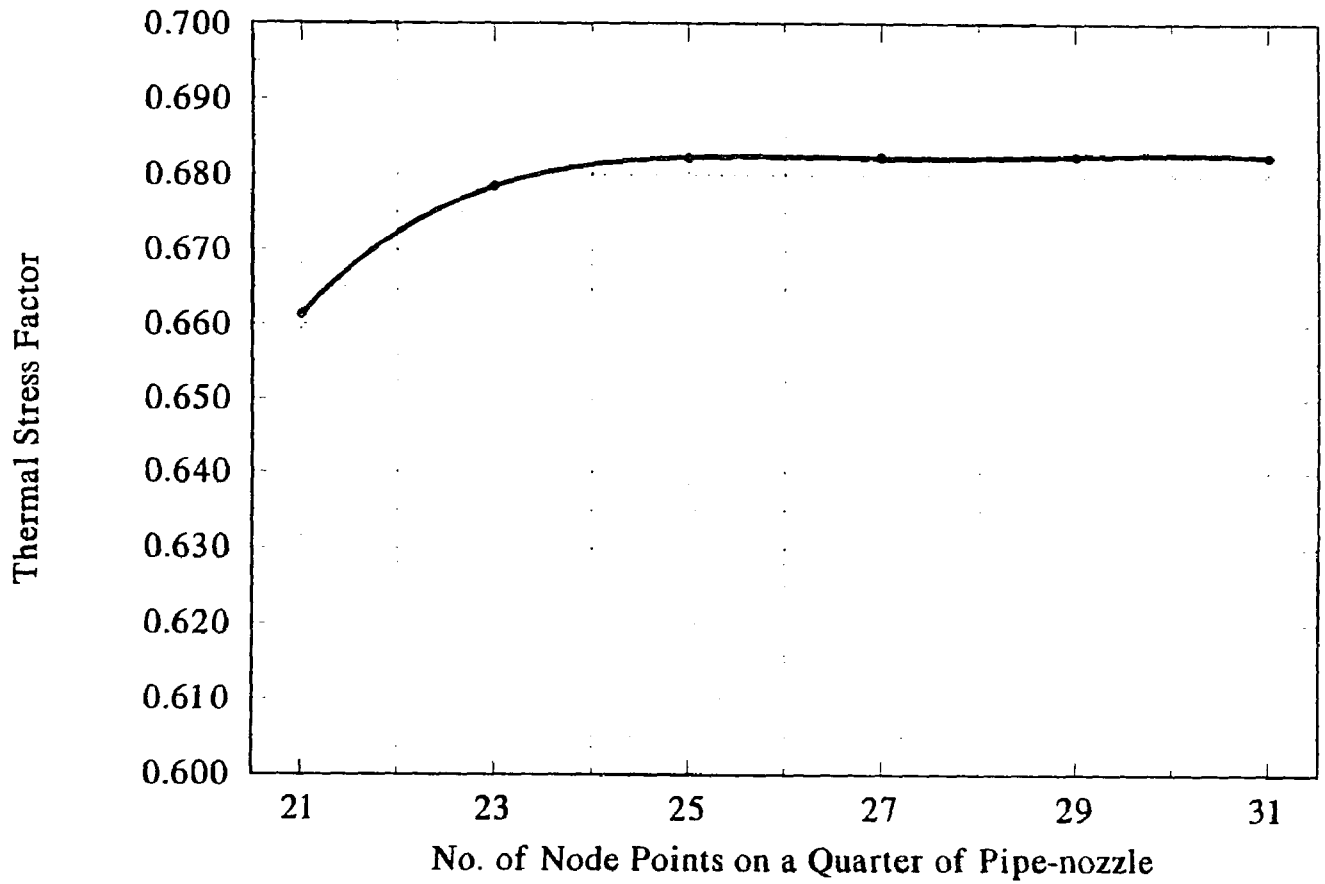

Figure B8 Convergence of node points at the juncture of pipe-nozzle for circumferential thermal stress factor at point C_1 of the pipe

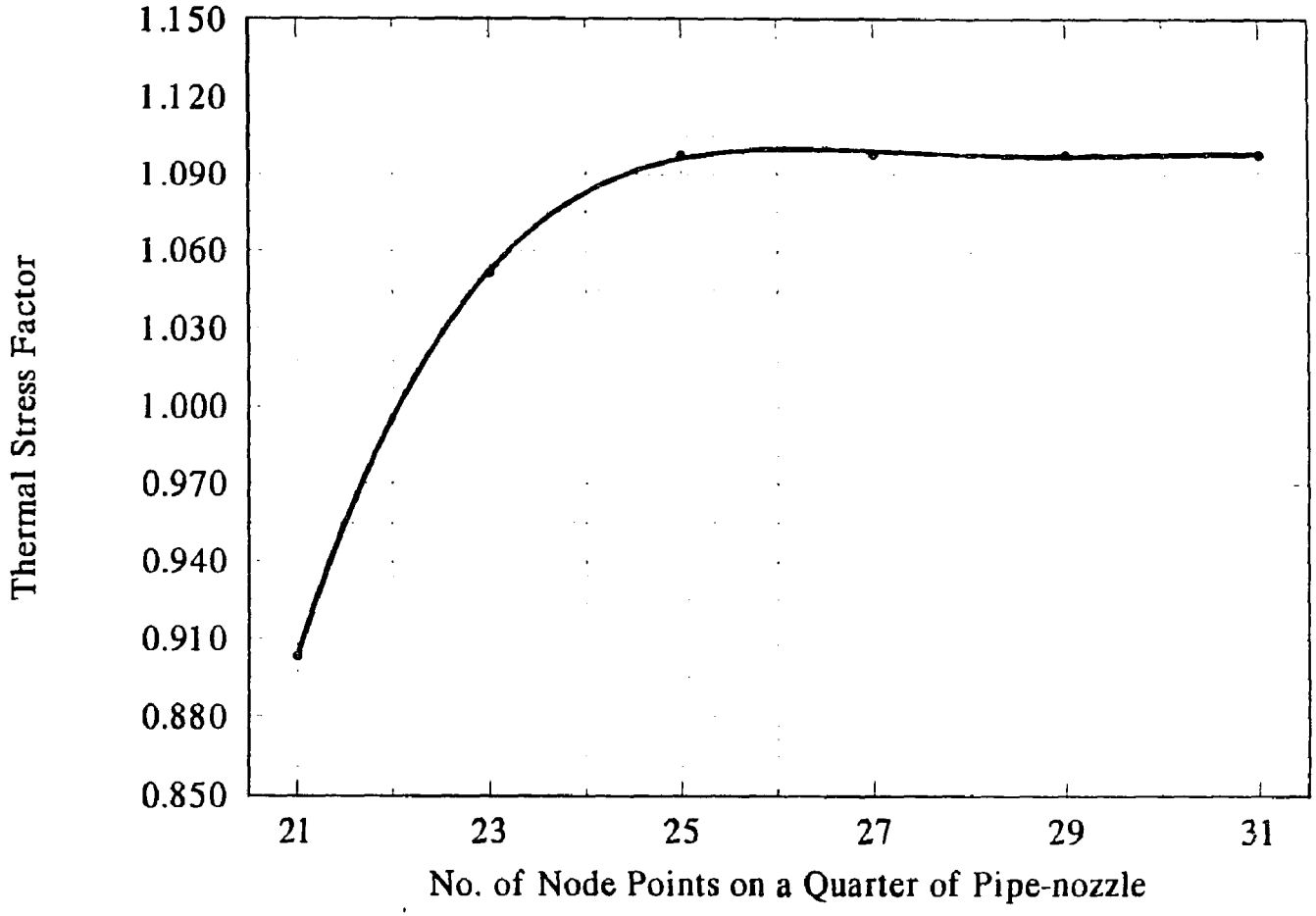

Figure B9 Convergence of node points at the juncture of pipe-nozzle for longitudinal thermal stress factor at point A of the nozzle

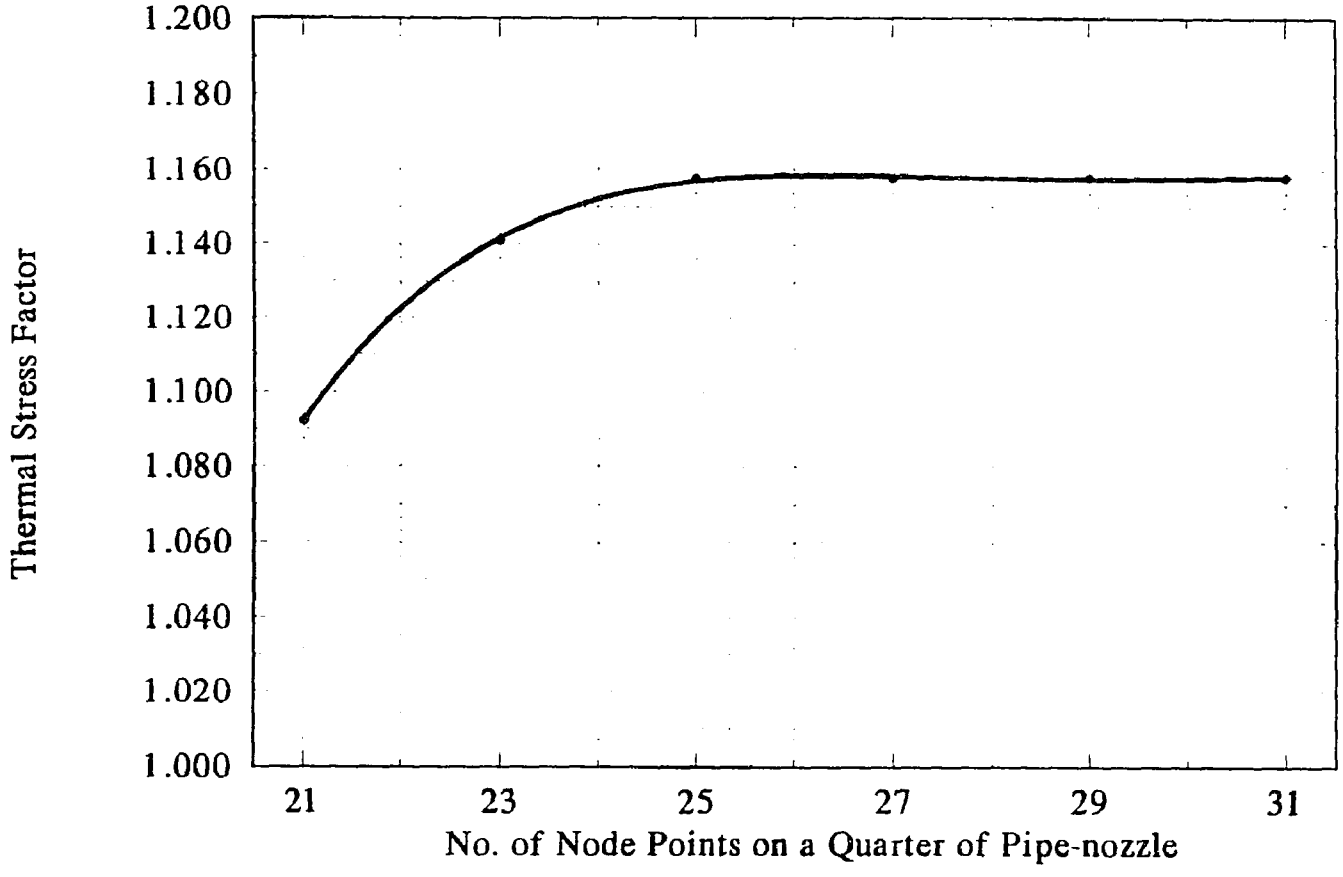

Figure B10 Convergence of node points at the juncture of pipe-nozzle for longitudinal thermal stress factor at point A_i of the nozzle

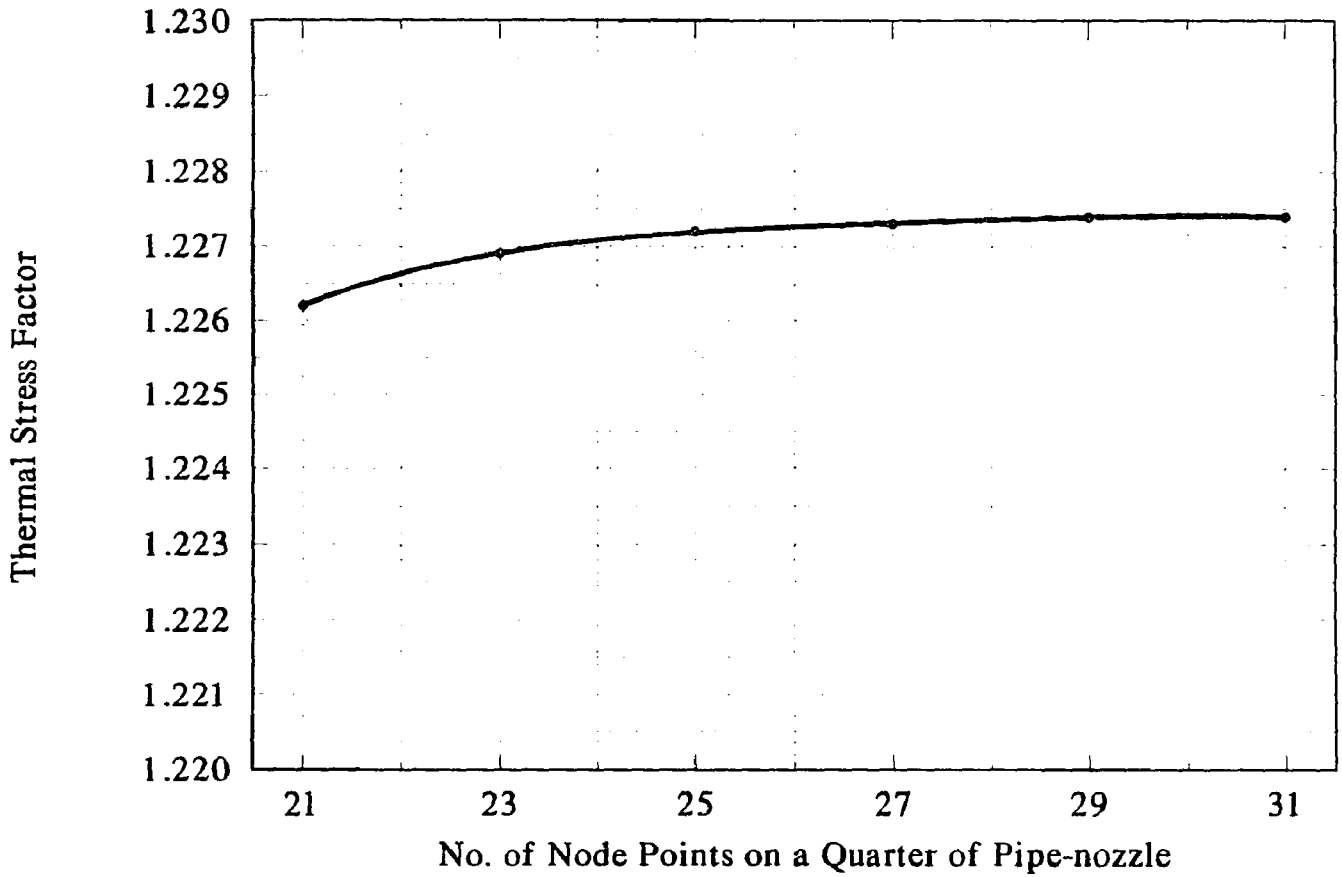

Figure B11 Convergence of node points at the juncture of pipe-nozzle for longitudinal thermal stress factor at point C_i of the nozzle

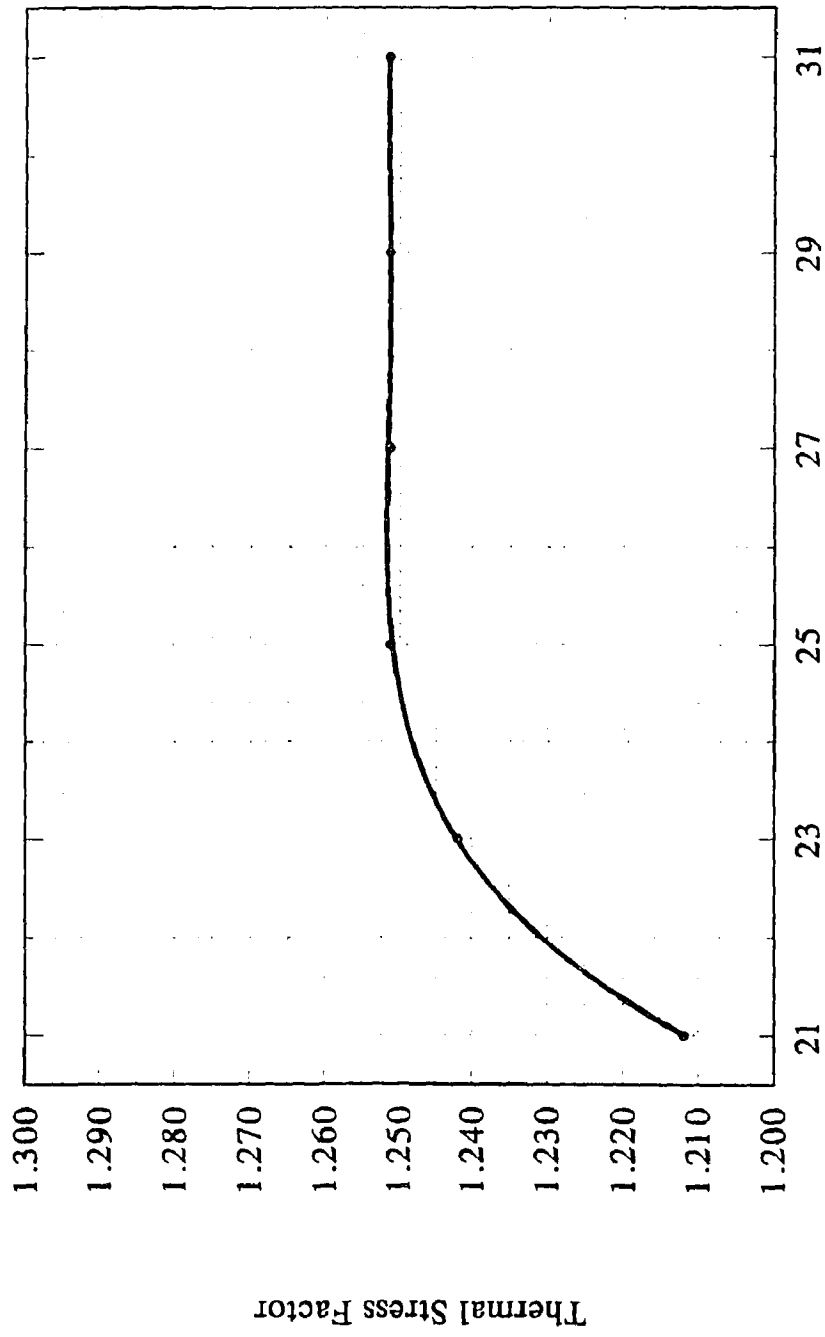

Figure B12 Convergence of node points at the juncture of pipe-nozzle for longitudinal thermal stress factor at point C_i of the nozzle

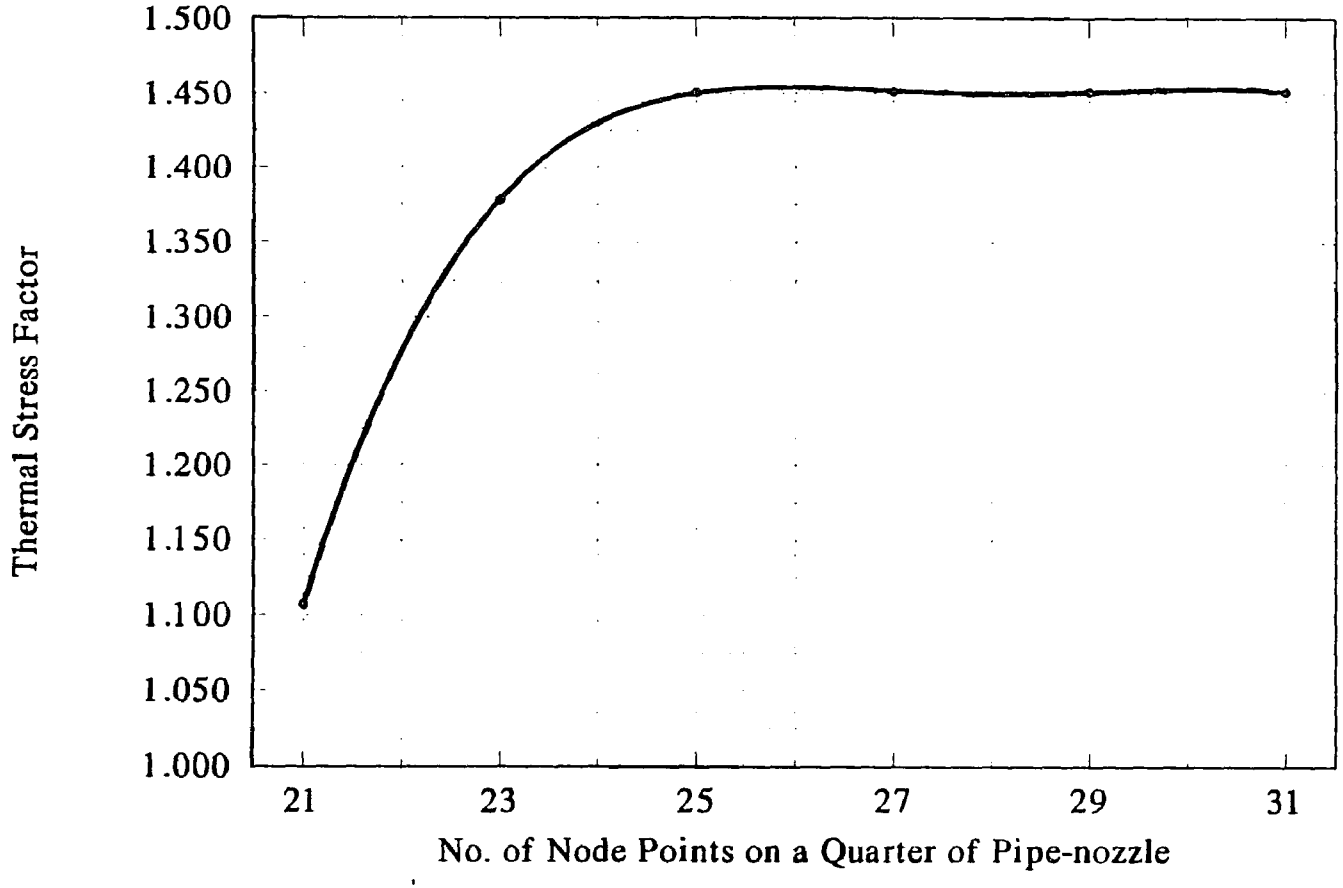

Figure B13 Convergence of node points at the juncture of pipe-nozzle for circumferential thermal stress factor at point A_u of the nozzle

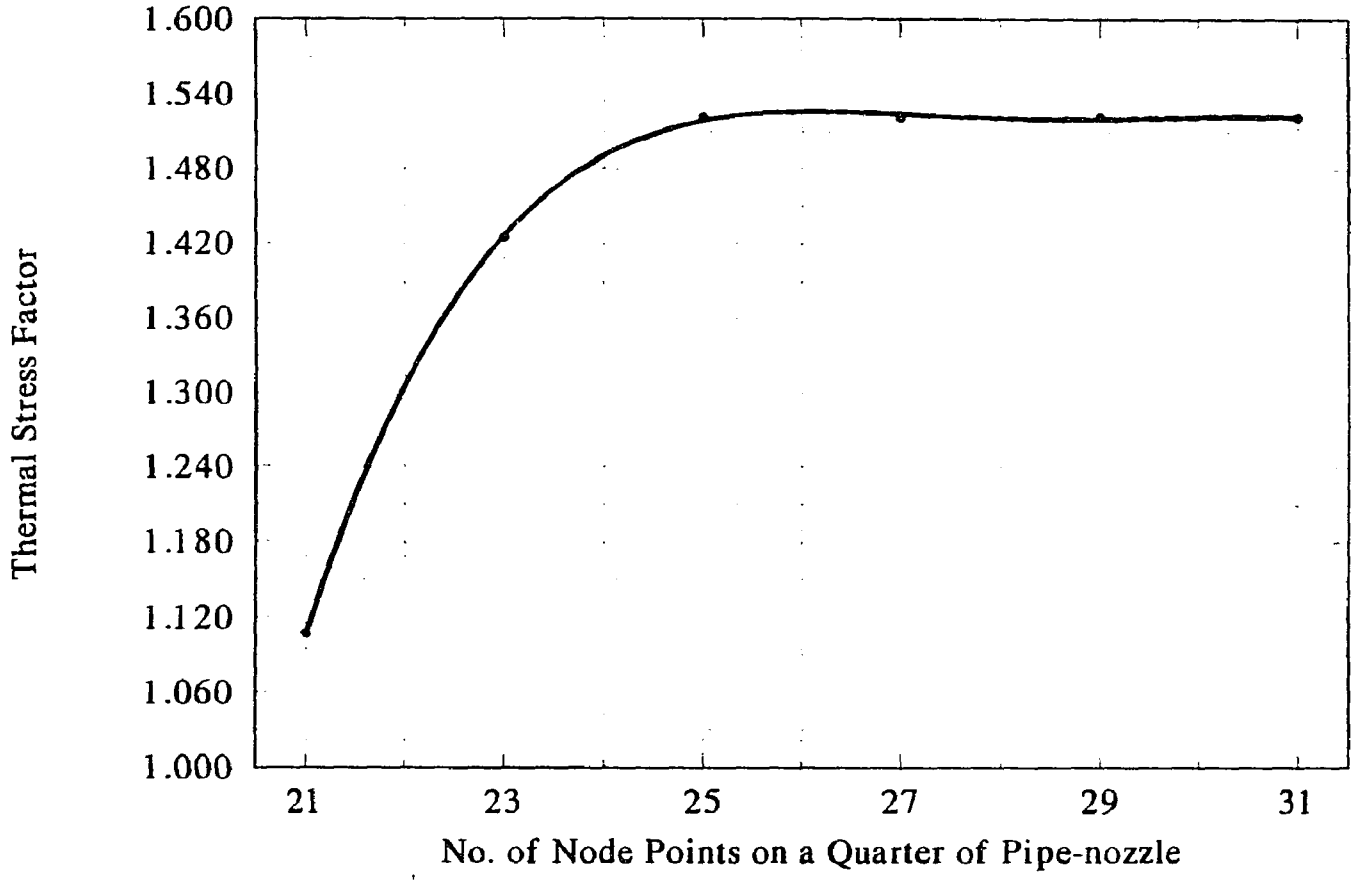

Figure B14 Convergence of node points at the juncture of pipe-nozzle for circumferential thermal stress factor at point A_1 of the nozzle

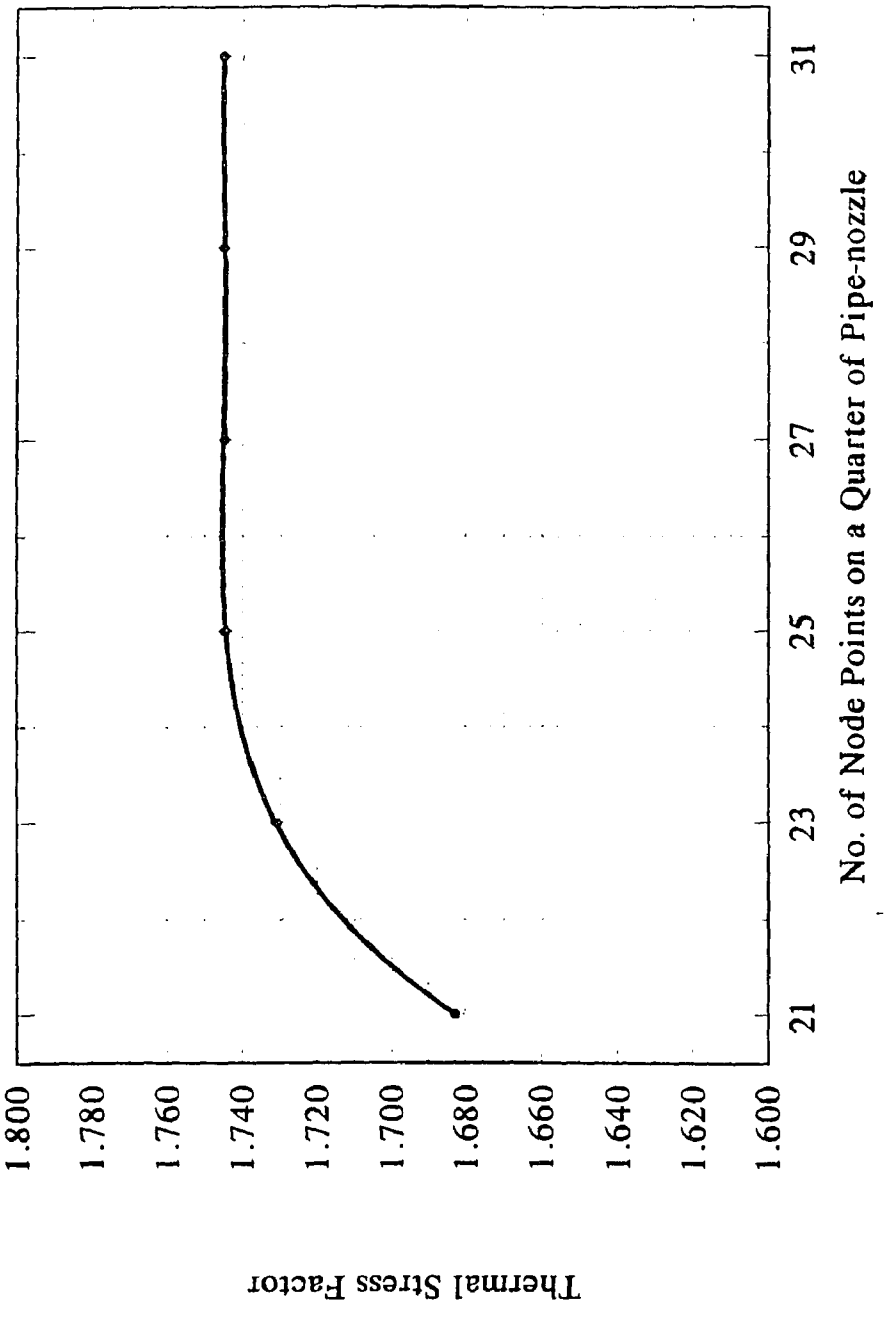

Figure B15 Convergence of node points at the juncture of pipe-nozzle for circumferential thermal stress factor at point C, of the nozzle

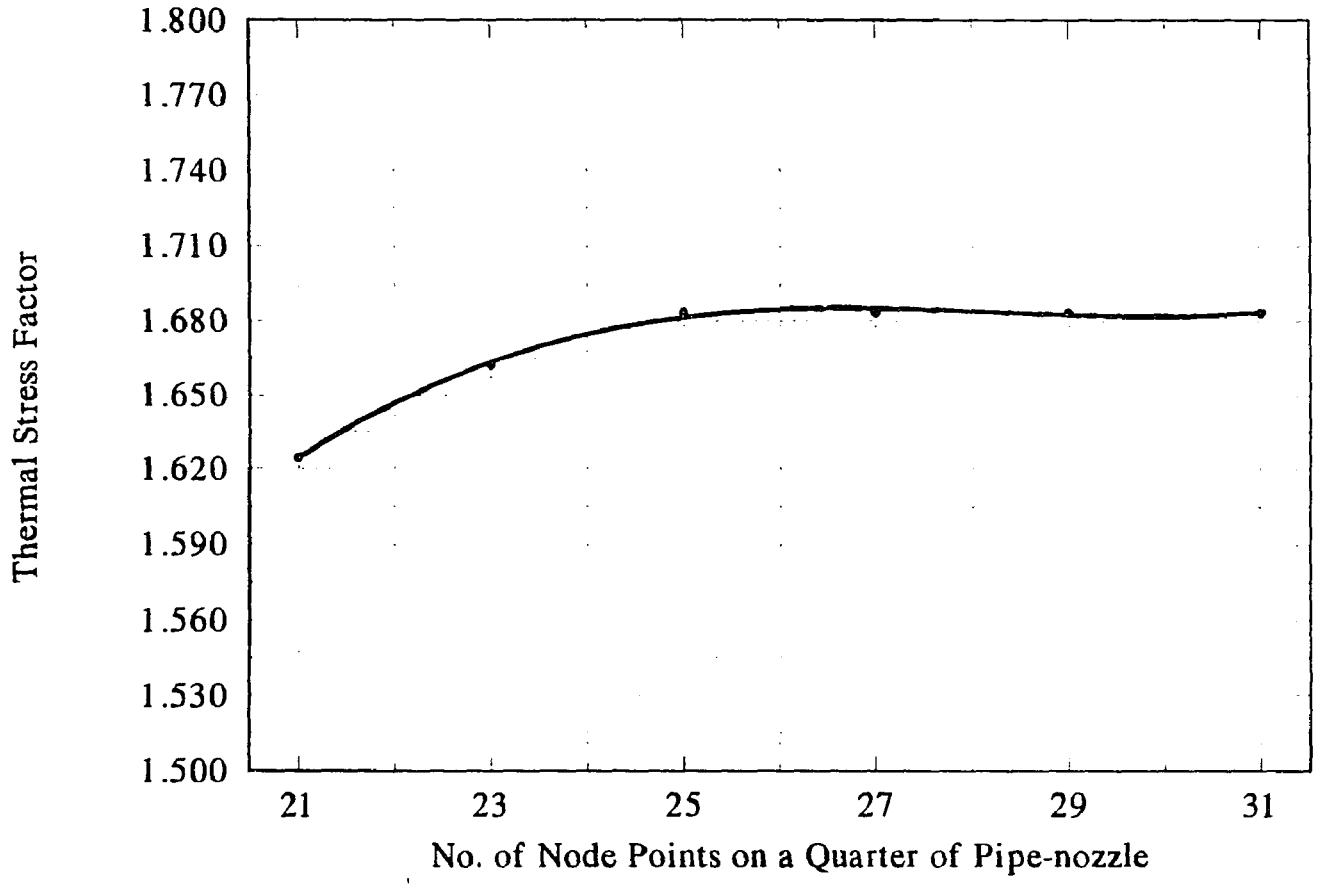

Figure B16 Convergence of node points at the juncture of pipe-nozzle for circumferential thermal stress factor at point C_i of the nozzle

APPENDIX C

ASYMPOTIC STUDY OF α_p AND α_n

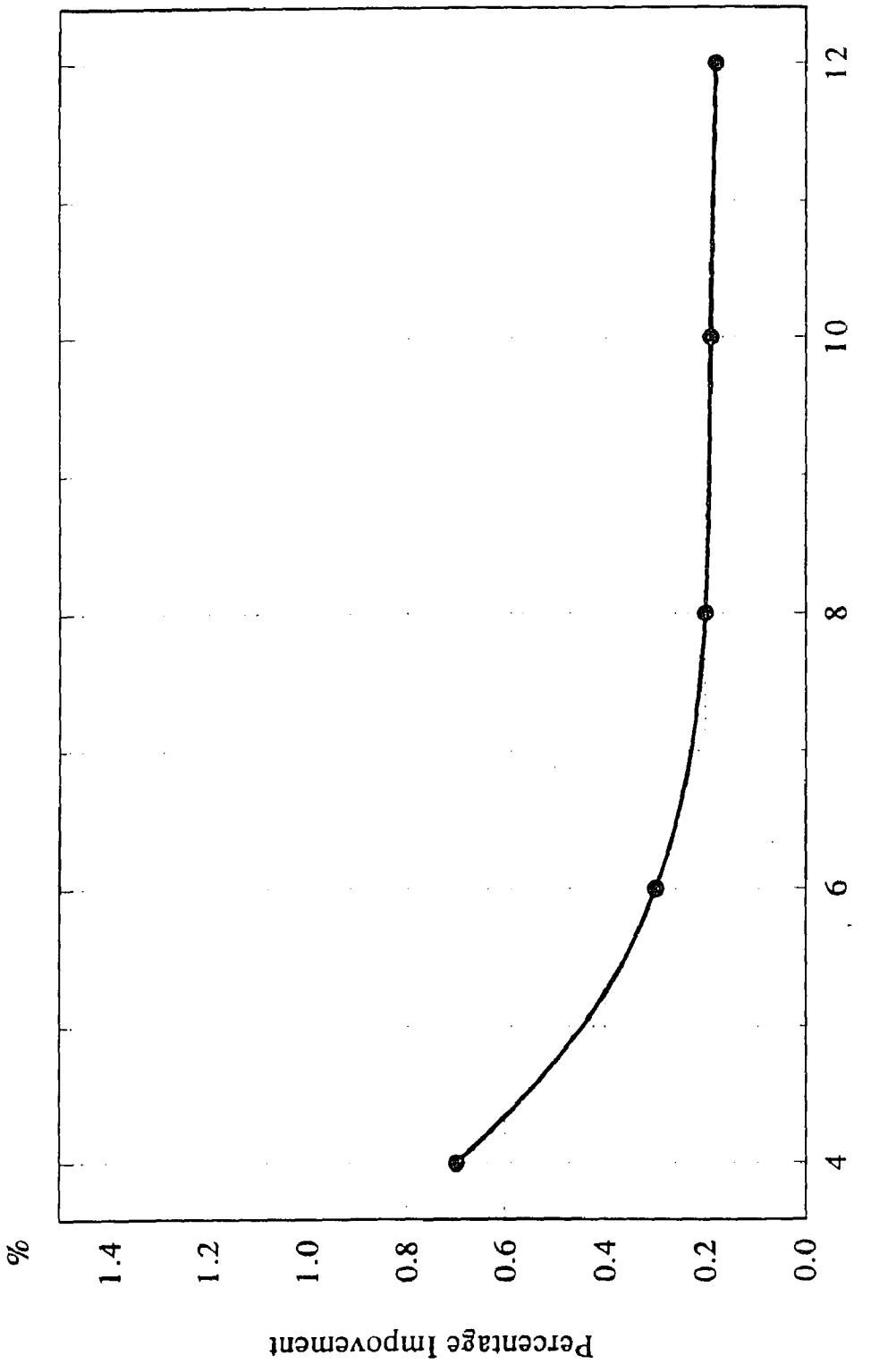

Figure C1 Percentage of improvement for larger α_p to previous α_p of longitudinal thermal stress factor at A_{ti} of the pipe

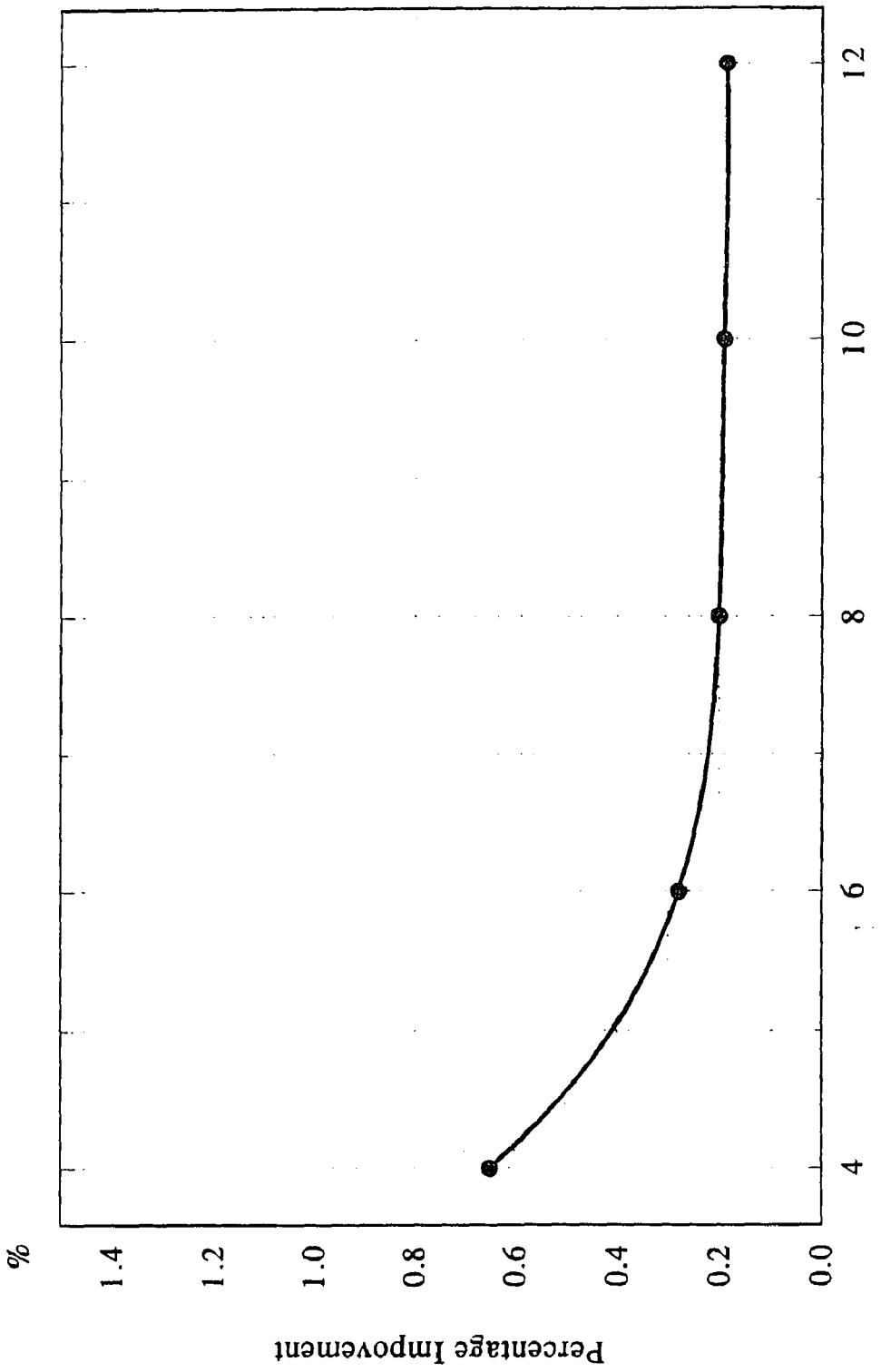

Figure C2 Percentage of improvement for larger α_p to previous α_p of longitudinal thermal stress factor at A_1 of the pipe

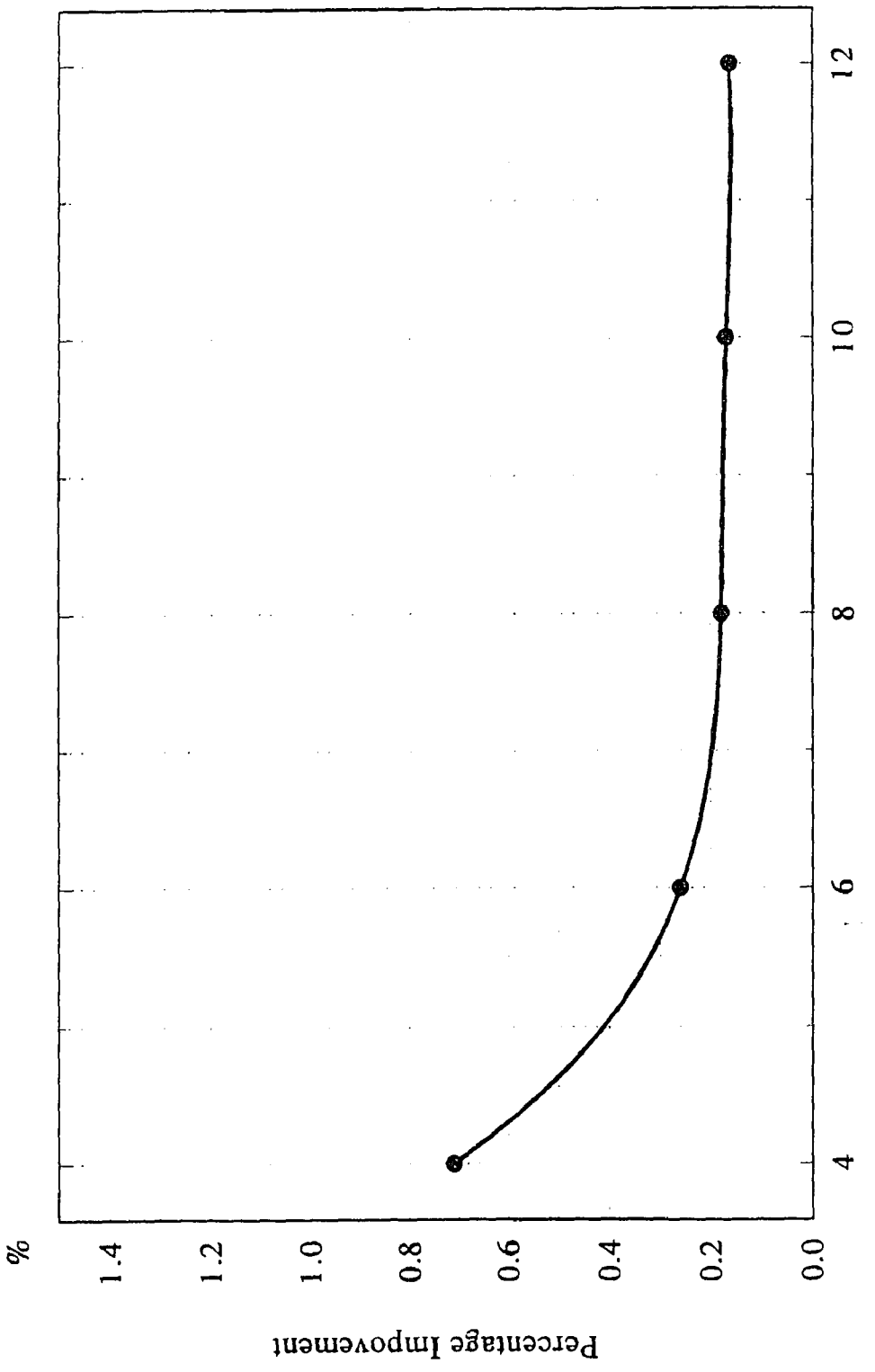

Figure C3 Percentage of improvement for larger α_p to previous α_p of longitudinal thermal stress factor at C_t of the pipe

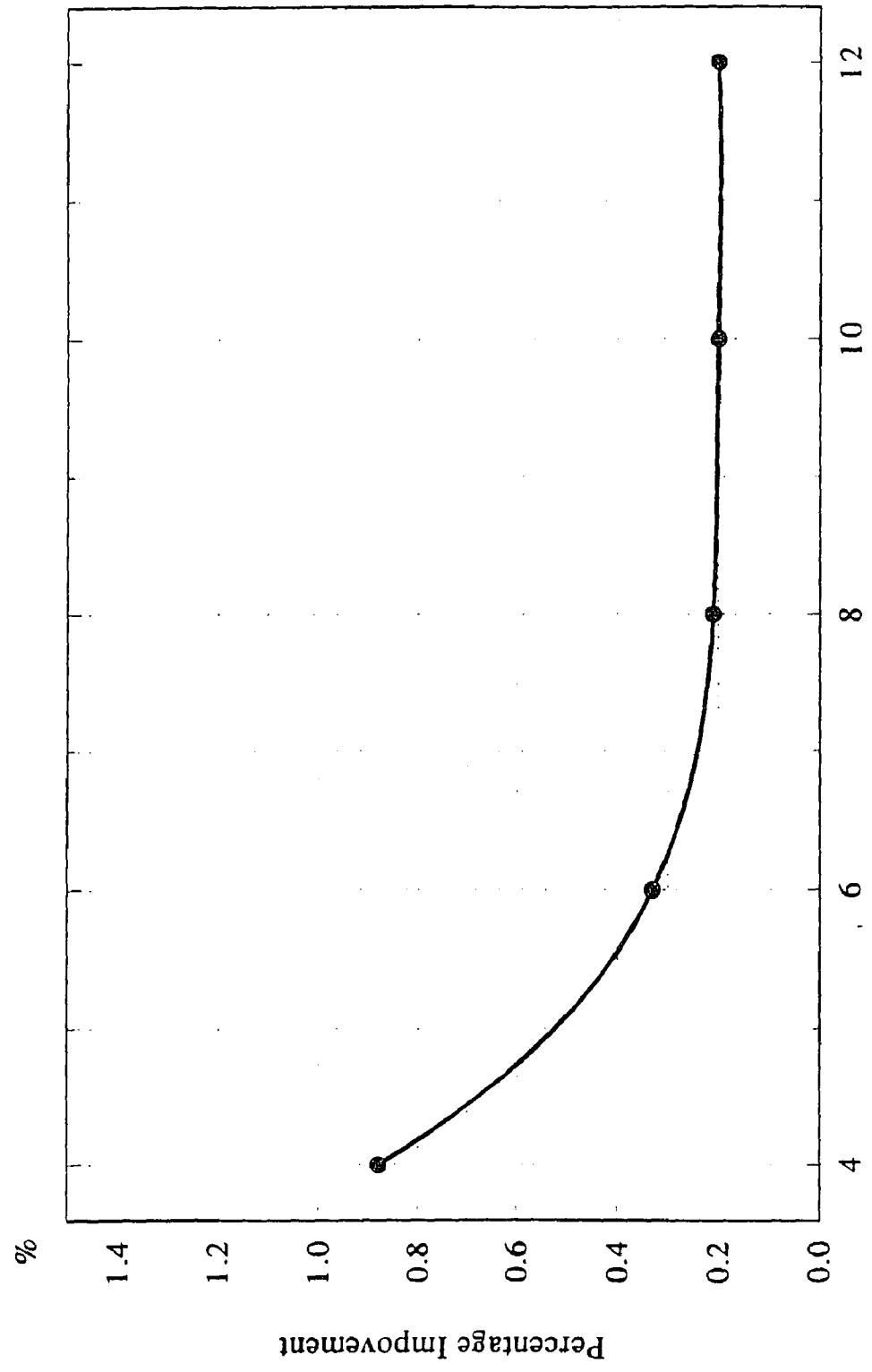

Figure C4 Percentage of improvement for larger α_p to previous α_p of longitudinal thermal stress factor at C_1 of the pipe

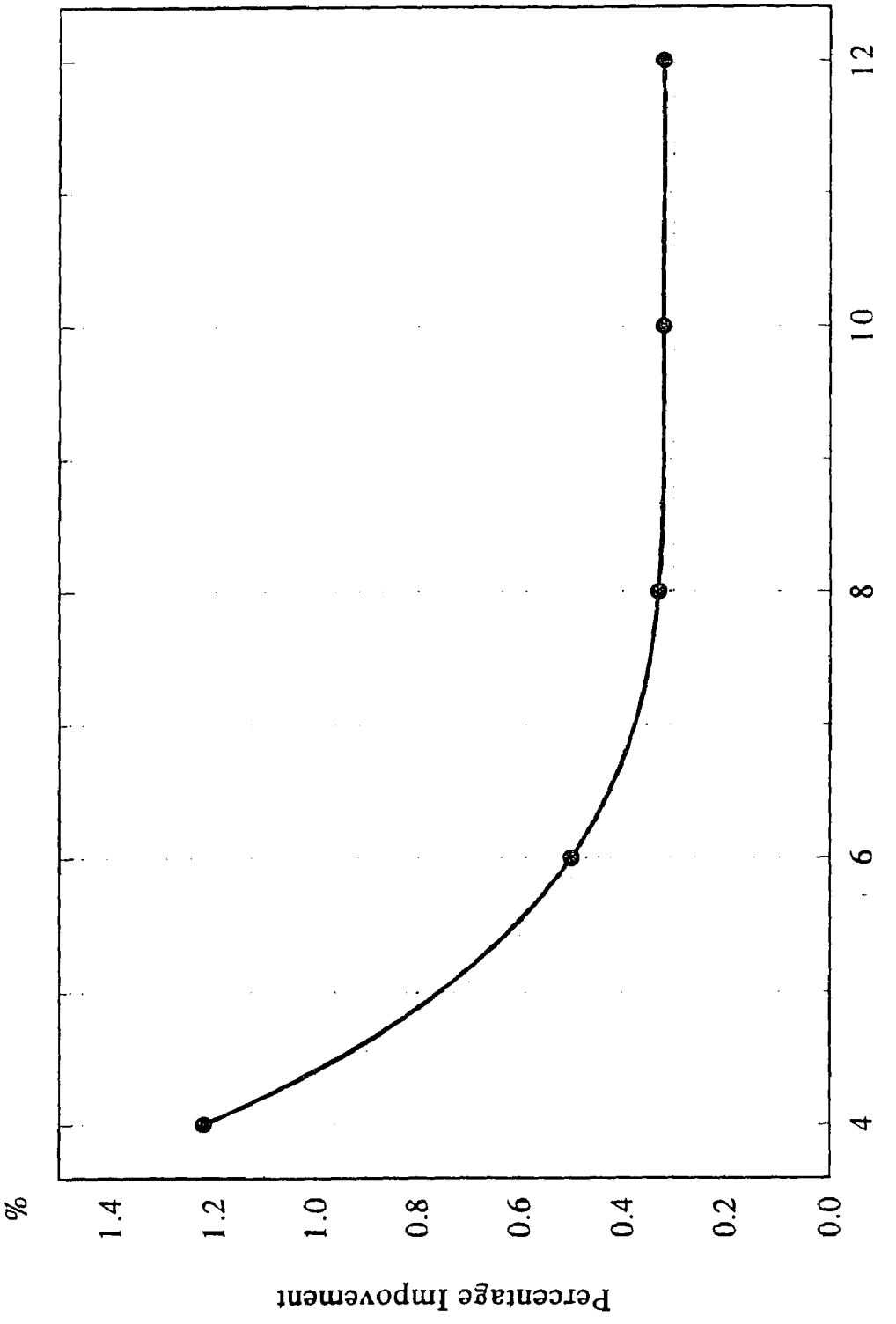

Figure C5 Percentage of improvement for larger α_p to previous α_p of circumferential thermal stress factor at A_1 of the pipe

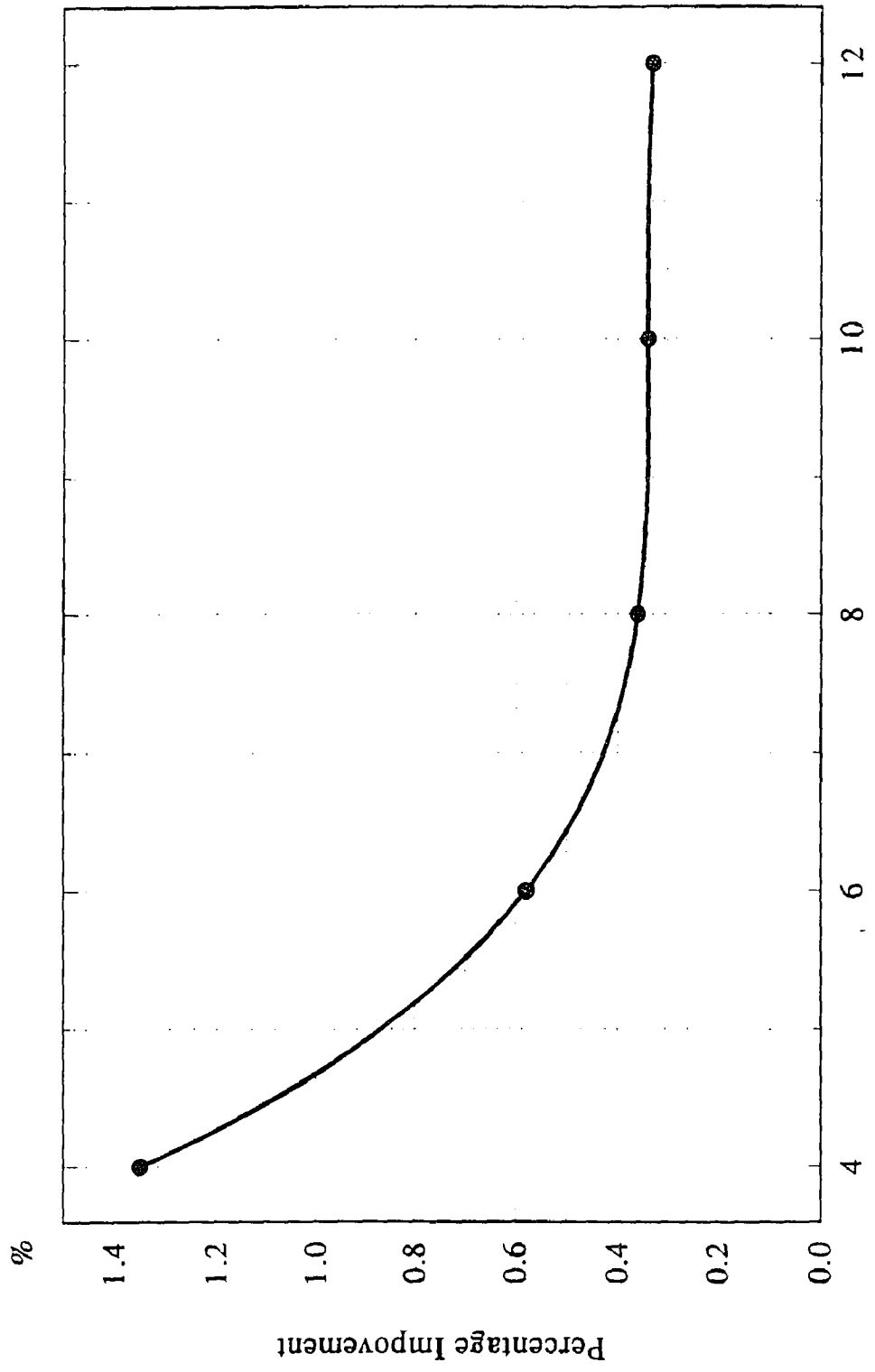

Figure C6 Percentage of improvement for larger α_p to previous α_p of circumferential thermal stress factor at A_1 of the pipe

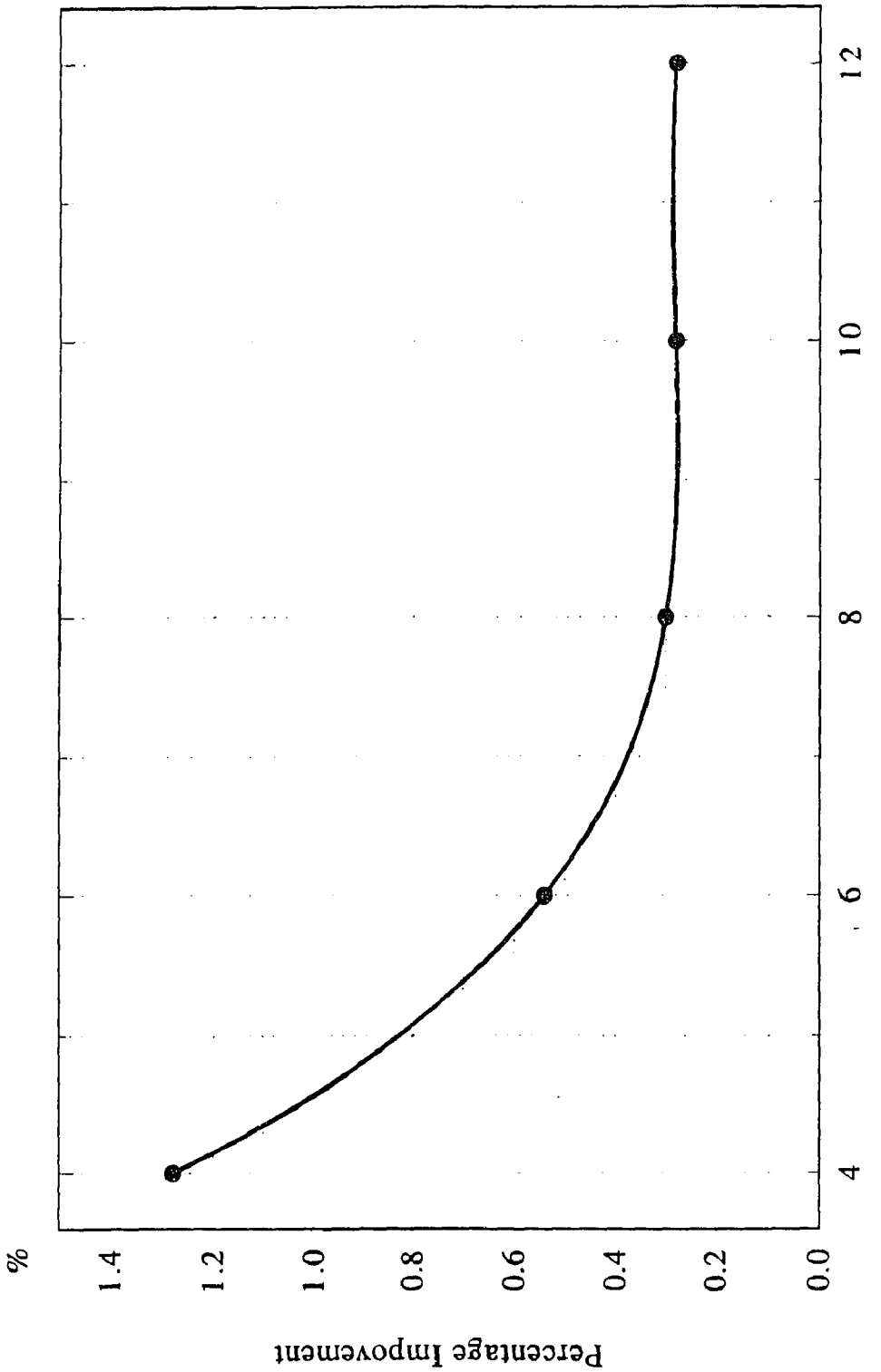

Figure C7 Percentage of improvement for larger α_p to previous α_p of circumferential thermal stress factor at C_1 of the pipe

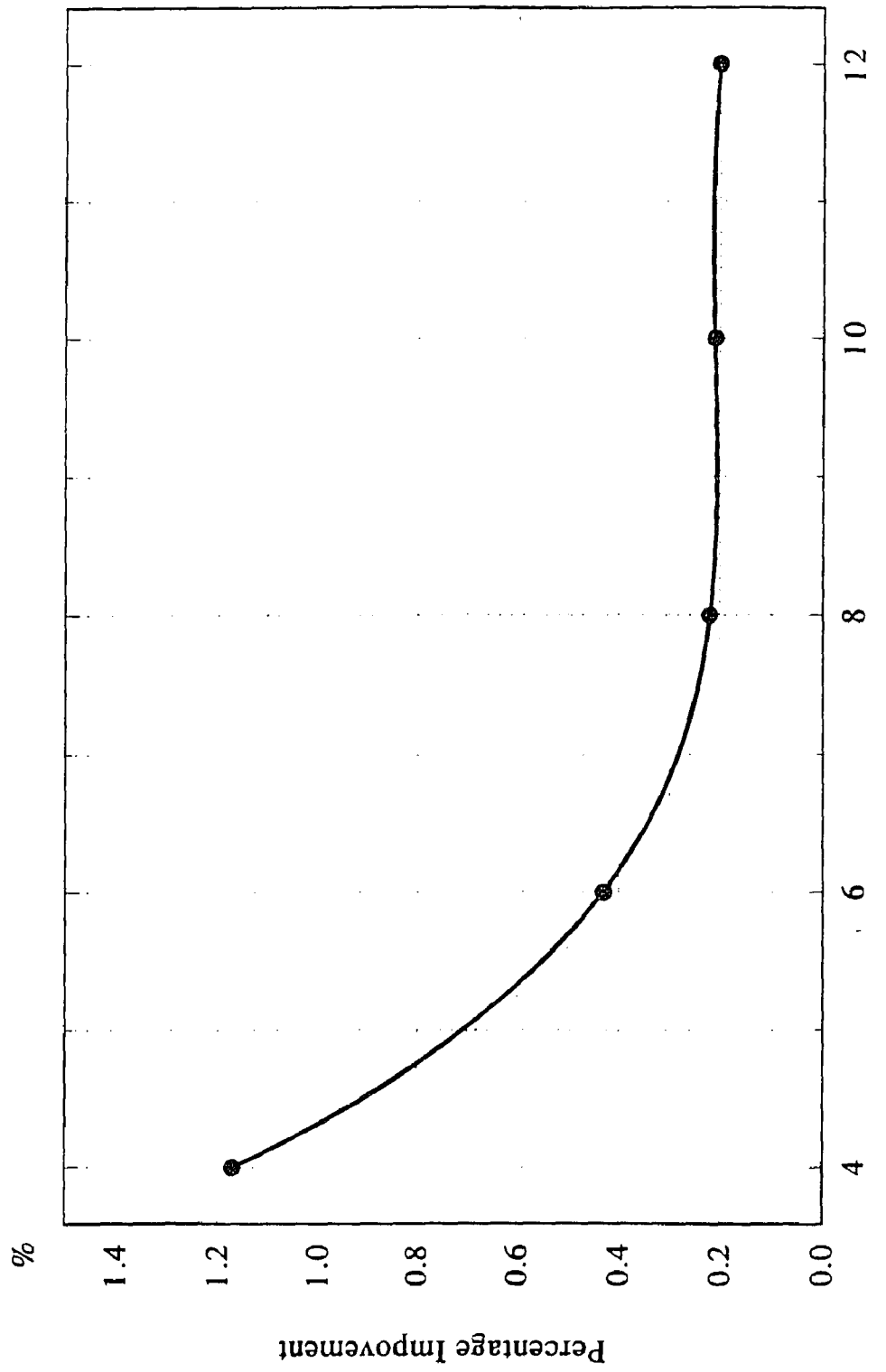

Figure C8 Percentage of improvement for larger α_p to previous α_p of circumferential thermal stress factor at C_1 of the pipe

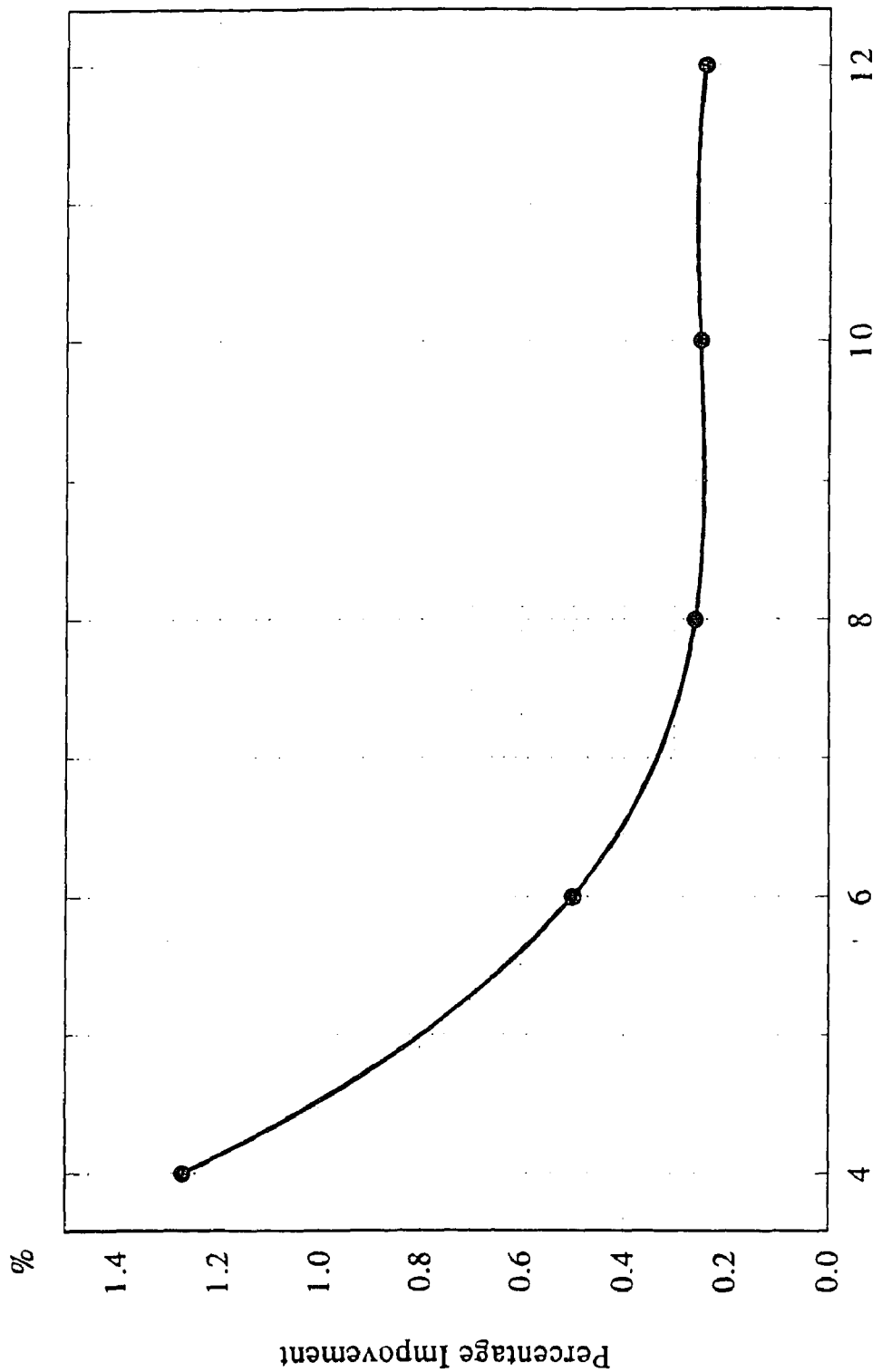

Figure C9 Percentage of improvement for larger α_p to previous α_p of longitudinal thermal stress factor at A_0 of the nozzle

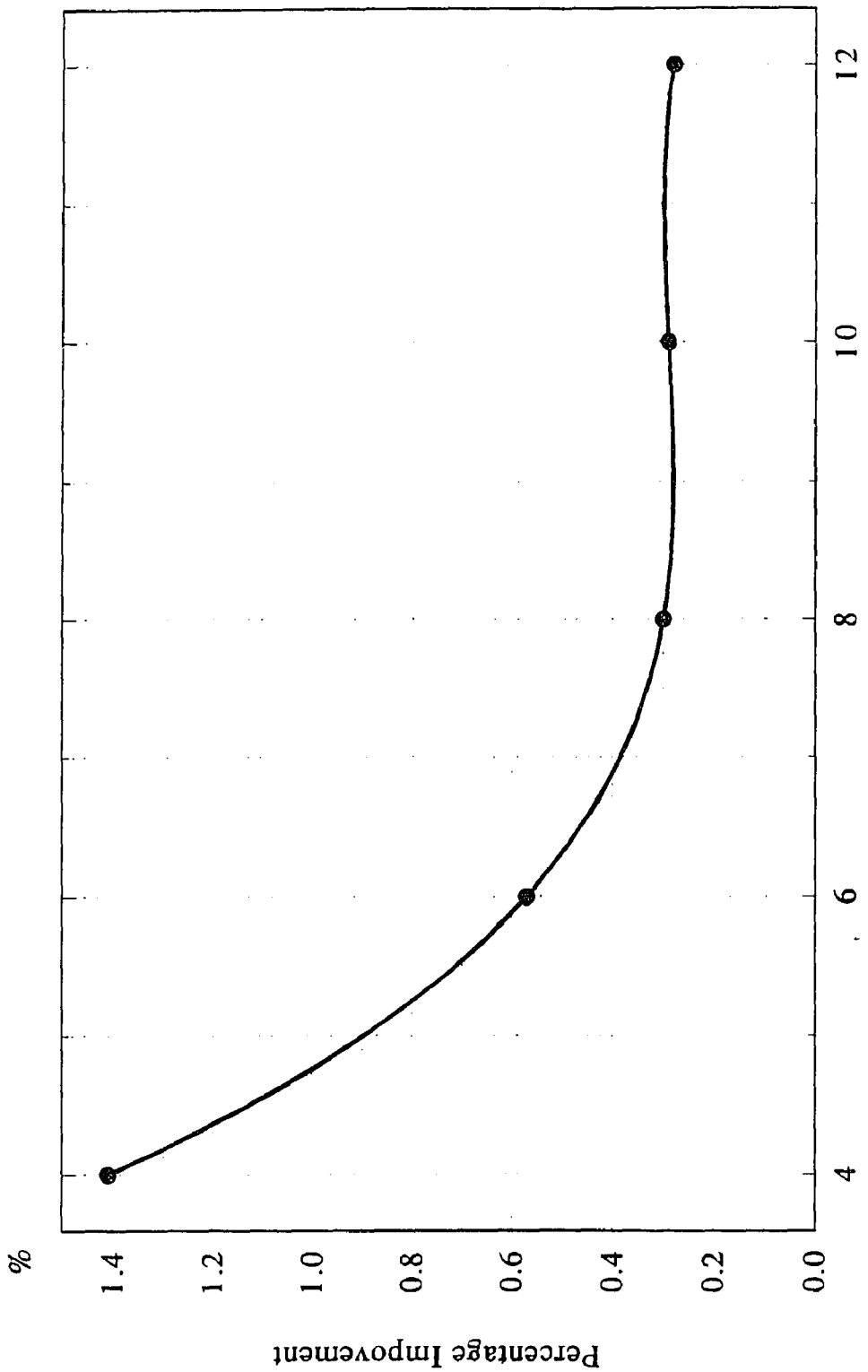

Figure C10 Percentage of improvement for larger α_p to previous α_p of longitudinal thermal stress factor at A_1 of the nozzle

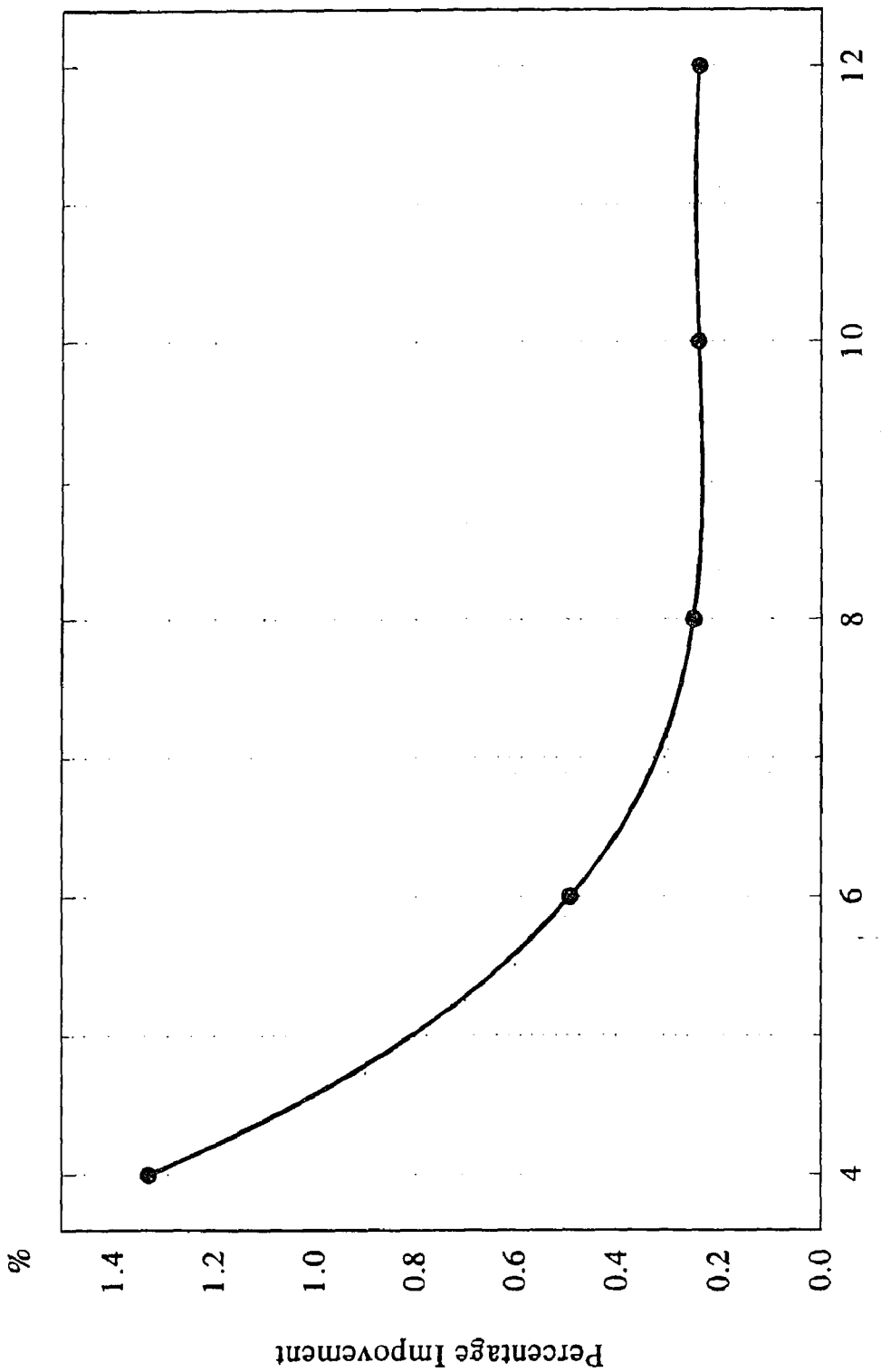

Figure C11 Percentage of improvement for larger α_p to previous α_p of longitudinal thermal stress factor at C_{∞} of the nozzle

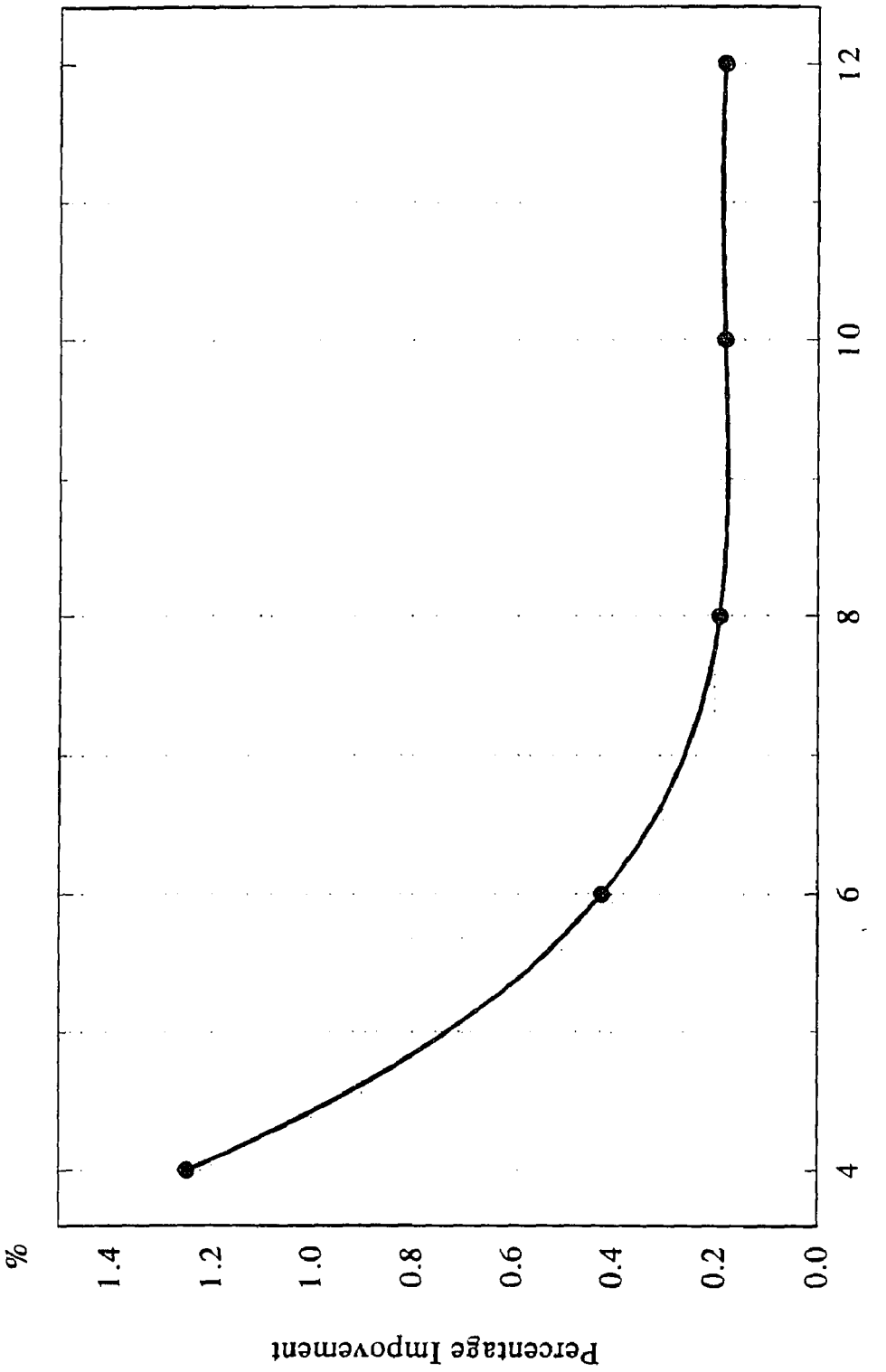

Figure C12 Percentage of improvement for larger α_p to previous α_p of longitudinal thermal stress factor at C_i of the nozzle

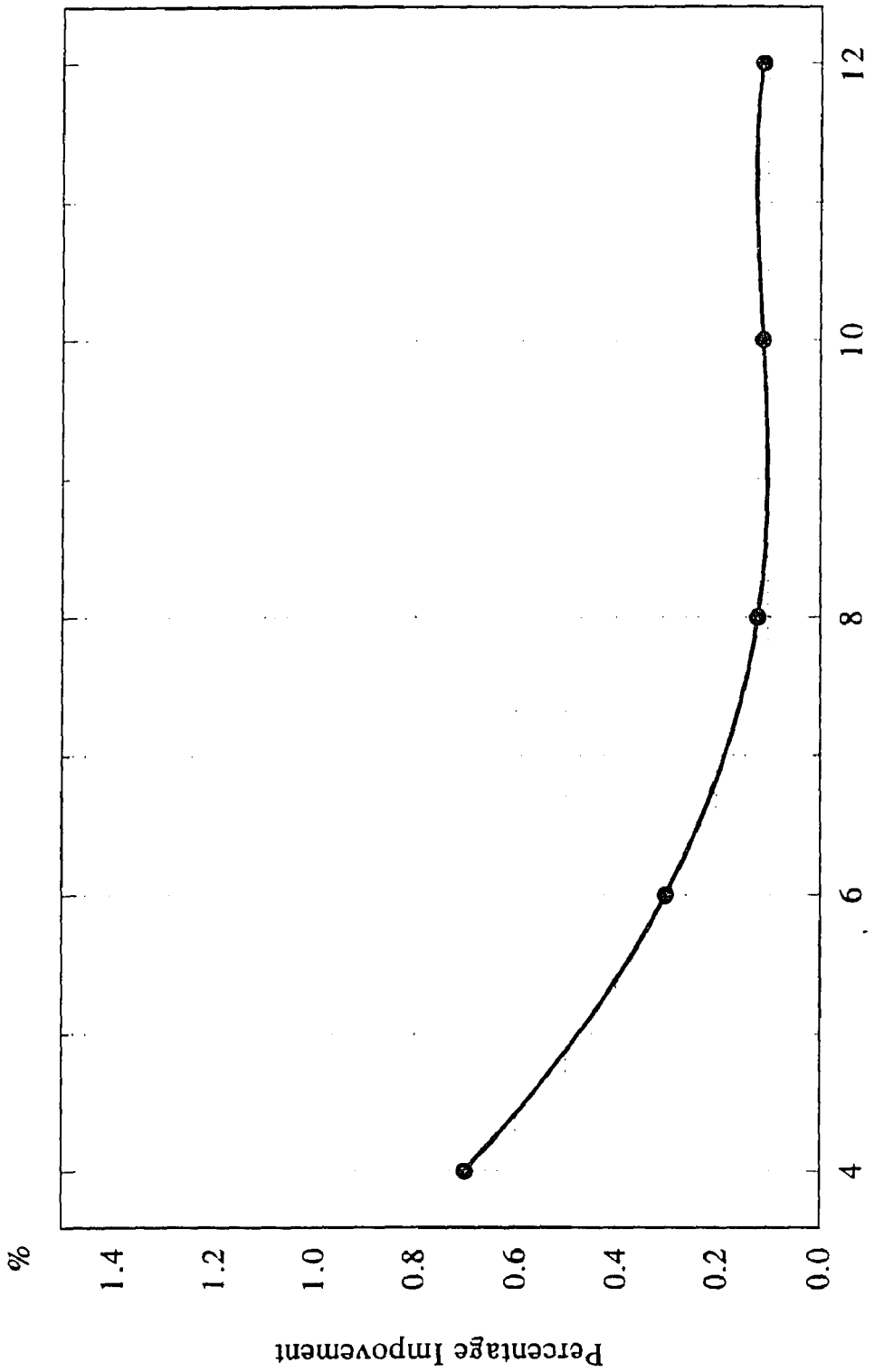

Figure C13 Percentage of improvement for larger α_p to previous α_p of circumferential thermal stress factor at $A_{..}$ of the nozzle

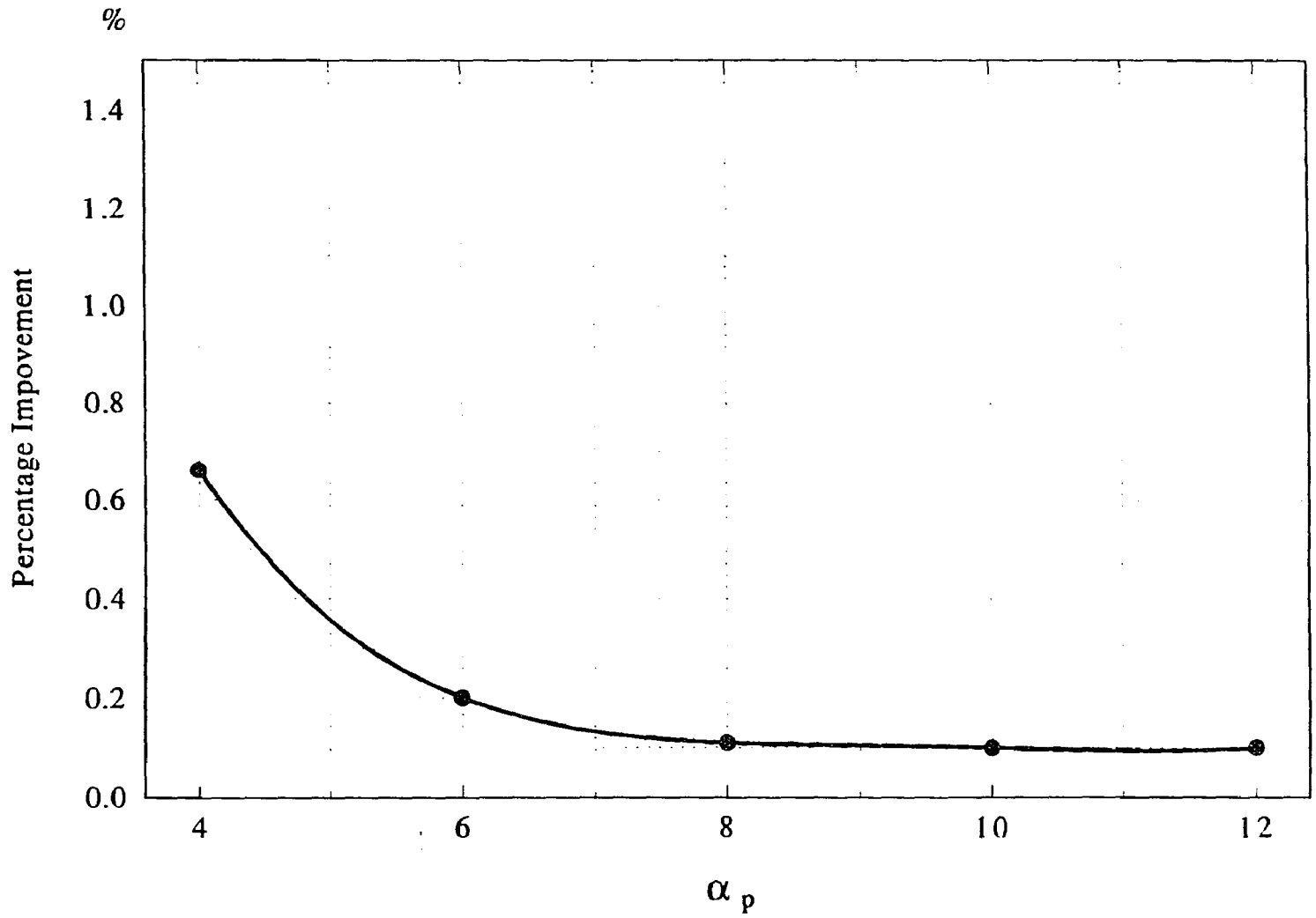

Figure C14 Percentage of improvement for larger α_p to previous α_p of circumferential thermal stress factor at A_i of the nozzle

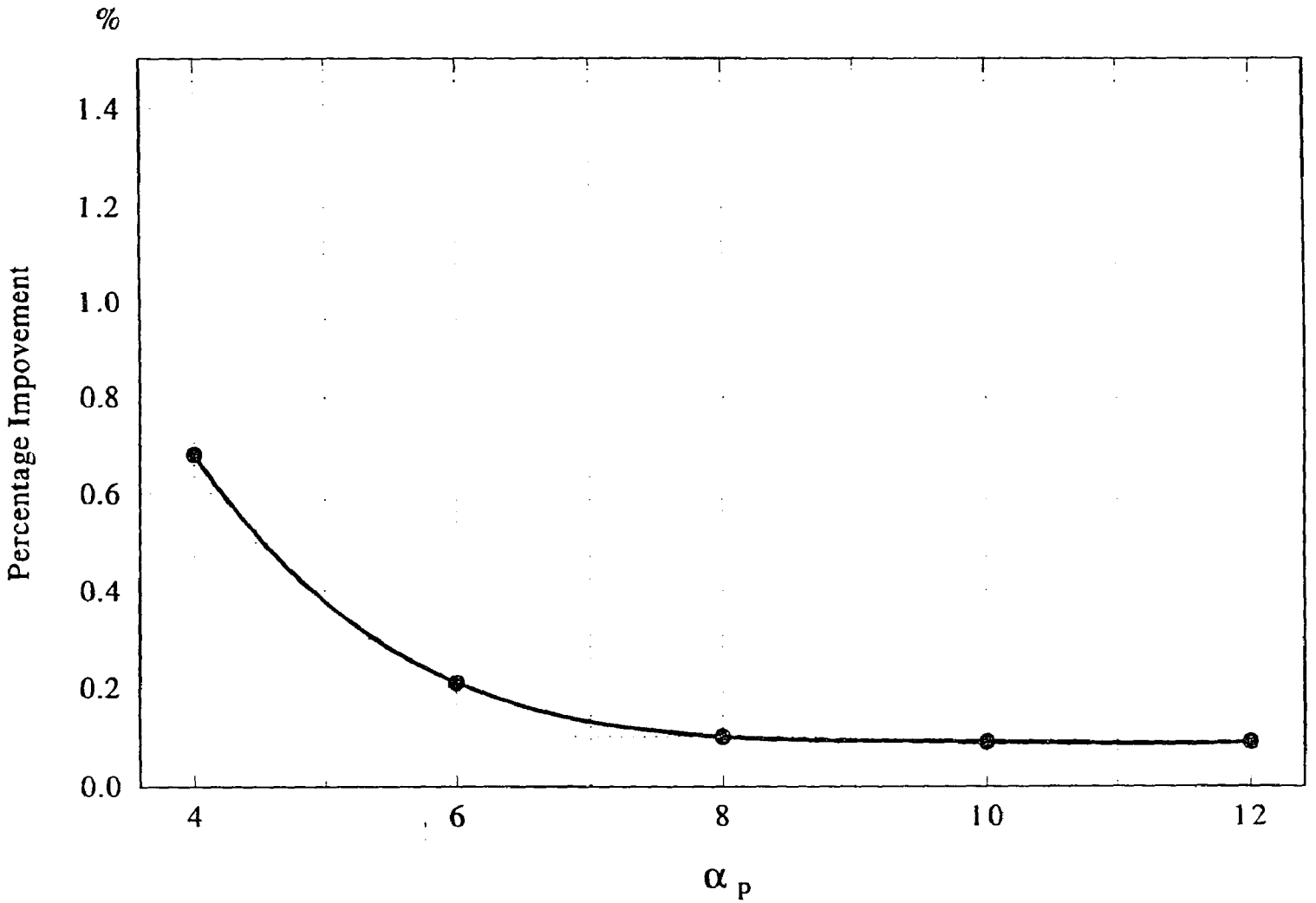

Figure C15 Percentage of improvement for larger α_p to previous α_p of circumferential thermal stress factor at C_{α} of the nozzle

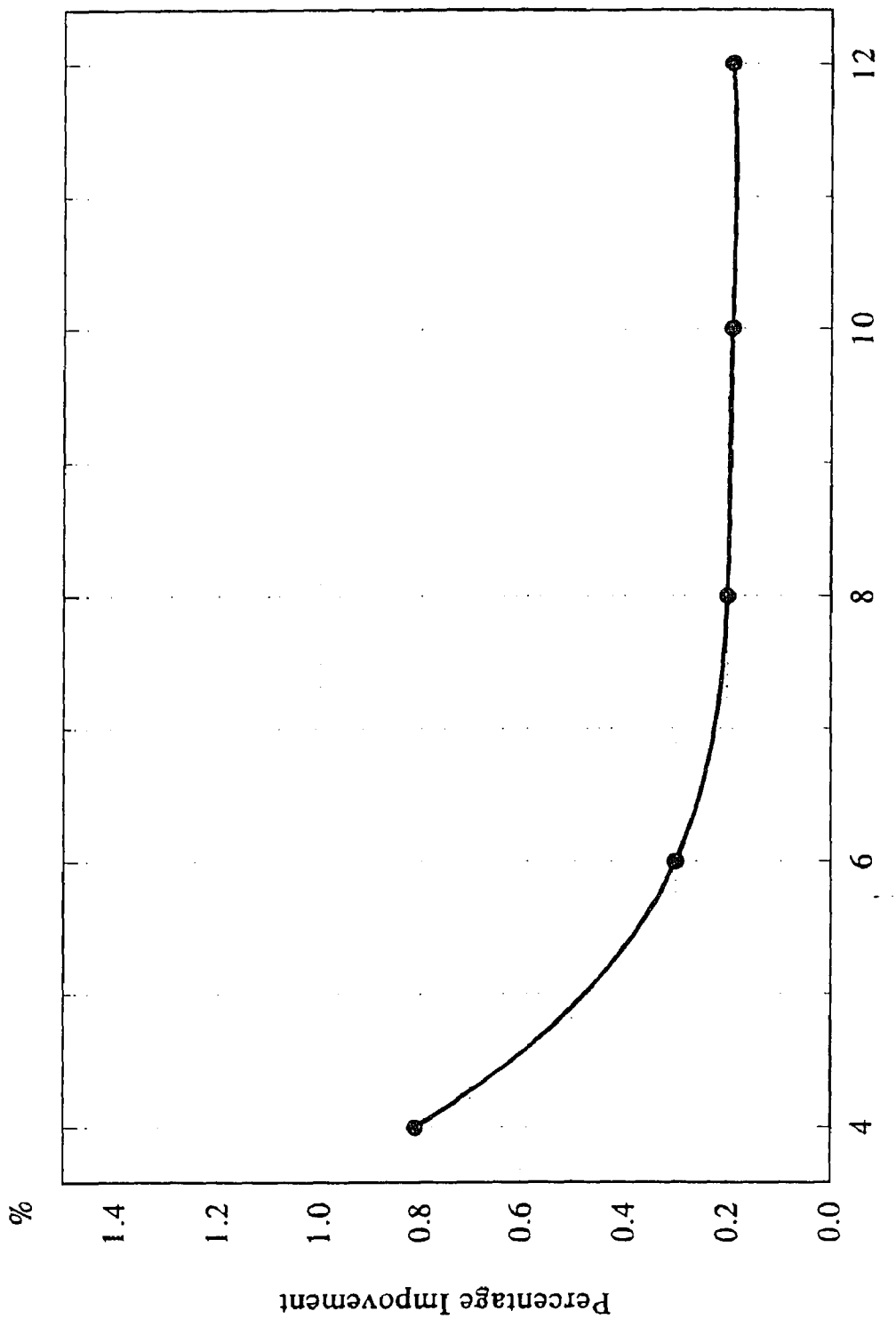

Figure C16 Percentage of improvement for larger α_p to previous α_p of circumferential thermal stress factor at C_i of the nozzle

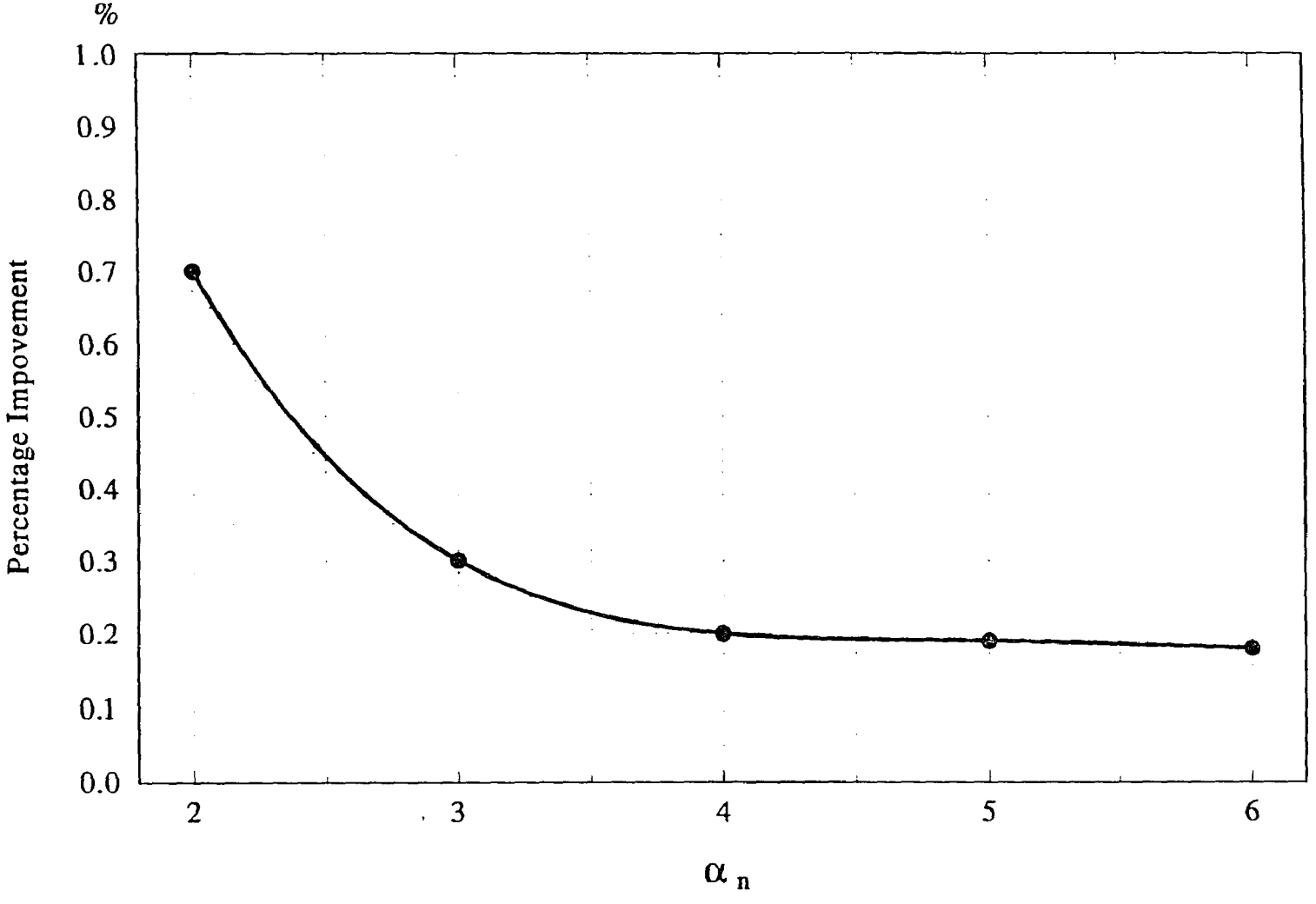

Figure C17 Percentage of improvement for larger α_n to previous α_n of longitudinal thermal stress factor at A_{t_1} of the pipe

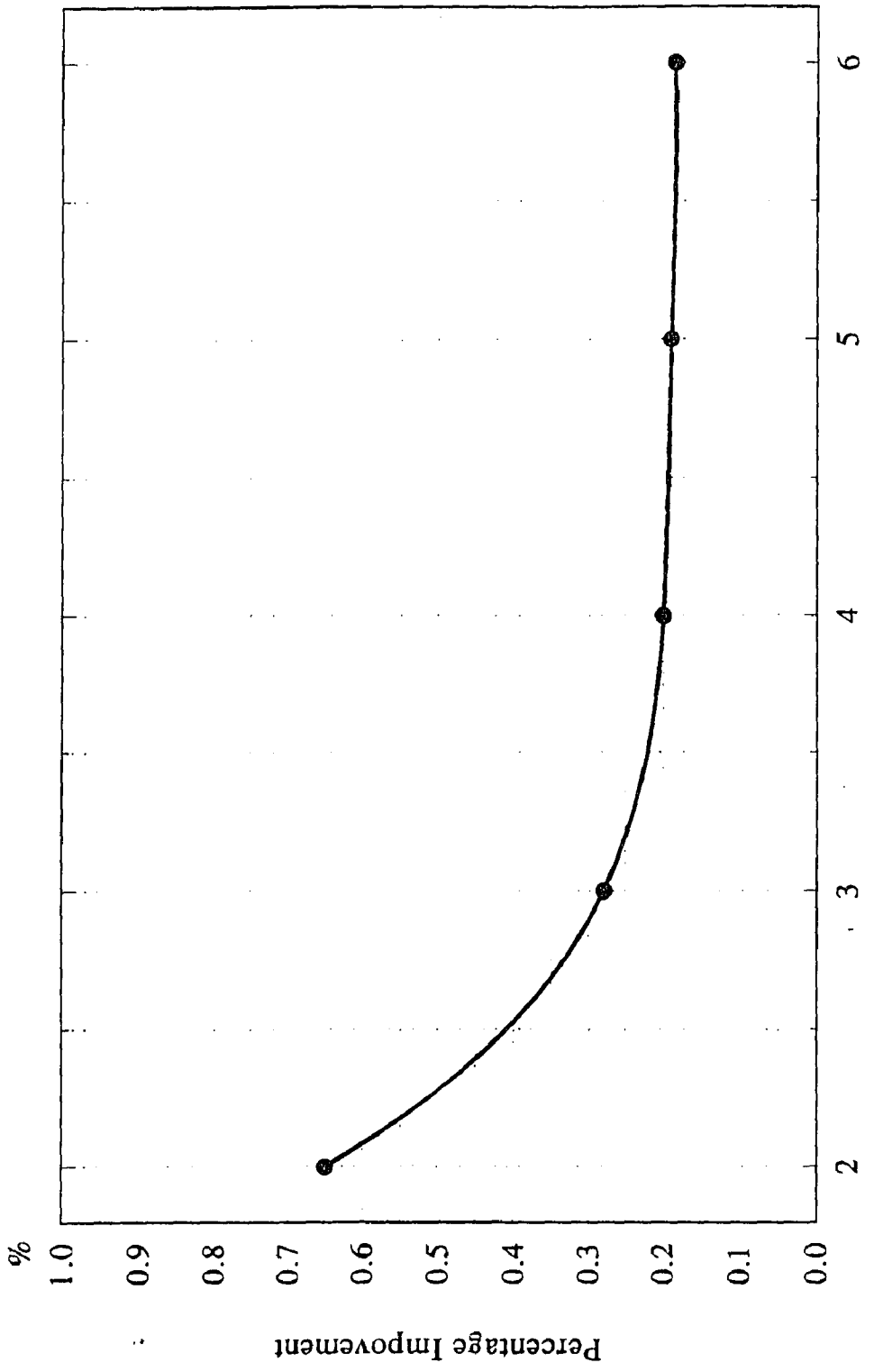

Figure C18 Percentage of improvement for larger α_n to previous α_n of longitudinal thermal stress factor at A_1 of the pipe

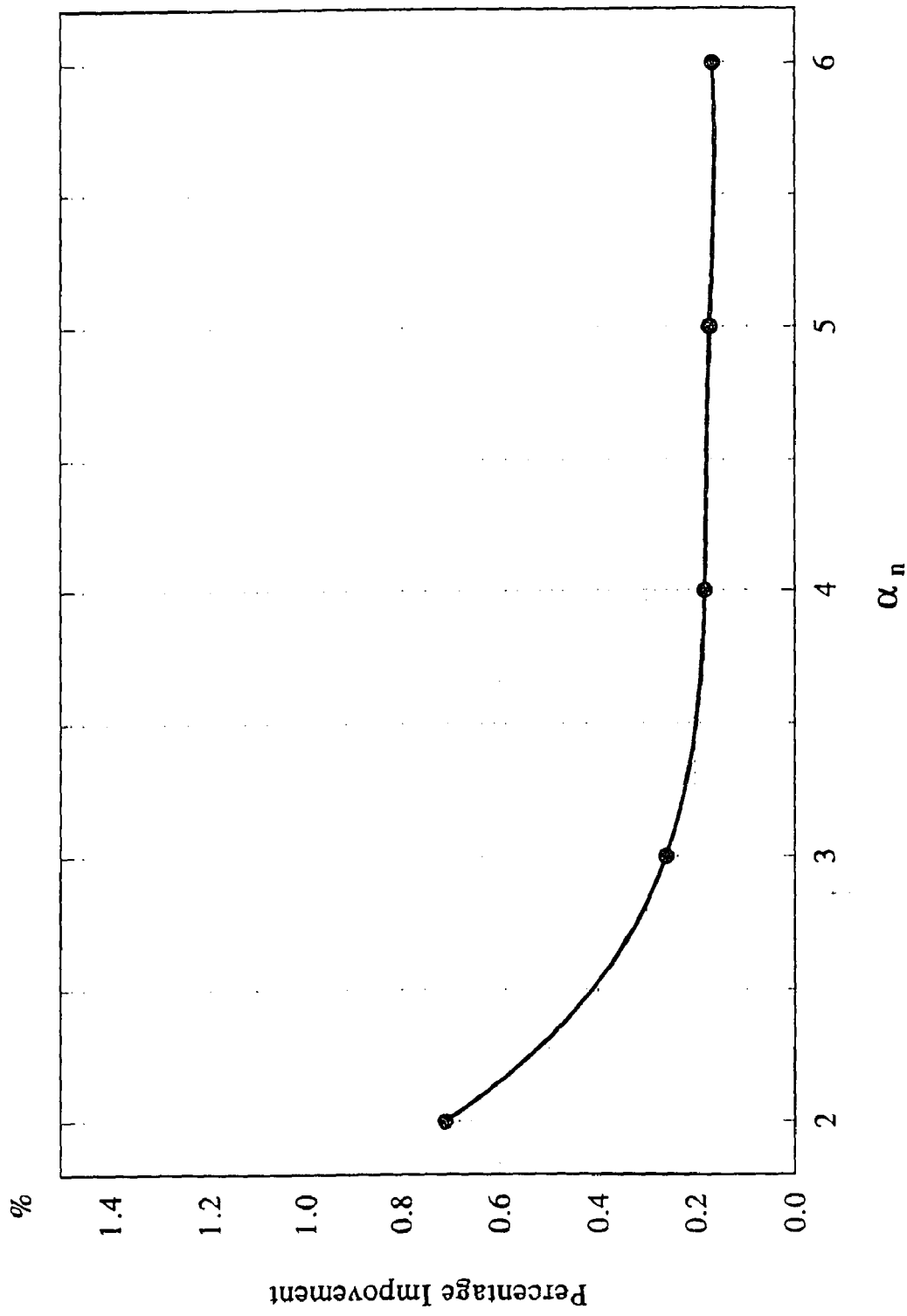

Figure C19 Percentage of improvement for larger α_n to previous α_n of longitudinal thermal stress factor at C_t of the pipe

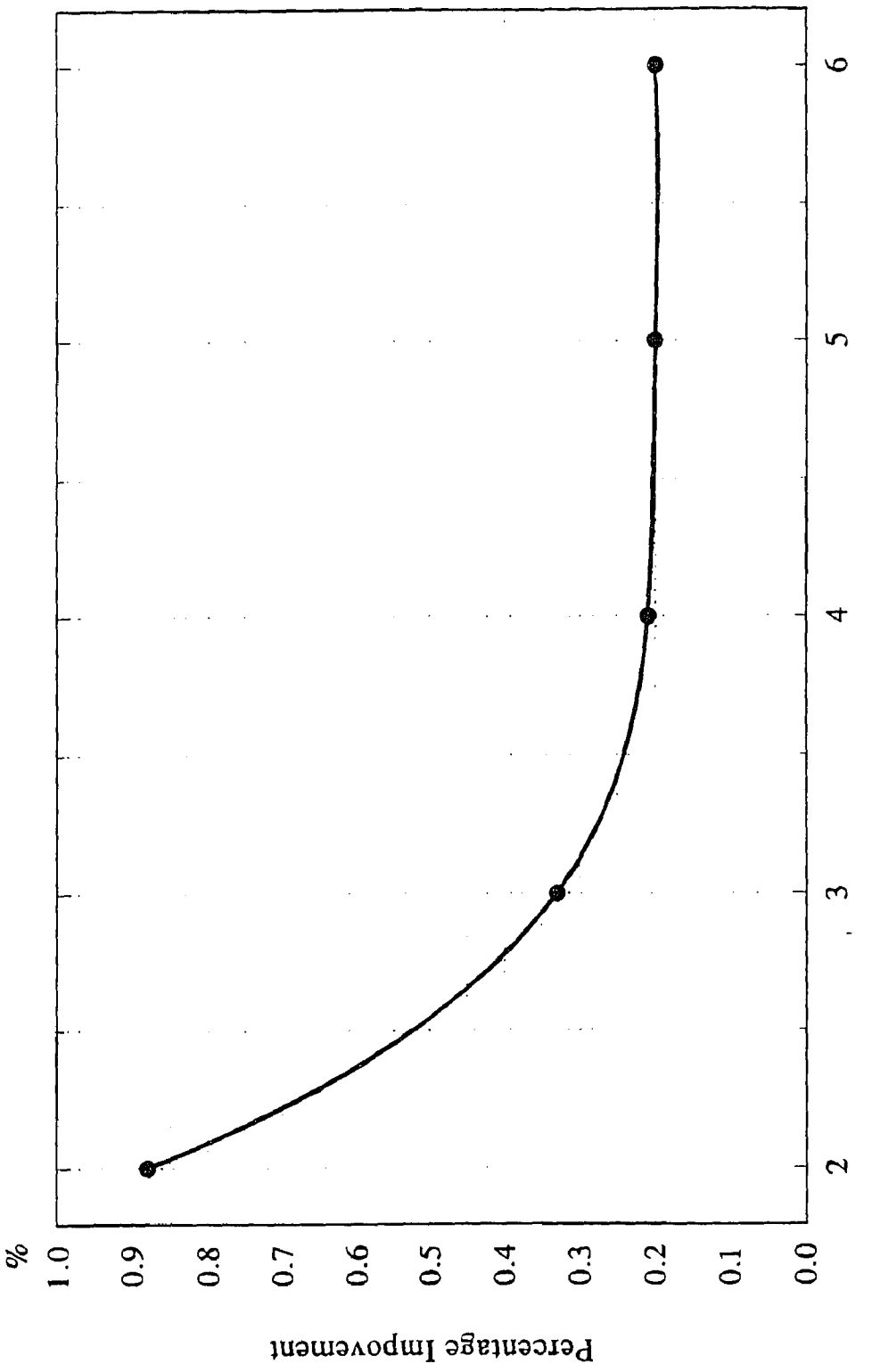

Figure C20 Percentage of improvement for larger α_n to previous α_n of longitudinal thermal stress factor at C_1 of the pipe

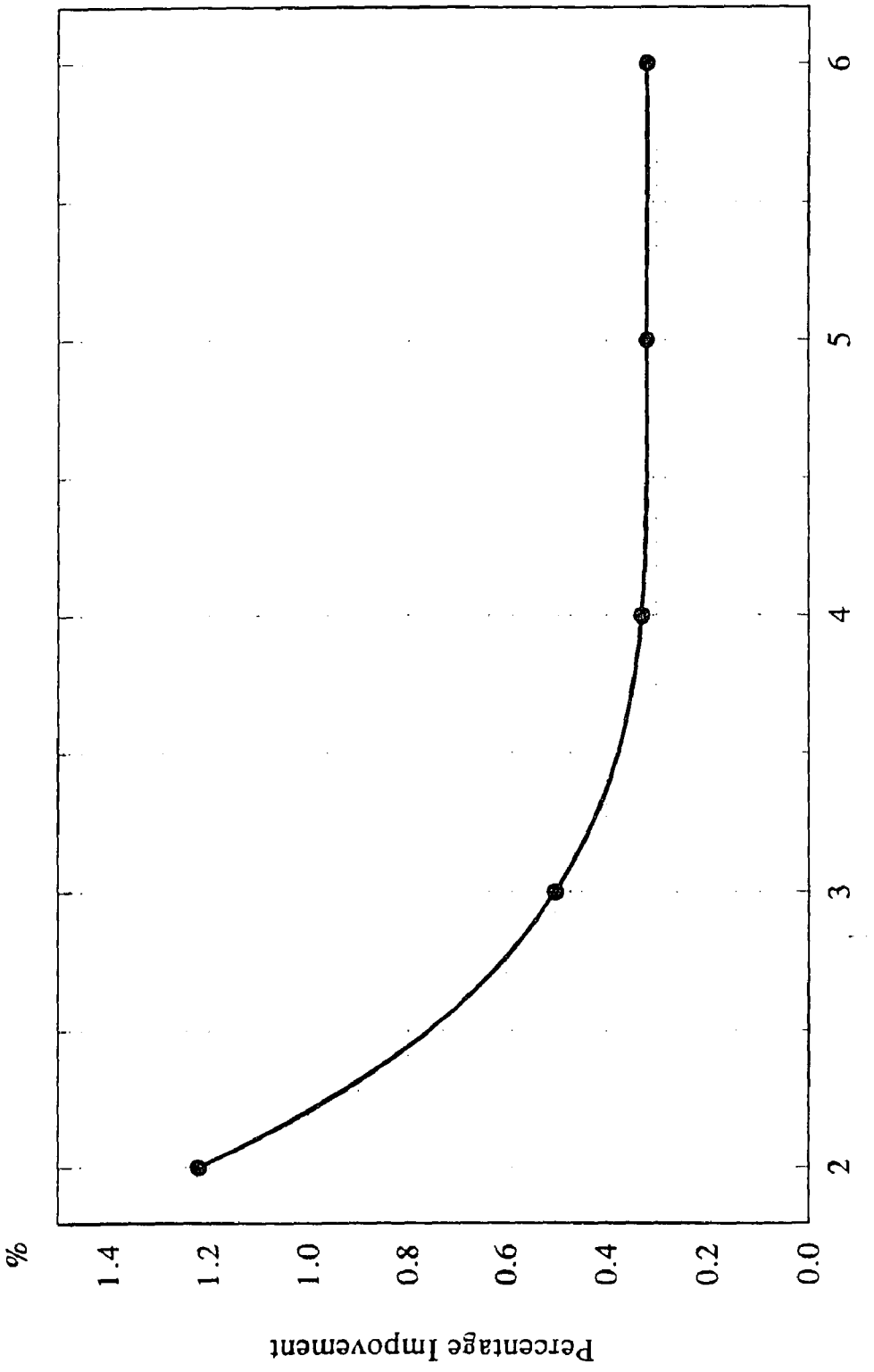

Figure C21 Percentage of improvement for larger α_n to previous α_n of circumferential thermal stress factor at A_i of the pipe

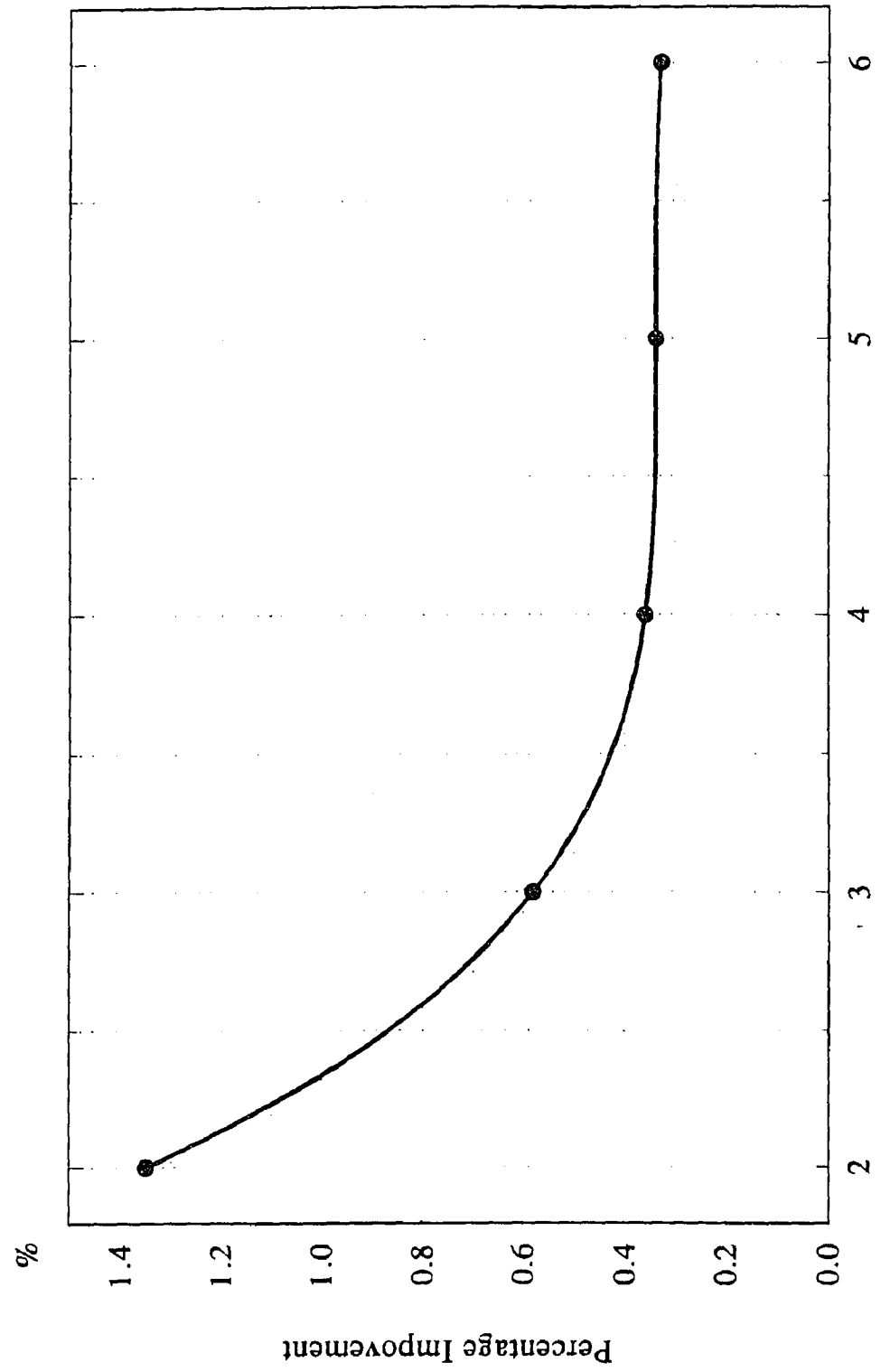

Figure C22 Percentage of improvement for larger α_n to previous α_n of circumferential thermal stress factor at A_1 of the pipe

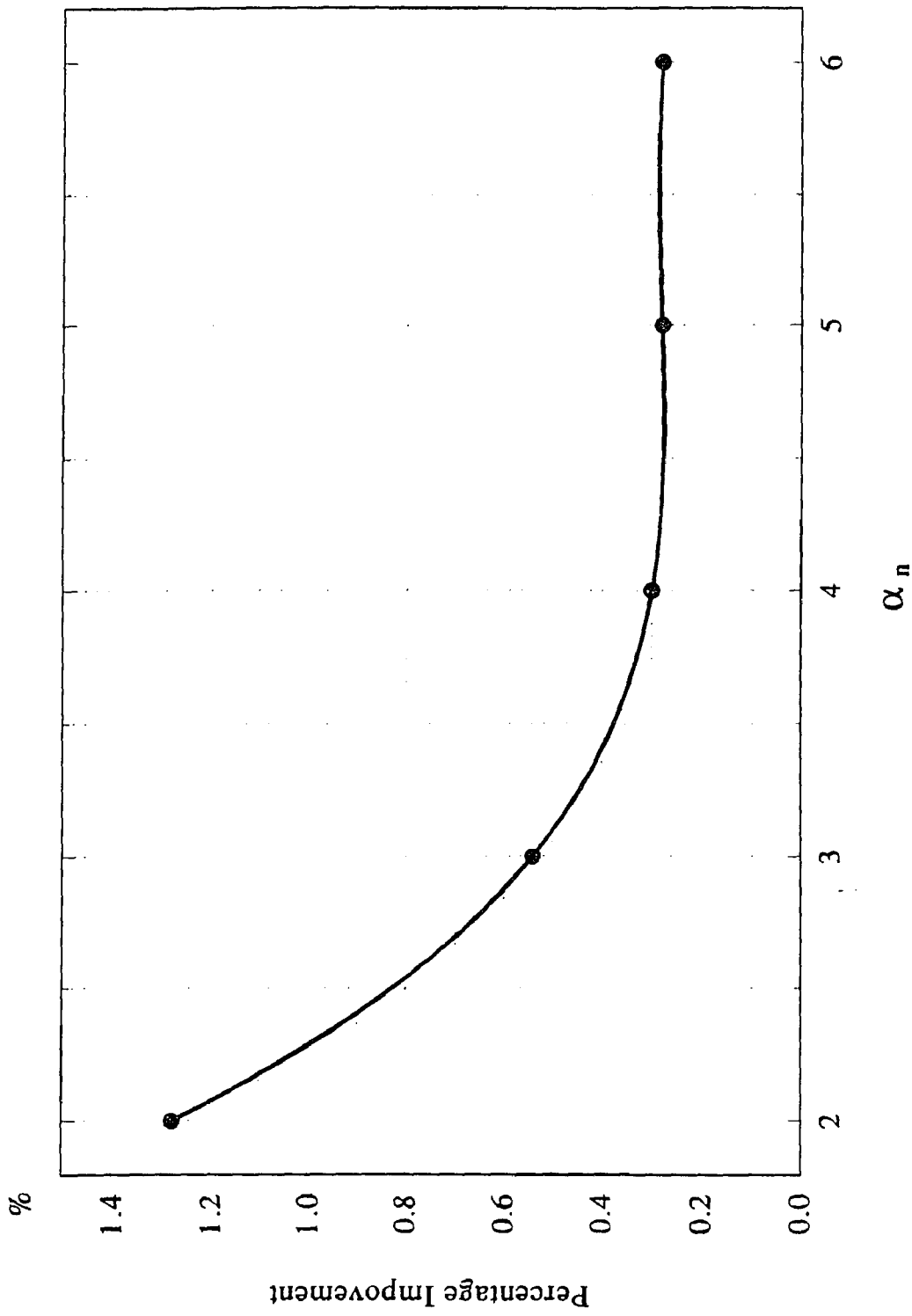

Figure C23 Percentage of improvement for larger α_n to previous α_n of circumferential thermal stress factor at C_1 of the pipe

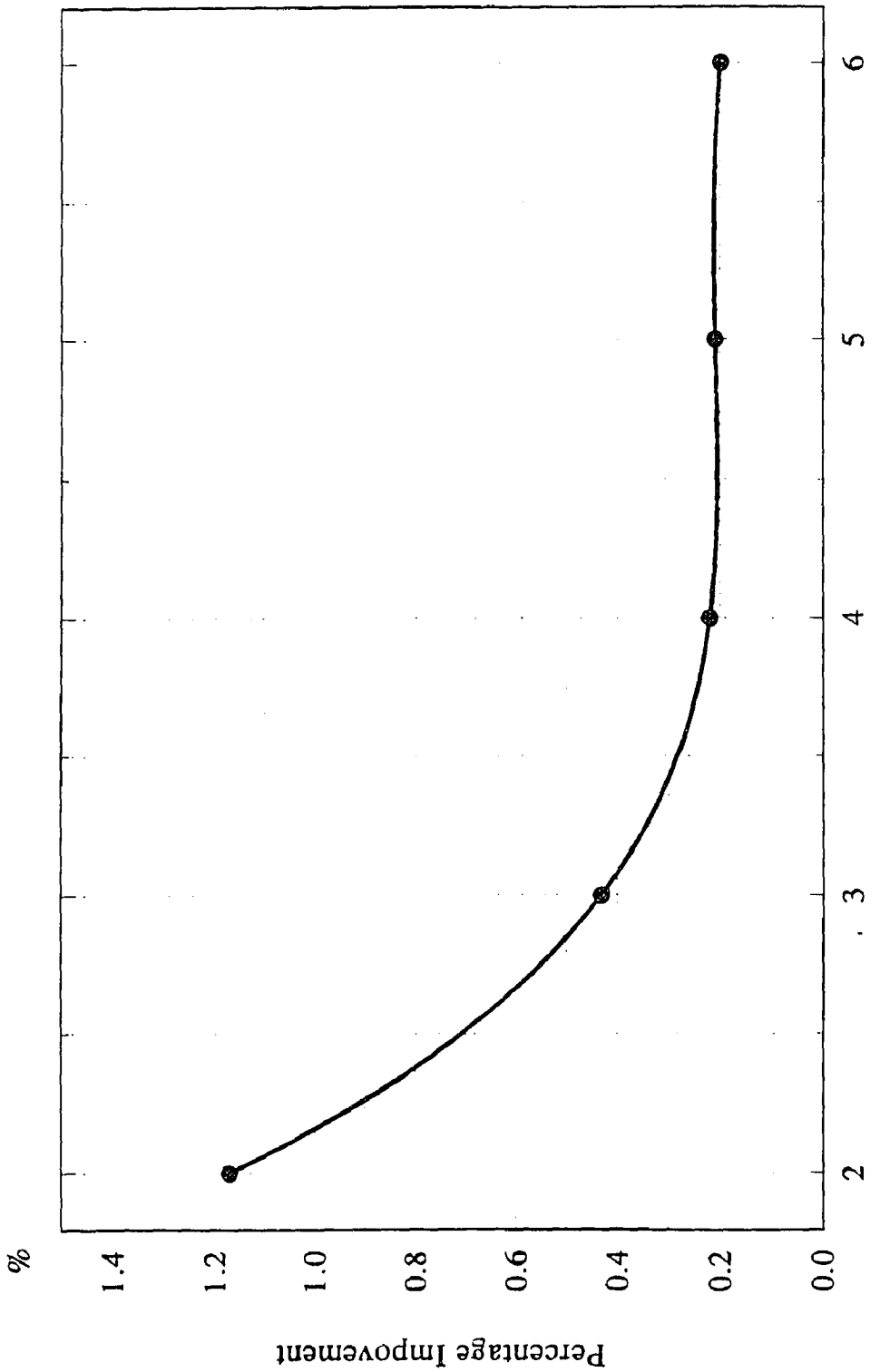

Figure C24 Percentage of improvement for larger α_n to previous α_n of circumferential thermal stress factor at C_1 of the pipe

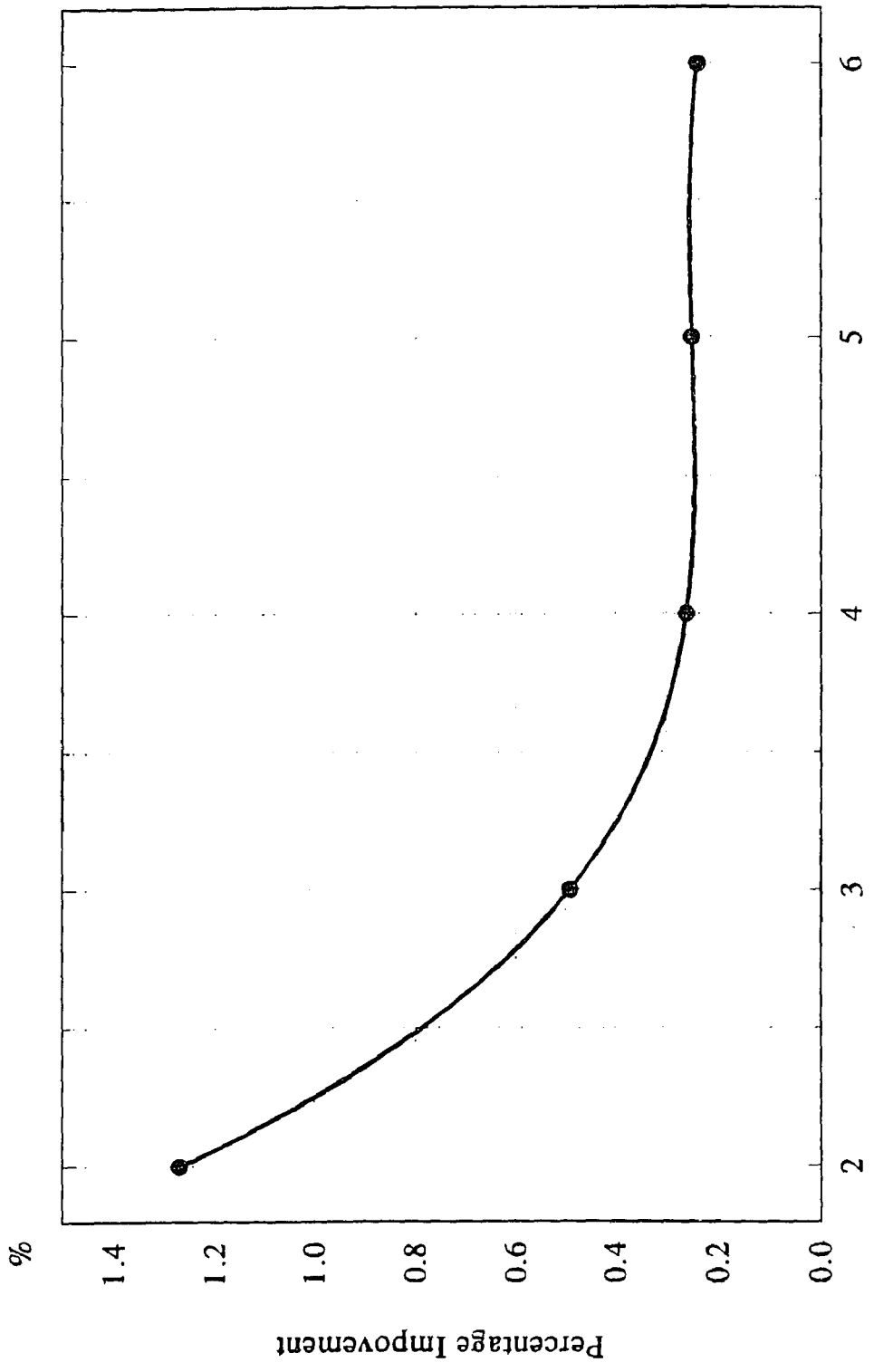

Figure C25 Percentage of improvement for larger α_n to previous α_n of longitudinal thermal stress factor at $A_{c'}$ of the nozzle

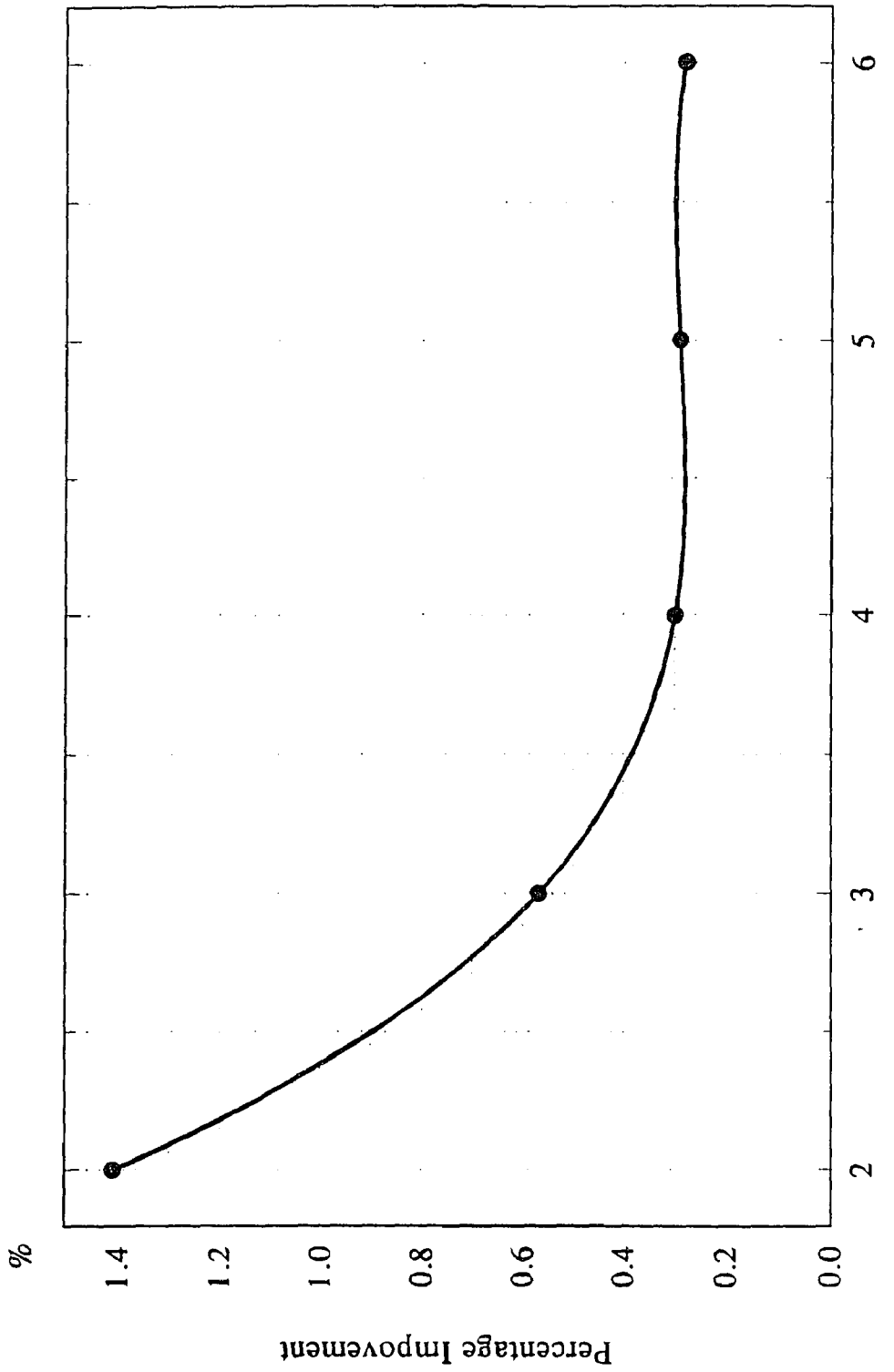

Figure C26 Percentage of improvement for larger α_n to previous α_n of longitudinal thermal stress factor at A_i of the nozzle

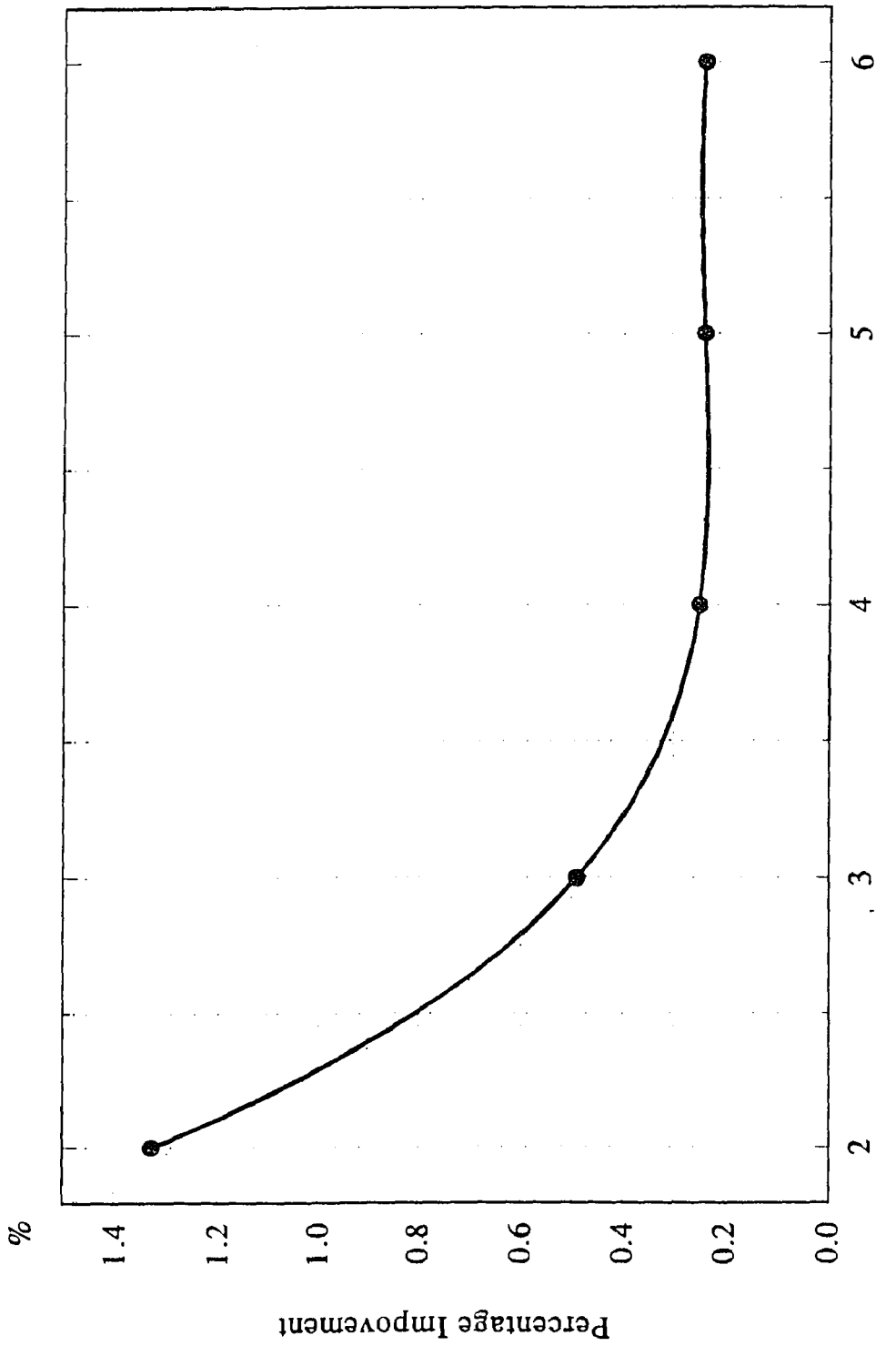

Figure C27 Percentage of improvement for larger α_n to previous α_n of longitudinal thermal stress factor at C_o of the nozzle

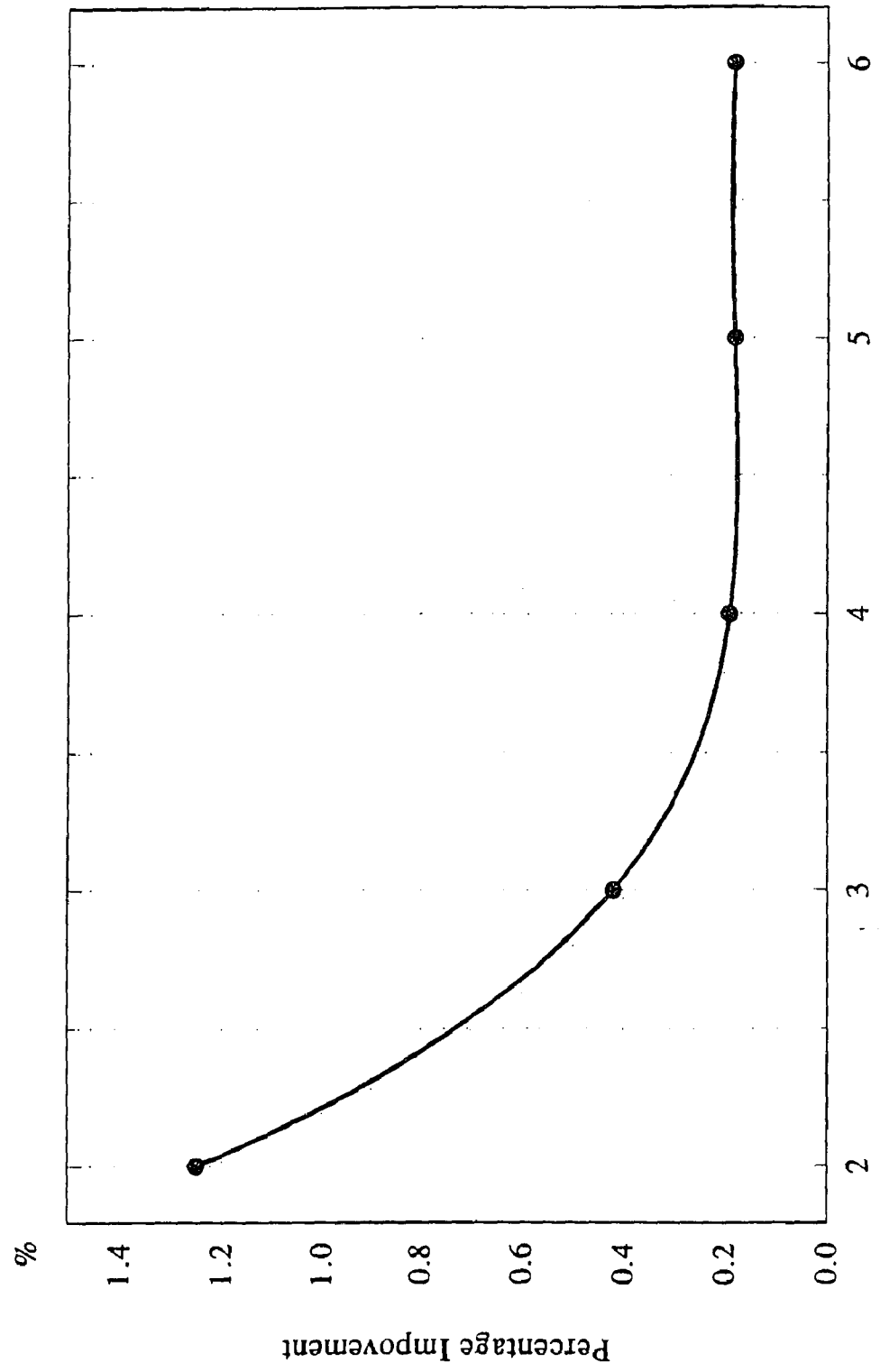

Figure C28 Percentage of improvement for larger α_n to previous α_n of longitudinal thermal stress factor at C_i of the nozzle

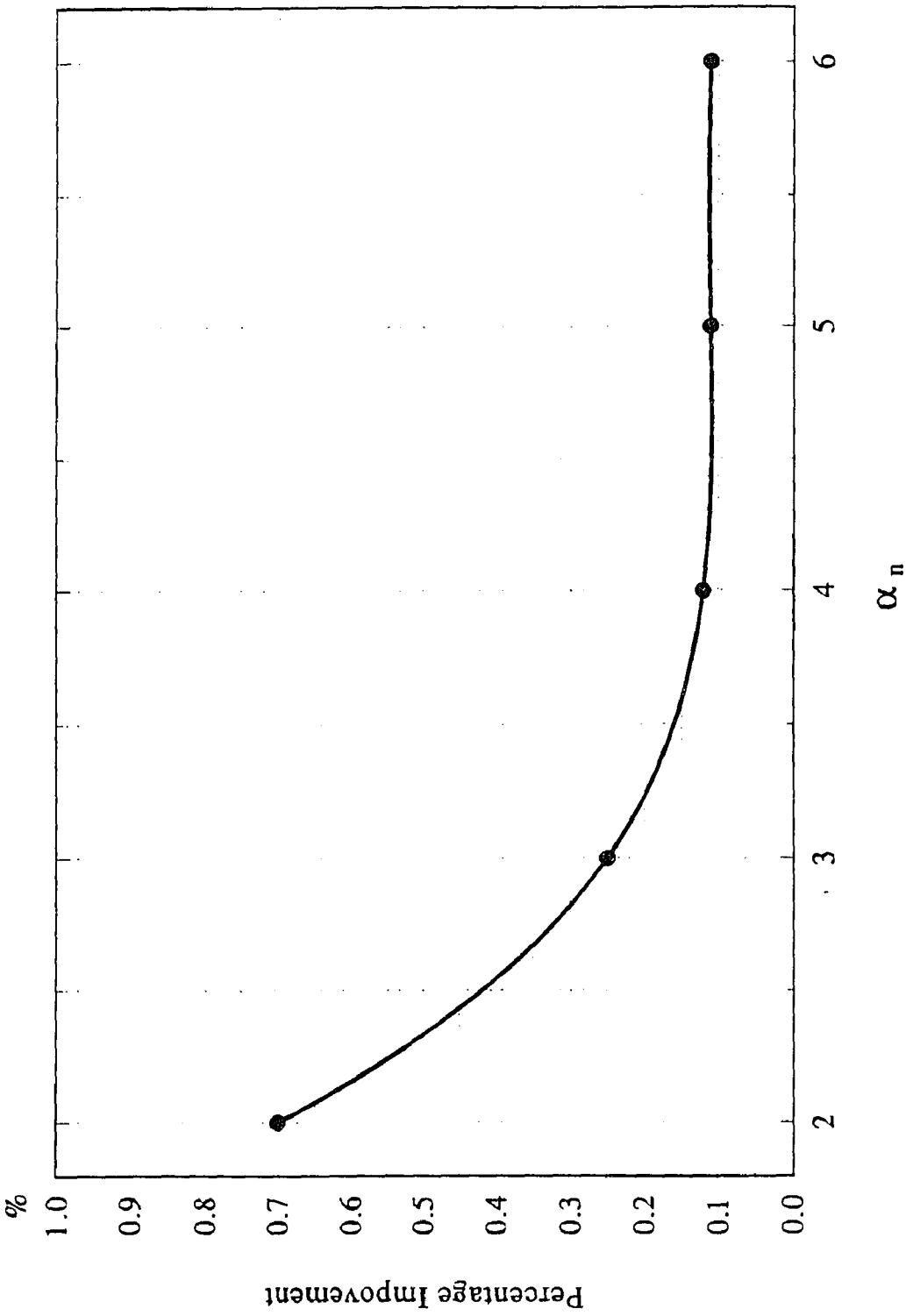

Figure C29 Percentage of improvement for larger α_n to previous α_n of circumferential thermal stress factor at A_i of the nozzle

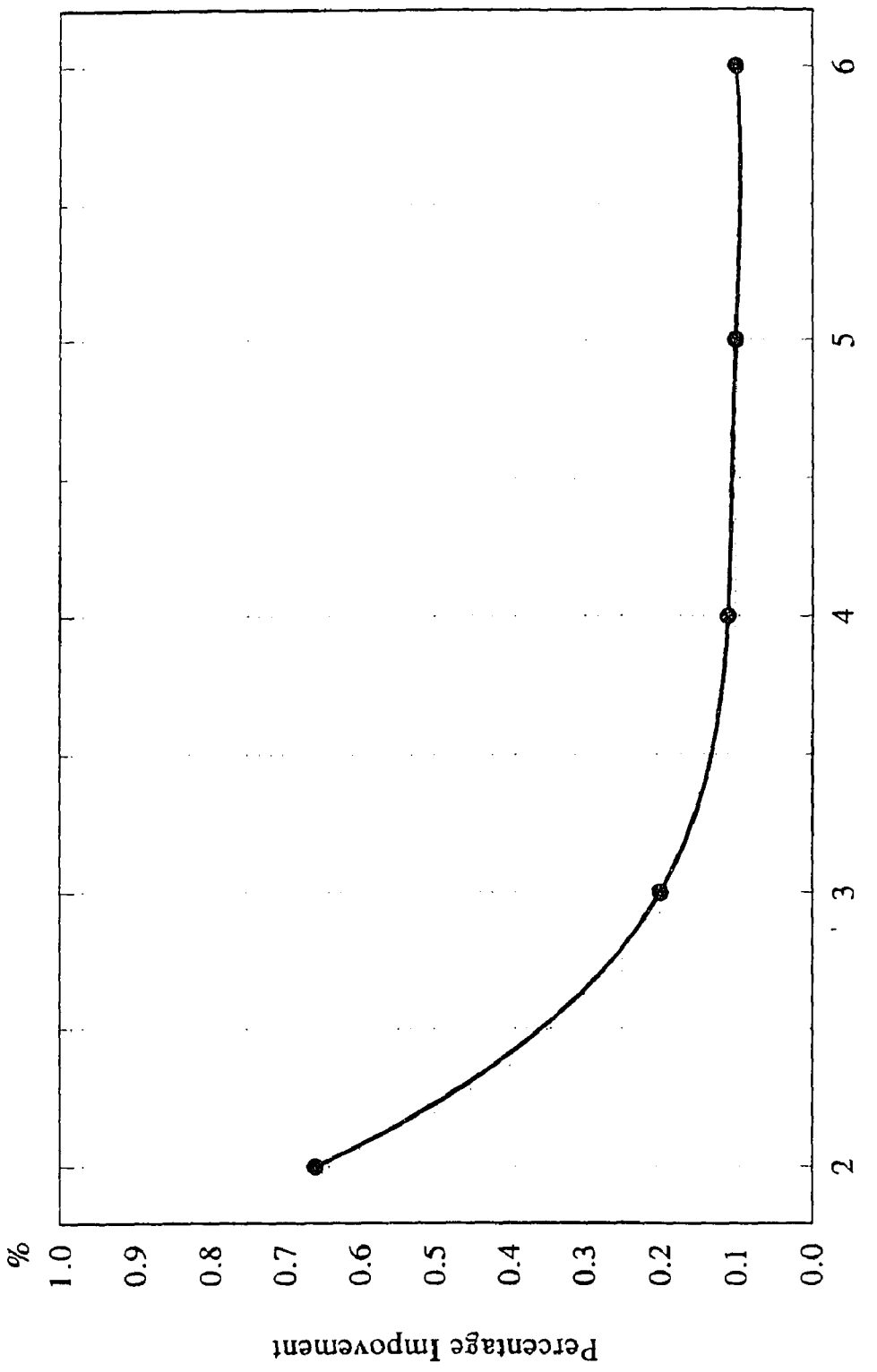

Figure C30 Percentage of improvement for larger α_n to previous α_n of circumferential thermal stress factor at A, of the nozzle

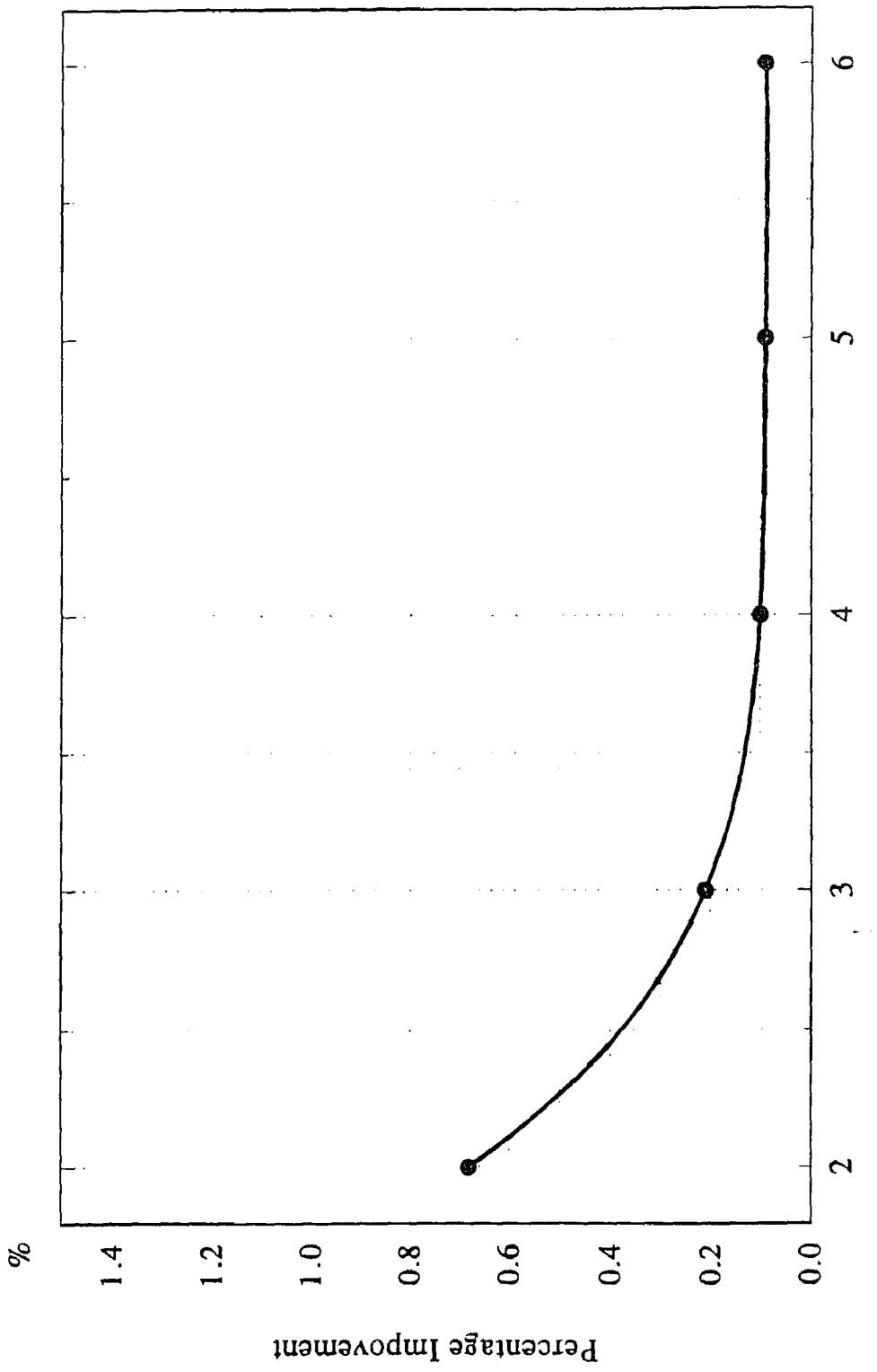

Figure C31 Percentage of improvement for larger α_n to previous α_n of circumferential thermal stress factor at C_o of the nozzle

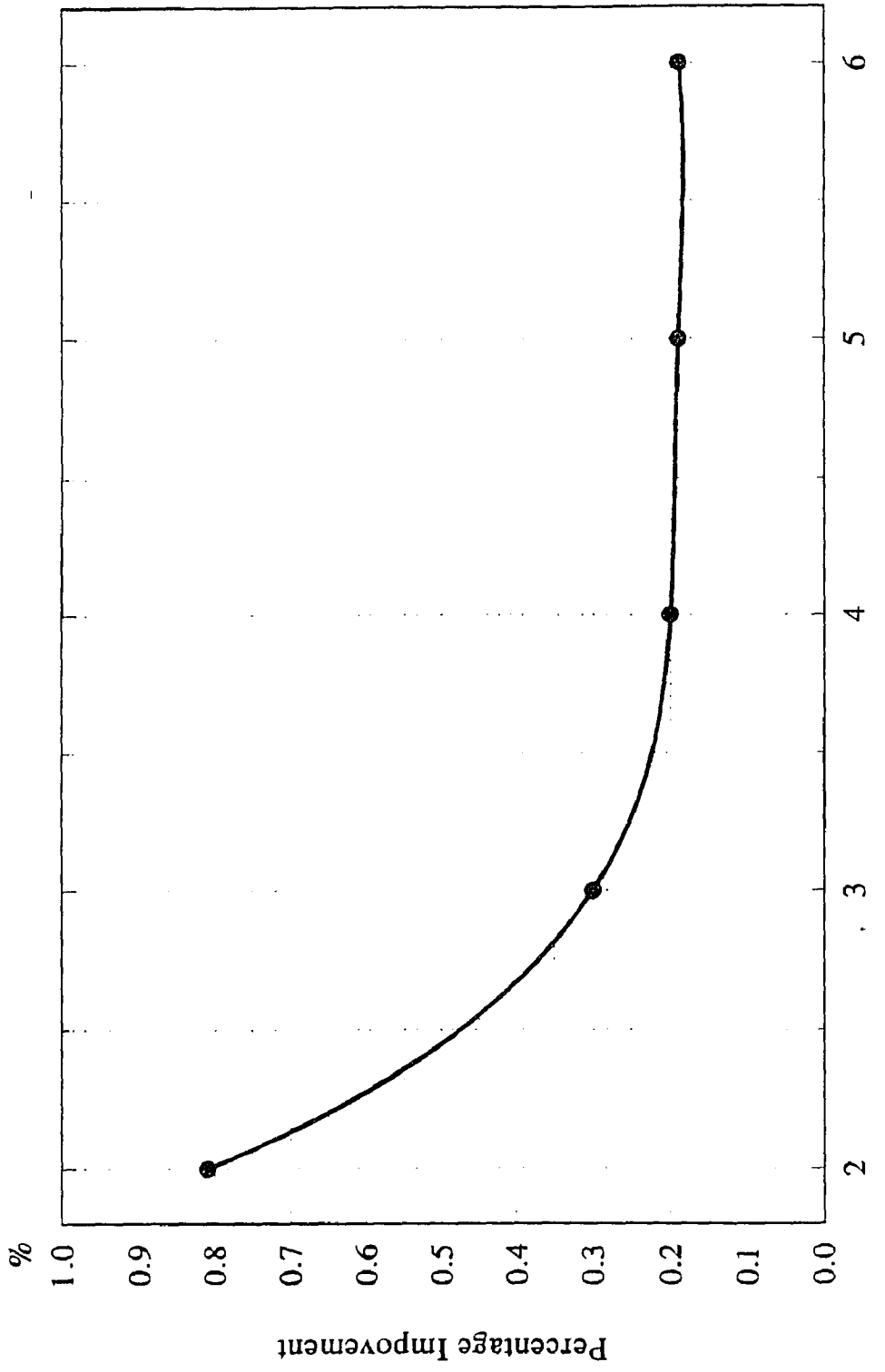

Figure C32 Percentage of improvement for larger α_n to previous α_n of circumferential thermal stress factor at C_1 of the nozzle

APPENDIX D

NORMALIZATION STUDIES

Table D-1 Material Properties, Geometric parameters and dimensions of case # 1 and case # 2

α_T = Thermal Expansion Coefficience	6.50e-06	in/in-°F
E = Young's Modulus	3.00e+07	psi
μ = Poisson's ratio	0.3	
Ti = Internal Temperature	500	°F
To = Environmental Temperature	100	°F
δT = Ti - To	400	°F
Pipe Material	347 SS	
Nozzle Material	347 SS	

Case # 1 :

α_p = Pipe length / pipe mean radius	8	
α_n = Noz. length / noz. mean radius	4	
β = Noz. mean rad. / pipe mean rad.	0.6	
γ = Pipe mean rad. / pipe thk.	50	
L_p = Pipe length	160	ins
L_n = Nozzle length	48	ins
R_p = Pipe mean radius	20	ins
R_n = Nozzle mean radius	12	ins
t_p = Pipe thickness	0.4	ins
t_n = Nozzle thickness = βt_p	0.24	ins

Case # 2:

α_p= pipe length / pipe mean radius	8	
α_n= noz. length / noz. mean radius	4	
β = noz. mean rad. / pipe mean rad.	0.6	
γ = pipe mean rad. / pipe thk.	50	
L_p = Pipe length	320	ins
L_n = Nozzle length	96	ins
R_p = Pipe mean radius	40	ins
R_n = Nozzle mean radius	24	ins
t_p = Pipe thickness	0.8	ins
t_n = Nozzle thickness = βt_p	0.48	ins

Table D-2 Thermal stresses & stress factors comparison table at node point A of case # 1 & case # 2

Formula for the Thermal stress factor :

Thermal stress factor (K_T) = $\frac{2\times\sigma_T\times(1}{E\times\alpha_T\times}$; Thermal Stress (σ_T) = $\frac{K_T\times E\times\alpha}{2\times(1-}$

(1) Node A on the outside surface of pipe:

Model	# 1	# 2
Longitudinal Thermal Stress (S_1), psi	35,355	35,355
Thermal Stress Factor	0.64	0.64

Circumferential Thermal Stress (S_2), psi	53,640	53,640
Thermal Stress Factor	0.96	0.96

(2) Node A on the inside surface of pipe:

Model	# 1	# 2
Longitudinal Thermal Stress (S_1), psi	-35,245	-35,245
Thermal Stress Factor	-0.63	-0.63

Circumferential Thermal Stress (S_2), psi	-55,485	-55,485
Thermal Stress Factor	-1	-1

(3) Node A on the outside surface of nozzle:

Model	# 1	# 2
Longitudinal Thermal Stress (S_1), psi	61,150	61,150
Thermal Stress Factor	1.1	1.1

Circumferential Thermal Stress (S_2), psi	80,850	80,850
Thermal Stress Factor	1.45	1.45

(4) Node A on the inside surface of nozzle:

Model	# 1	# 2
Longitudinal Thermal Stress (S_1), psi	-64,495	-64,495
Thermal Stress Factor	-1.16	-1.16

Circumferential Thermal Stress (S_2), psi	-84,755	-84,755
Thermal Stress Factor	-1.52	-1.52

Table D-3 Thermal stresses & stress factors comparison table at node point C of case # 1 & case # 2

Formula for the Thermal stress factor :

Thermal stress factor (K_T) $= \frac{2\times\sigma_T\times(1-\mu)}{E\times\alpha_T\times\delta T}$; Thermal Stress (σ_T) $= \frac{K_T\times E\times\alpha_T\times\delta T}{2\times(1-\mu)}$

(5) Node C on the outside surface of pipe:

Model	# 1	# 2
Longitudinal Thermal Stress (S_1), psi	54,470	54,470
Thermal Stress Factor	0.98	0.98
Circumferential Thermal Stress (S_2), psi	40,210	40,210
Thermal Stress Factor	0.72	0.72

(6) Node C on the inside surface of pipe:

Model	# 1	# 2
Longitudinal Thermal Stress (S_1), psi	-55,950	-55,950
Thermal Stress Factor	-1	-1
Circumferential Thermal Stress (S_2), psi	-38,010	-38,010
Thermal Stress Factor	-0.68	-0.68

(7) Node C on the outside surface of nozzle:

Model	# 1	# 2
Longitudinal Thermal Stress (S_1), psi	68,365	68,365
Thermal Stress Factor	1.23	1.23
Circumferential Thermal Stress (S_2), psi	97,205	97,205
Thermal Stress Factor	1.75	1.75

(8) Node C on the inside surface of nozzle:

Model	# 1	# 2
Longitudinal Thermal Stress (S_1), psi	-69,705	-69,705
Thermal Stress Factor	-1.25	-1.25
Circumferential Thermal Stress (S_2), psi	-93,775	-93,775
Thermal Stress Factor	-1.68	-1.68

Table D-4 Material Properties, Geometric parameters and dimensions of case # 3 and case # 4

α_T = Thermal Expansion Coefficience	6.50e-06	in/in-°F
E = Young's Modulus	3.00e+07	psi
μ = Poisson's ratio	0.3	
Ti = Internal Temperature	500	°F
To = Environmental Temperature	100	°F
δT = Ti - To	400	°F
Pipe Material	347 SS	
Nozzle Material	347 SS	

Case # 3 :

α_p = Pipe length / pipe mean radius	8	
α_n = Noz. length / noz. mean radius	4	
β = Noz. mean rad. / pipe mean rad.	0.3	
γ = Pipe mean rad. / pipe thk.	100	
L_p = Pipe length	160	ins
L_n = Nozzle length	24	ins
R_p = Pipe mean radius	20	ins
R_n = Nozzle mean radius	6	ins
t_p = Pipe thickness	0.2	ins
t_n = Nozzle thickness = βt_p	0.06	ins

Case # 4 :

α_p = Pipe length / pipe mean radius	8	
α_n = Noz. length / noz. mean radius	4	
β = Noz. mean rad. / pipe mean rad.	0.3	
γ = Pipe mean rad. / pipe thk.	100	
L_p = Pipe length	80	ins
L_n = Nozzle length	12	ins
R_p = Pipe mean radius	10	ins
R_n = Nozzle mean radius	3	ins
t_p = Pipe thickness	0.1	ins
t_n = Nozzle thickness = βt_p	0.03	ins

Table D-5 Thermal stresses & stress factors comparison table at node point A of case # 3 & case # 4

Formula for the Thermal stress factor :

Thermal stress factor (K_T) = $\frac{2\times\sigma_T\times(1-\mu)}{E\times\alpha_T\times\delta T}$; Thermal Stress (σ_T) = $\frac{K_T\times E\times\alpha_T\times\delta T}{2\times(1-\mu)}$

(1) Node A on the outside surface of pipe:

Model	# 3	# 4
Longitudinal Thermal Stress (S_1), psi	27,985	27,985
Thermal Stress Factor	0.5	0.5
Circumferential Thermal Stress (S_2), psi	59,390	59,390
Thermal Stress Factor	1.07	1.07

(2) Node A on the inside surface of pipe:

Model	# 3	# 4
Longitudinal Thermal Stress (S_1), psi	-27,885	-27,885
Thermal Stress Factor	-0.5	-0.5
Circumferential Thermal Stress (S_2), psi	-30,835	-30,835
Thermal Stress Factor	-0.55	-0.55

(3) Node A on the outside surface of nozzle:

Model	# 3	# 4
Longitudinal Thermal Stress (S_1), psi	58,810	58,810
Thermal Stress Factor	1.06	1.06
Circumferential Thermal Stress (S_2), psi	21,840	21,840
Thermal Stress Factor	0.39	0.39

(4) Node A on the inside surface of nozzle:

Model	# 3	# 4
Longitudinal Thermal Stress (S_1), psi	-51,120	-51,120
Thermal Stress Factor	-0.92	-0.92
Circumferential Thermal Stress (S_2), psi	-19,200	-19,200
Thermal Stress Factor	-0.35	-0.35

Table D-6 Thermal stresses & stress factors comparison table at node point C of case # 3 & case # 4

Formula for the Thermal stress factor :

Thermal stress factor (K_T) = $\frac{2\times\sigma_T\times(1-\mu)}{E\times\alpha_T\times\delta T}$; Thermal Stress (σ_T) = $\frac{K_T\times E\times\alpha_T\times\delta T}{2\times(1-\mu)}$

(5) Node C on the outside surface of pipe:

Model	# 3	# 4
Longitudinal Thermal Stress (S_1), psi	102,150	102,150
Thermal Stress Factor	1.83	1.83
Circumferential Thermal Stress (S_2), psi	153,650	153,650
Thermal Stress Factor	2.76	2.76

(6) Node C on the inside surface of pipe:

Model	# 3	# 4
Longitudinal Thermal Stress (S_1), psi	-71,780	-71,780
Thermal Stress Factor	-1.29	-1.29
Circumferential Thermal Stress (S_2), psi	-142,850	-142,850
Thermal Stress Factor	-2.56	-2.56

(7) Node C on the outside surface of nozzle:

Model	# 3	# 4
Longitudinal Thermal Stress (S_1), psi	90,555	90,555
Thermal Stress Factor	1.63	1.63
Circumferential Thermal Stress (S_2), psi	154,700	154,700
Thermal Stress Factor	2.78	2.78

(8) Node C on the inside surface of nozzle:

Model	# 3	# 4
Longitudinal Thermal Stress (S_1), psi	-80,155	-80,155
Thermal Stress Factor	-1.44	-1.44
Circumferential Thermal Stress (S_2), psi	-147,600	-147,600
Thermal Stress Factor	-2.65	-2.65

Table D-7 Material Properties, Geometric parameters and dimensions of case # 5 and case # 6

α_T = Thermal Expansion Coefficience	6.50e-06	in/in-°F
E = Young's Modulus	3.00e+07	psi
μ = Poisson's ratio	0.3	
Ti = Internal Temperature	500	°F
To = Environmental Temperature	100	°F
δT = Ti - To	400	°F
Pipe Material	347 SS	
Nozzle Material	347 SS	

Case # 5 :

α_p = Pipe length / pipe mean radius	8	
α_n = Noz. length / noz. mean radius	4	
β = Noz. mean rad. / pipe mean rad.	0.9	
γ = Pipe mean rad. / pipe thk.	20	
L_p = Pipe length	160	ins
L_n = Nozzle length	72	ins
R_p = Pipe mean radius	20	ins
R_n = Nozzle mean radius	18	ins
t_p = Pipe thickness	1	ins
t_n = Nozzle thickness = βt_p	0.9	ins

Case # 6:

α_p = Pipe length / pipe mean radius	8	
α_n = Noz. length / noz. mean radius	4	
β = Noz. mean rad. / pipe mean rad.	0.9	
γ = Pipe mean rad. / pipe thk.	20	
L_p = Pipe length	240	ins
L_n = Nozzle length	108	ins
R_p = Pipe mean radius	30	ins
R_n = Nozzle mean radius	27	ins
t_p = Pipe thickness	1.5	ins
t_n = Nozzle thickness = βt_p	1.35	ins

Table D-8 Thermal stresses & stress factors comparison table at node point A of case # 5 & case # 6

Formula for the Thermal stress factor :

Thermal stress factor (K_T) = $\frac{2\times\sigma_T\times(1-\mu)}{E\times\alpha_T\times\delta T}$; Thermal Stress (σ_T) = $\frac{K_T\times E\times\alpha_T\times\delta T}{2\times(1-\mu)}$

(1) Node A on the outside surface of pipe:

Model	# 5	# 6
Longitudinal Thermal Stress (S_1), psi	20,455	20,455
Thermal Stress Factor	0.37	0.37

Circumferential Thermal Stress (S_2), psi	33,850	33,850
Thermal Stress Factor	0.61	0.61

(2) Node A on the inside surface of pipe:

Model	# 5	# 6
Longitudinal Thermal Stress (S_1), psi	-19,995	-19,995
Thermal Stress Factor	-0.36	-0.36

Circumferential Thermal Stress (S_2), psi	-31,300	-31,300
Thermal Stress Factor	-0.56	-0.56

(3) Node A on the outside surface of nozzle:

Model	# 5	# 6
Longitudinal Thermal Stress (S_1), psi	54,050	54,050
Thermal Stress Factor	0.97	0.97

Circumferential Thermal Stress (S_2), psi	49,530	49,530
Thermal Stress Factor	0.89	0.89

(4) Node A on the inside surface of nozzle:

Model	# 5	# 6
Longitudinal Thermal Stress (S_1), psi	-55,320	-55,320
Thermal Stress Factor	-0.99	-0.99

Circumferential Thermal Stress (S_2), psi	-49,630	-49,630
Thermal Stress Factor	-0.89	-0.89

Table D-9 Thermal stresses & stress factors comparison table at node point C of case # 5 & case # 6

Formula for the Thermal stress factor :

Thermal stress factor (K_T) = $\frac{2\times\sigma_T\times(1-\mu)}{E\times\alpha_T\times\delta T}$; Thermal Stress (σ_T) = $\frac{K_T\times E\times\alpha_T\times\delta T}{2\times(1-\mu)}$

(5) Node C on the outside surface of pipe:

Model	# 5	# 6
Longitudinal Thermal Stress (S_1), psi	49,290	49,290
Thermal Stress Factor	0.89	0.89
Circumferential Thermal Stress (S_2), psi	29,135	29,135
Thermal Stress Factor	0.52	0.52

(6) Node C on the inside surface of pipe:

Model	# 5	# 6
Longitudinal Thermal Stress (S_1), psi	-47,540	-47,540
Thermal Stress Factor	-0.85	-0.85
Circumferential Thermal Stress (S_2), psi	-33,840	-33,840
Thermal Stress Factor	-0.61	-0.61

(7) Node C on the outside surface of nozzle:

Model	# 5	# 6
Longitudinal Thermal Stress (S_1), psi	57,015	57,015
Thermal Stress Factor	1.02	1.02
Circumferential Thermal Stress (S_2), psi	58,880	58,880
Thermal Stress Factor	1.06	1.06

(8) Node C on the inside surface of nozzle:

Model	# 5	# 6
Longitudinal Thermal Stress (S_1), psi	-58,560	-58,560
Thermal Stress Factor	-1.05	-1.05
Circumferential Thermal Stress (S_2), psi	-59,060	-59,060
Thermal Stress Factor	-1.06	-1.06

Table D-10 Material Properties, Geometric parameters and dimensions of case # 7 and case # 8

α_T = Thermal Expansion Coefficience	6.50e-06	in/in-°F
E = Young's Modulus	3.00e+07	psi
μ = Poisson's ratio	0.3	
Pipe Material	347 SS	
Nozzle Material	347 SS	

α_p = Pipe length / pipe mean radius	8	
α_n = Noz. length / noz. mean radius	4	
β = Noz. mean rad. / pipe mean rad.	0.6	
γ = Pipe mean rad. / Pipe thk.	50	
L_p = Pipe length	160	ins
L_n = Nozzle length	48	ins
R_p = Pipe radius	20	ins
R_n = Nozzle radius	12	ins
t_p = Pipe thickness	0.4	ins
t_n = Nozzle thickness = βt_p	0.24	ins

Case # 7:

Ti = Internal Temperature	500	°F
To = Environmental Temperature	100	°F
δT = Ti - To	400	°F

Case # 8:

Ti = Internal Temperature	1,000	°F
To = Environmental Temperature	100	°F
δT = Ti - To	900	°F

Table D-11 Thermal stresses & stress factors comparison table at node point A of case # 7 & case # 8

Formula for the Thermal stress factor :

Thermal stress factor (K_T) = $\frac{2\times\sigma_T\times(1-\mu)}{E\times\alpha_T\times\delta T}$; Thermal Stress (σ_T) = $\frac{K_T\times E\times\alpha_T\times\delta T}{2\times(1-\mu)}$

(1) Node A on the outside surface of pipe:

Model	# 7	# 8
Longitudinal Thermal Stress (S_1), psi	35,355	79,555
Thermal Stress Factor	0.63	0.63
Circumferential Thermal Stress (S_2), psi	53,640	120,700
Thermal Stress Factor	0.96	0.96

(2) Node A on the inside surface of pipe:

Model	# 7	# 8
Longitudinal Thermal Stress (S_1), psi	-35,245	-79,305
Thermal Stress Factor	-0.63	-0.63
Circumferential Thermal Stress (S_2), psi	-55,485	-124,800
Thermal Stress Factor	-1	-1

(3) Node A on the outside surface of nozzle:

Model	# 7	# 8
Longitudinal Thermal Stress (S_1), psi	61,150	137,550
Thermal Stress Factor	1.1	1.1
Circumferential Thermal Stress (S_2), psi	80,850	181,900
Thermal Stress Factor	1.45	1.45

(4) Node A on the inside surface of nozzle:

Model	# 7	# 8
Longitudinal Thermal Stress (S_1), psi	-64,495	-146,650
Thermal Stress Factor	-1.16	-1.17
Circumferential Thermal Stress (S_2), psi	-84,755	-189,350
Thermal Stress Factor	-1.52	-1.51

Table D-12 Thermal stresses & stress factors comparison table at node point C of case # 7 & case # 8

Formula for the Thermal stress factor :

Thermal stress factor (K_T) = $\frac{2\times\sigma_T\times(1-\mu)}{E\times\alpha_T\times\delta T}$, Thermal stress (σ_T) = $\frac{K_T\times E\times\alpha_T\times\delta T}{2\times(1-\mu)}$

(5) Node C on the outside surface of pipe:

Model	# 7	# 8
Longitudinal Thermal Stress (S_1), psi	54,470	122,550
Thermal Stress Factor	0.98	0.98
Circumferential Thermal Stress (S_2), psi	40,210	90,470
Thermal Stress Factor	0.72	0.72

(6) Node C on the inside surface of pipe:

Model	# 7	# 8
Longitudinal Thermal Stress (S_1), psi	-55,950	-125,900
Thermal Stress Factor	-1	-1
Circumferential Thermal Stress (S_2), psi	-38,010	-85,520
Thermal Stress Factor	-0.68	-0.68

(7) Node C on the outside surface of nozzle:

Model	# 7	# 8
Longitudinal Thermal Stress (S_1), psi	68,360	153,800
Thermal Stress Factor	1.23	1.23
Circumferential Thermal Stress (S_2), psi	97,205	218,700
Thermal Stress Factor	1.74	1.74

(8) Node C on the inside surface of nozzle:

Model	# 7	# 8
Longitudinal Thermal Stress (S_1), psi	-69,705	-156,850
Thermal Stress Factor	-1.25	-1.25
Circumferential Thermal Stress (S_2), psi	-93,775	-211,000
Thermal Stress Factor	-1.68	-1.68

APPENDIX E

COMPARISON OF DATA - CASE 2

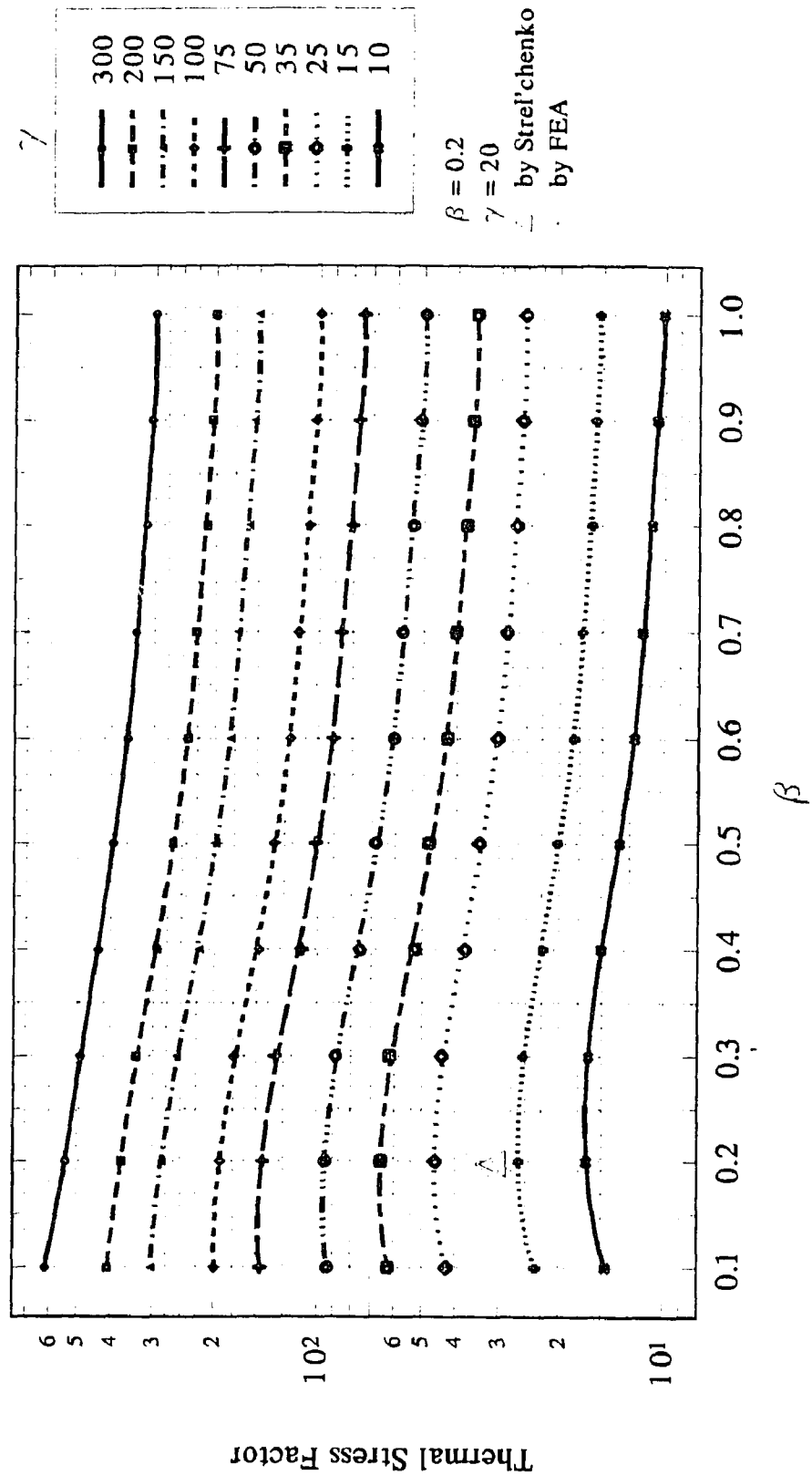

Figure E1 Data comparison of thermal stress factor in the longitudinal direction at point A_o of the nozzle

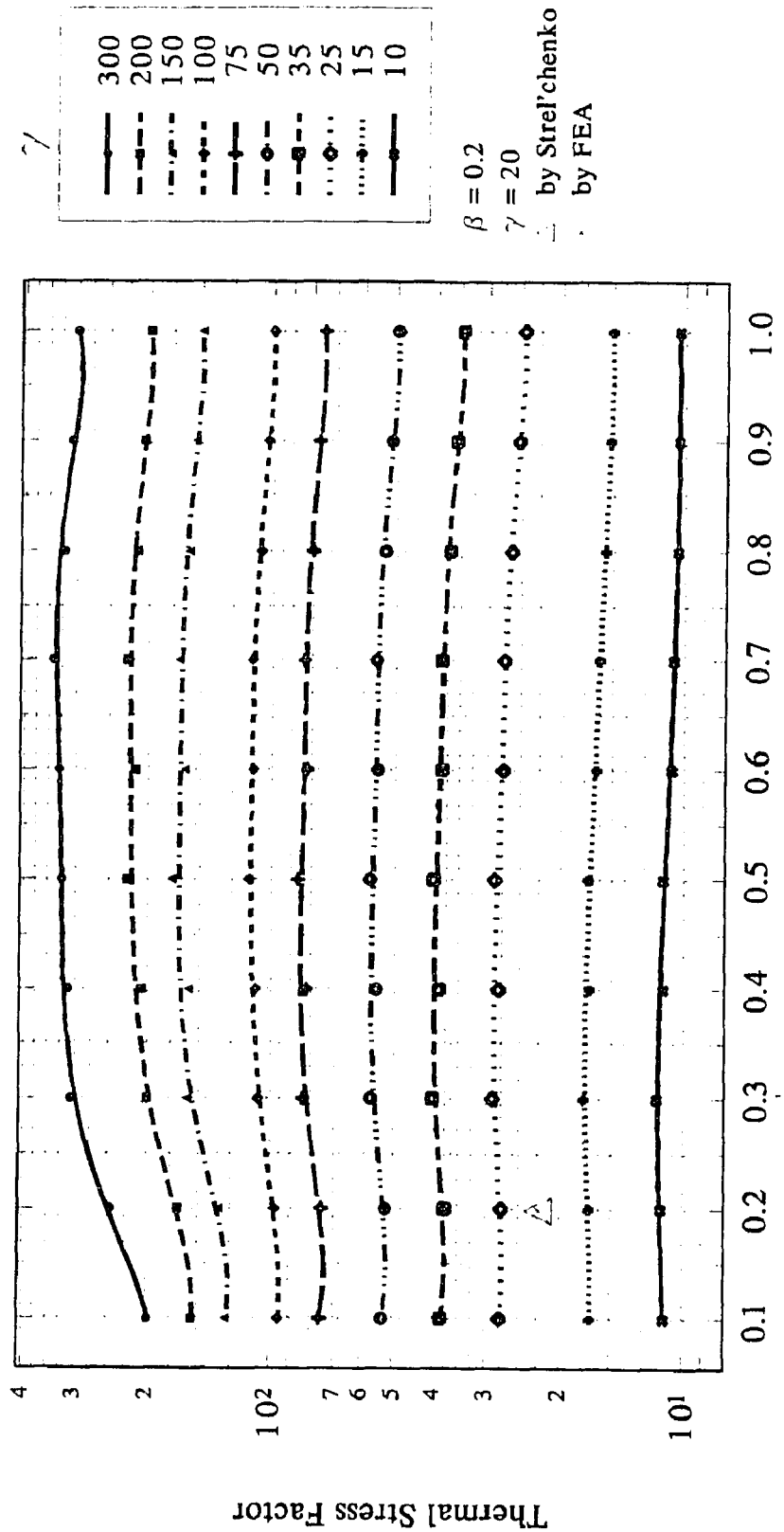

Figure E2 Data comparison of thermal stress factor in the longitudinal direction at point A_1 of the nozzle

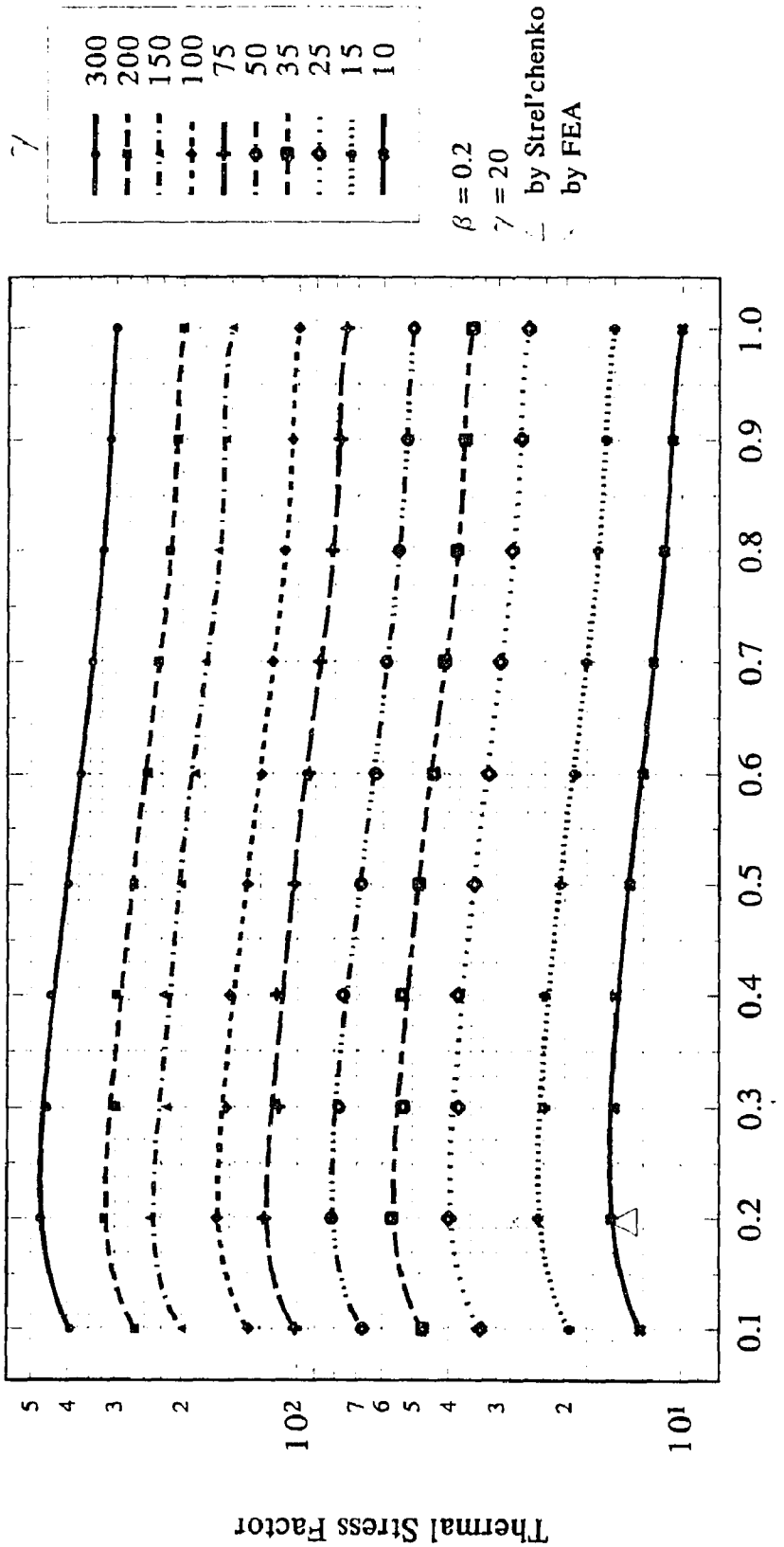

Figure E3 Data comparison of thermal stress factor in the longitudinal direction at point C_o of the nozzle

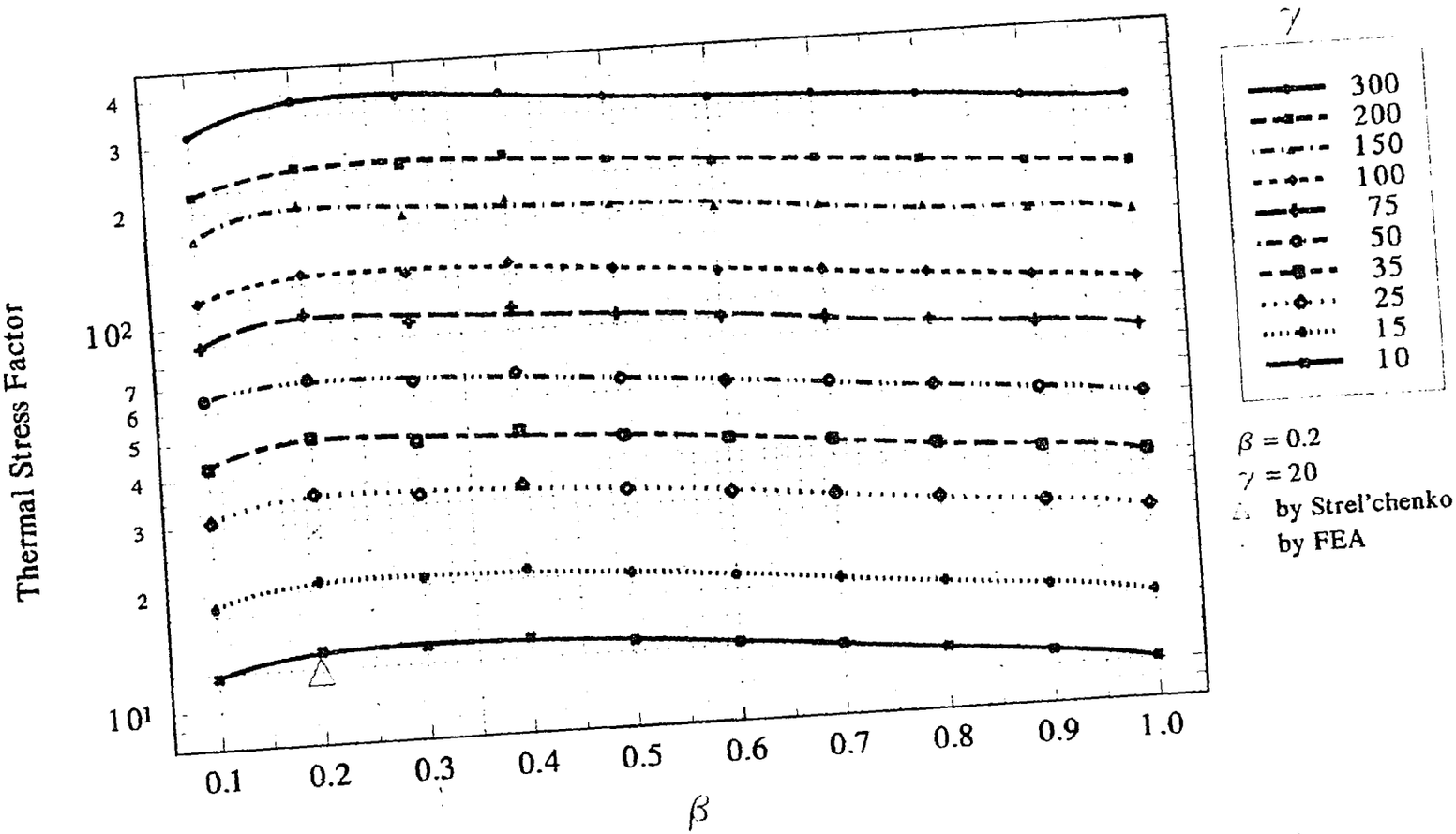

Figure E4 Data comparison of thermal stress factor in the longitudinal direction at point C, of the nozzle

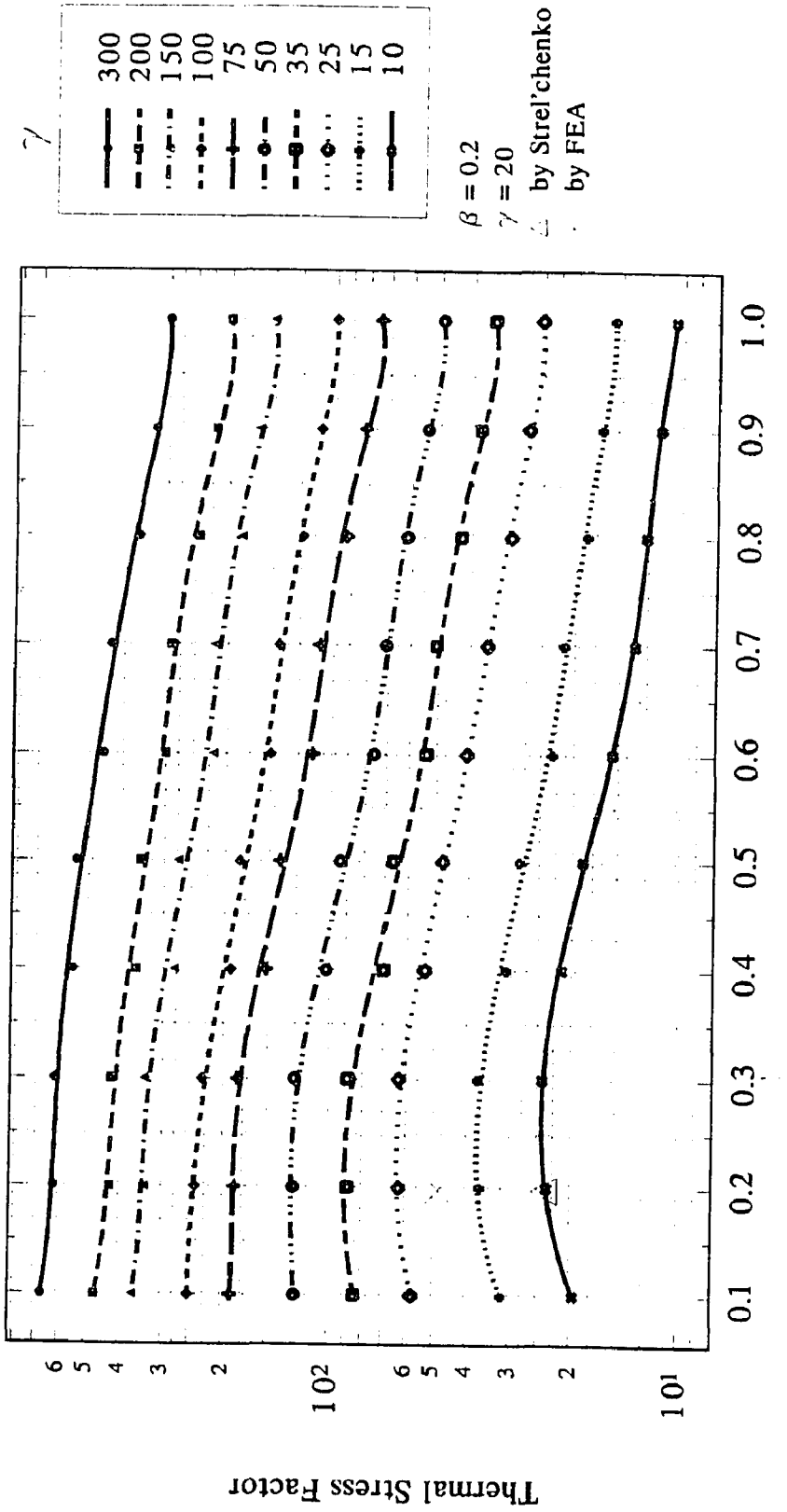

Figure E5 Data comparison of thermal stress factor in the circumferential direction at point A_o of the nozzle

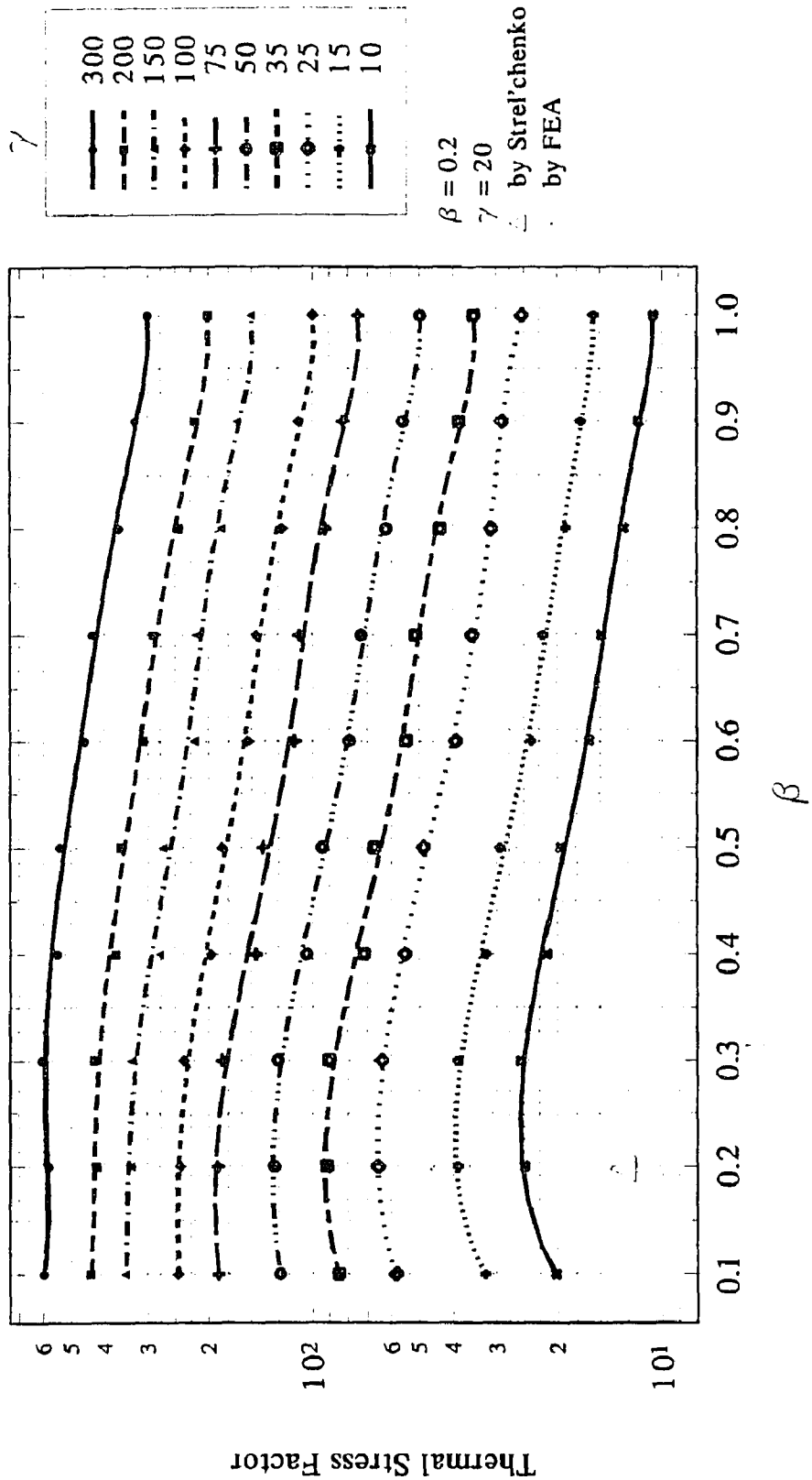

Figure E6 Data comparison of thermal stress factor in the circumferential direction at point A, of the nozzle

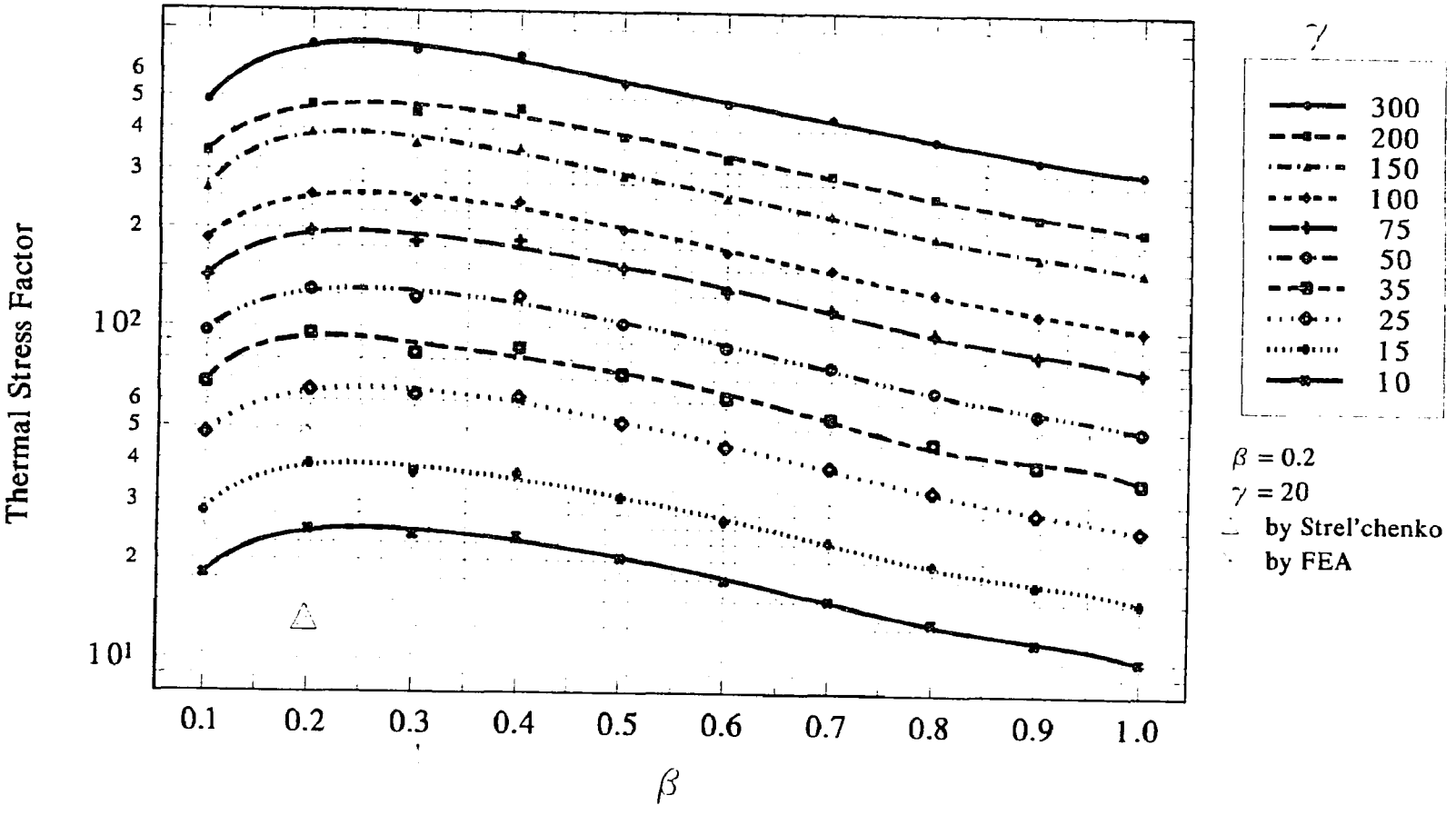

Figure E7 Data comparison of thermal stress factor in the circumferential direction at point C_o of the nozzle

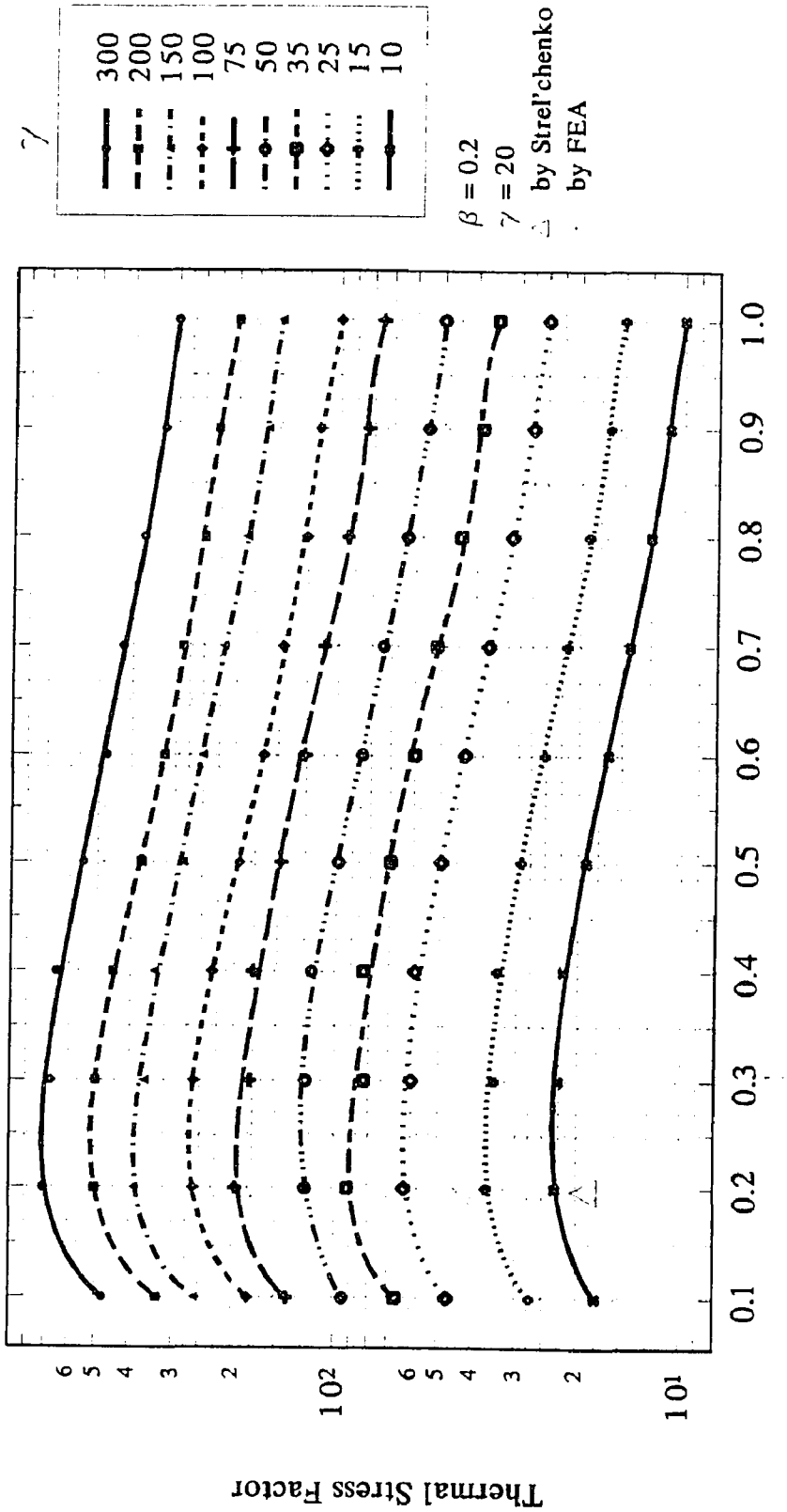

Figure E8 Data comparison of thermal stress factor in the circumferential direction at point C_i of the nozzle

REFERENCES

[1] D. H. Van Campen, "Mechanical and Thermal Stresses in Cylinder-to-Cylinder Intersections of Equal or Nearly Equal Diameters," *Ist International Conference on Pressure Vessel Tech., Part 1, Design & Analysis*, Sept. 29 - Oct. 2, 1969, pp. 293 - 307.

[2] K. R. Wichman, A. G. Hopper, and J. L. Mershon, "Local stresses in Spherical and Cylindrical Shells due to External Loadings," *Welding Research Council Bulletin 107.*

[3] S. Stepanek, "Stress Concentration in the Nozzle Ring of a Pressure Vessel," *Nuclear Engineering and Design*, v.2 , 1965 , pp.211 - 223.

[4] N. C. Lind, "Approximate Stress-Concentration Analysis for Pressured Branch Pipe Connections," *ASME Paper 67-WA/PVP-7*, 1967, pp.1 - 8.

[5] P. P. Bijlarrd and R. J. Dohrmann, "Stresses in Junction of Nozzle to Cylindrical Pressure Vessel for Equal Diameter of Vessel and Nozzle," *Nuclear Engineering and Design*, v.5, 1967, pp. 349 - 365.

[6] W. F. Riley, "Experimental Determination of Stress Distribution in Thin-Walled Cylindrical and Spherical Pressure Vessel with Circular Nozzle," *Welding Research Council Bulletin , n.108*, 1965, pp. 1 - 11.

[7] E. C. Rodabaugh, T. J. Atterbury, R. L. Cloud, and F. J. Witt, "Evaluation of Experimental and Theoretical Data on Radial Nozzle in Pressure Vessel," *USAEC Report, TID-24343*, Phase 5, 19666 - 67, PP. 1 - 58.

[8] F. J. Witt, R. C. Gwaltney, R. L. Maxwell, R. W. Holland, "A Comparsion of Theoretical and Experimental Results from Spherical Shell with a Single Radially Attached Nozzle," *ASME Journal of Engineering for Power*, v.89, 1967, pp. 333 - 340.

[9] P. P. Bijlarrd, R. J. Dohrmann, and J. M. Duke, "Thermal Stress Analysis of Nonuniformly Heated Cylindrical Shell and Its Application to Steam Generator Membrane Wall," *ASME Journal of Engineering for Power*, Jan., 1968, pp. 73 - 81.

[10] D. Manschot, "A Computation Method for Thermal Stresses in Thin-Walled Tees, " *Report KR-170, Laboratory for Nuclear Engineering* , University of Technology, Delft, June, 1968.

[11] E. T. Cranch, and O. H. Griffith, "Discontinuity Thermal Stresses in Shallow Spherical Shells," *1st International Conference on Pressure Vessel Technology, Pat 1, Design & Analysis*, Sept.. 1969, pp. 435 - 449.

[12] N. Krishnamurthy, "Three Dimensional Finite Element Analysis of Thick Walled Pipe-nozzle Junction with Curved Transition," *1st International Conference on Structural Mechanics in Reactor Technology*, Paper G2/7, 1971, pp. 215 - 237.

[13] K. Fullard, "The Calculation of Thermal Stresses in a Cylinder-to-cylinder Intersection by Means of Finite Element," *International Journal of Pressure Vessel and Piping*, v.1, n.3, July, 1973, pp. 177 - 198.

[14] D. H. Van Campen, and H. A. Spaas, "On the Stresses Distribution in Nozzle-to-Cylinder Connections, for Small Diameter Ratios," *Nuclear Engineering and Design*, v.21, 1972, pp. 368 - 395.

[15] K. Fullard, "Thermal Stresses in a Nozzle-drum Intersection," *International Conference of Structural Mechanics in Reactor Technology*, Paper G2/4, 1973.

[16] R. A. Goodell, "An Analytical and Experimental Investigation of a Nozzle-to-cylindrical Shell Junction," *Pressure Vessel and Piping - Analysis and Computers, ASME*, New York, 1974, pp. 141 - 157.

[17] R. C. Gwaltney, S. E. Bolt, and J. W. Byrson, "Theoretical and Experimental Stress Analysis of ORNL Thin-shell Cylinder-to-cylinder Model 4," *ERDA Report ORNL-5019*, Oak Ridge National Laboratory, June, 1975.

[18] F. Cesari, "Equivalent Nozzle in Thermomechanical Problems," *TRANS. International Conference on Structural Mechanics in Reactor Technology*, Paper G8/8 , Aug. 1977.

[19] A. H. Gantayat, and G. H. Powell, "Finite Element Analysis of Thin and Thick Walled Tubular Tee Joints," *TRANS., International Conference on Structural Mechanics in Reactor Technology*, Paper F1/1, Aug, 1977.

[20] J. Jayaraman, and K. P. Rao, "Thermal Stresses in a Spherical Shell with a Conical Nozzle," *Nuclear Engineering and Design*, v.48, n.2-3, Aug. , 1978, pp. 367 - 375.

[21] G. D. Gupta, M. S. Rao, T. V. Narayanan, A. C. Gangadharan, "Thermoelastic Analysis of Nonaxisymmetrically Heated Thick Cylindrical Shells," *Journal of Pressure Vessel Technology*, v. 100, Feb., 1978, pp. 107 - 111.

[22] S. J. Brown, "Thermal Transient Stress Analysis of Cylinder-to-cylinder Structures by the Finite Element Method ," *ASME paper 78-PVP-76*, June, 1978, PP. 1 - 12.

[23] S. J. Brown, "On the Mechanical and Thermal Transient Analysis of Cylinder-to-cylinder Vessels by a Finite Plate Method," *International Journal of Pressure Vessel and Piping,* v. 7, n. 1, Jan., 1979, pp. 31 - 64.

[24] J. W. Bryson, W. G. Johnson, and B. R. Bass, "Stresses in Reinforced Nozzle-cylinder Attachments under - a Parametric Study," *International Stress Indices and Stress Intensification Factors of Pressure Vessel and Piping Component, ASME,* N.Y., pp. 51 - 65, 1981.

[25] T. N. Truc, A. Bazergui, "Experimental Thermal Stresses at Attachment / Cylinder Intersections," *CANCAM Proceedings - Canadian Congress of Applied Mechanics,* 8th, v. 2, 1981, pp. 531 - 532.

[26] G. V. Ranjan, G. N. Brooks, and R. Huet, "An Improved Method of Stress Analysis for Cylinder-to-cylinder Intersections," *ASME Paper 82-PVP-41,* 1982.

[27] D. Lapointe, C. A. Laberge, and R. Baldur, "Plate-Cylinder Intersections Subjected to Thermal Loads," *Proceeding of the 5th International Conference on Numerical Methods in Thermal Problems,* 1987.

[28] R. Baldur, C. A. Laberge, and D. Lapointe, "Numerical Design Method for Thermally Loaded Plate-cylinder Intersections," *Journal of Pressure Vessel Technology,* v.110, Nov. 1988, pp. 361 - 366.

[29] W. J. Stikvoort, "Piping Reactions on Pressure Vessel Nozzles," *Chemical Engineering,* v. 93, n. 13, July, 1986, pp. 51 - 53.

[30] R. Sundaravadiveler, M. Hariharan, and C. Ganapathy, "Formula for Variation of Stress Concentration around Intersection in Tubular Joint," *Journal of Energy Resources, Technology, TRANS. ASME,* v. 110, n.4, Dec., 1988, pp. 237 - 245.

[31] G. N. Brooks, "Shell Solution for Reinforced Cylinder to Sphere Intersection," *Journal of Pressure Vessel Technology,* v. 110, n. 1, Feb., 1988, pp . 64 - 69.

[32] V. Kumer, and A. V. Singh, "Analysis of Pad-reinforced Nozzle in Pressure Vessel Head," *Journal of Pressure Vessel Technology,* v.111, n.3, Aug. , 1989, pp. 218.

[33] A. Y. Kuo, and T. Y. Hsu, "Stress Analysis of Reinforced Nozzle-cylindrical Shell Intersection under Internal Pressure or Nozzle Radial Thermal Expansion," *Journal of Pressure Vessel Technology,* v. 110, Nov., 1988, pp. 367 - 373.

[34] V. I. Savchenko, and V. V. Nakonechvyi, "Stress Concentration Around Opening in Conical Shells," *Strength of Material,* Oct., 1988, pp. 254 - 258.

[35] Y. C. Lam, and P. O. Trauner, "Finite Element Analysis of a Desuperheater Vessel Steam Inlet Nozzle Subjected to Thermal Loads," *International Journal of Pressure Vessel and Piping*, v. 39, n. 3, 1989, pp. 171 - 187.

[36] A. S. Strel'chenko, I. G. Strel'chenko, and L. A. Sheptun, "Stress State of a Variable Thickness Cylindrical Shell with a Constant Thickness Branch Pipe," *Soviet Applied Mechanics*, v. 24, n. 9, March, 1989, pp. 883 - 890.

[37] A. S. Strel'chenko, I. G. Strel'chenko, and L. A. Sheptun, "Temperature Stress in T-shaped Intersection of Constant and Variable Thickness," *Soviet Applied Mechanics*, v. 26, n.12, June, 1991, pp. 1155 - 1162.

[38] H. Moini, T. P. Mitchell, "Stress Analysis of a Thick-Walled Pressure Vessel Nozzle Junction," *International Journal of Pressure Vessel and Piping* , v. 46, 1991, pp. 67 - 74.

[39] K. Watashi, I. Furuhashi, and A. Imzau, "Simplified Method for Stress Estimation of Nozzles," *ASME, Pressure Vessel and Piping*, PVP v. 163, New York, 1989, pp. 57 - 66.

[40] I. Furuhashi and K. Watashi, "A Simplified Method of Stress Calculation of a Nozzle Subjected to a Thermal Transient," *International Journal of Pressure Vessel and Piping*, v. 45, 1991, pp. 131 - 162.

[41] ALGOR User Manual, *ViziCad Plus, Vol.1 , & vol. 2* , ALGOR Inc., 1992.

[42] ALGOR User Manual, *Linear Stress and Vibration*, , ALGOR, Inc., 1992.

[43] S. P. Timoshenko and J. N. Goodier, *Theory of Elasticity* , McGraw-Hill Book Company, New York, 1970.

[44] J. F. Harvey, *Theory and Design of Pressure Vessels*, Van Nostrand Reinhold, New York, 1991.

[45] J. Lin, "Stress Analysis of Pipe-nozzle Junction in Pressure Vessel Shell Design," Master Thesis, New Jersey Institute of Technology, Newark, 1993.